

NOTE TO USERS

This reproduction is the best copy available.

UMI[®]

GEOMETRIC AND QUASI-STATIC THERMAL ERROR COMPENSATION
OF A LASER DIGITIZER ON A COORDINATE MEASURING MACHINE

By

JOHN O. HARRIS, B.ENG., M.E.SC.

A Thesis

Submitted to the School of Graduate Studies

in Partial Fulfilment of the Requirements

for the Degree

Doctor of Philosophy

McMaster University

© Copyright by John O. Harris, September 2004

Half Title Page

GEOMETRIC ERROR COMPENSATION OF A LASER DIGITIZER ON A CMM

10/10/10
10/10/10
10/10/10

Descriptive Note

DOCTOR OF PHILOSOPHY

(Mechanical Engineering)

McMaster University

Hamilton, Ontario

TITLE: Geometric and Quasi-static Thermal Error Compensation of A Laser
Digitizer on A Coordinate Measuring Machine

AUTHOR: John O. Harris, B.Eng. (McMaster University), M.E.Sc. (University of
Western Ontario)

SUPERVISOR: Dr. Allan D. Spence

NUMBER OF PAGES: xix, 195

Abstract

Coordinate measuring machines (CMM) are widely used in inspection and reverse engineering. There is increasing interest in using optical sensors, such as laser digitizers, to take advantage of their high data acquisition rates and the fact that they are a non-contact measurement suitable for soft materials or delicate parts. The issue to be addressed is the fact that the sensors and CMMs are made by different manufacturers, so there is no integration of the error compensation scheme. As well, unlike conventional touch trigger probes, correction of the laser digitizer pose must be explicitly incorporated.

The purpose of this study was to develop a mathematical algorithm that would improve the accuracy of data collected with a laser digitizer mounted on a CMM. To this end, an algorithm was developed to compensate for the variations in digitizer pose. It compensates for both positional errors and angular errors, whether caused by CMM geometric component error or quasi-static thermal error.

To implement and verify the error compensation, tests were made using a Hymarc laser digitizer mounted on a DEA Iota 1102 CMM. The thesis proposes using an optical ballbar, an adaptation of the traditional ballbar recommended by ASME Standard B89.4. The scan plane coordinates of the digitizer, the CMM axis scale positions and temperatures were recorded simultaneously in real time. The CMM error compensation algorithm was then used to post process the data to obtain improved global part coordinates. Accuracy of a laser equipped CMM is improved from 67 μm to 17 μm . The

benefits of using optical sensors can be improved by incorporating this error compensation scheme into an integrated optical metrology system.

Acknowledgements

Serendipity is when things just happen right. I was introduced to Dr. Spence at an open house of Memex Inc. We talked, with me saying how difficult it was to go back to school for a Ph.D., and him saying how few people in industry wanted to pursue advanced education. I acknowledge my most sincere gratitude to Dr. Spence for his leadership, expertise and unending support. I am proud and grateful to have the good fortune of his mentorship and friendship.

The help with calibrating the CMM and the loan of a traditional ballbar and laser interferometer by Omni-Tech CMM services (Canada) Inc. was greatly appreciated, as was the support of Hymarc Technologies Inc.

Equipment was purchased using a Canada Foundation for Innovation/Ontario Innovation Trust (CFI/OIT) grant, Materials & Manufacturing Ontario, and National Centres of Excellence Auto 21.

Special appreciation is extended to the Mechanical Engineering Department staff, both in the office and in the labs, for their assistance and encouragement over the years. My colleagues at the Dimensional Modelling Systems Laboratory (DMSL), Harley Chan, Dave Chang, Phil Mitchell and Peng Wu have made our endeavours at McMaster memorable and irreplaceable. Harley assisted with machine operation, and Dave helped when I got "Blue Screen" problems.

Thank you to my children, Peter and Tara and their spouses, for their support and understanding. In addition, thank you, Renée, for your weekly admonition to "Study, study, study." It has become my catch phrase for this degree.

And a final comment from Vigenere:

XMEFF IAKQM DEIQD QMBMU ZMEFT

QBDAR QEEAD EBXMK QPQSA SMYQE

Table Of Contents

Descriptive Note	ii
Abstract.....	iii
Acknowledgements	v
Table Of Contents	vii
List Of Illustrations.....	xii
List Of Tables	xv
List Of Symbols	xvii
List Of Abbreviations	xviii
Chapter 1	1
Introduction.....	1
1.1. Background.....	2
1.2. Coordinate Measuring Machines	4
1.3. Lasers For Measurement.....	6
1.4. Accuracy	7
1.5. Error Mapping And Compensation.....	11
1.6. Thermal Effects.....	11
1.7. Justification.....	12
1.8. Scope Of Thesis	13

1.9. Outline	14
Chapter 2	16
Literature Review	16
2.1. Metrology.....	16
2.2. Coordinate Measuring Machines	18
2.2.1. CMM Types And Structures	19
2.3. Probing.....	24
2.3.1. Touch Probes	24
2.3.2. Laser Digitizers Based On Triangulation.....	25
2.4. Accuracy And Precision Machining	28
2.5. Sources Of Errors.....	29
2.5.1. Errors In CMMs	29
2.5.1.1. Quasi Static Errors	30
2.5.1.2. Dynamic Errors	33
2.5.1.3. Software Induced Errors	34
2.6. CMM Calibration Standards.....	35
2.6.1. ASME B89.....	37
2.6.2. VDI/VDE 2617	38
2.6.3. ISO 10360 And ISO 14253.....	39
2.6.4. Other	41
2.7. Integration With CAD/CAM	42
2.8. Measurement And Modelling Of Errors	43

2.8.1. CMM Modelling And Error Description	44
2.8.2. Use Of Homogeneous Transformation Matrix	51
2.9. Error Reduction.....	51
2.9.1. Changes To CMM Structure	52
2.9.2. Software Compensation Of Measurements	52
2.10. Thermal Errors	55
2.11. Summary	56
Chapter 3	58
CMM Error Mapping.....	58
3.1. Geometric Component Errors	58
3.2. CMM Error Measurement	60
3.2.1. Storing Error Measurements	63
3.3. Error Measurement	64
3.4. CMM Error Map At Specific Temperatures	68
3.5. Error Map At 20 °C	86
3.6. Error Map At 25 °C	91
3.7. Error Map At 30 °C	96
Chapter 4	101
Laser Digitizer	101
4.1. Laser Digitizer	101
4.2. Digitizer Mount.....	105
4.3. Euler Angle Method Of Digitizer Alignment Calibration For Pose Attitude.....	106

4.4. Laser Digitizer Alignment Calibration	111
Chapter 5	113
Error Compensation	113
5.1. Implementation Of Error Correction Scheme.....	113
5.2. CMM Position Error Compensation	115
5.3. HTM For Laser Digitizer Alignment.....	116
5.4. Error Correction For Attitude Of Laser Digitizer Mount	123
5.5. Laser Digitizer Pose Attitude And Position Compensation.....	125
5.6. Interpolation Between Map Points	126
5.7. Summary.....	127
Chapter 6	129
Test Results And Analysis	129
6.1. Tests	129
6.1.1. Equipment	131
6.1.2. Measurements On Sphere	131
6.1.3. Calculation Of Sphere Centre	132
6.1.4. Interpolation Between Error Map Points	132
6.2. Initial Squareness Tests (22 °C)	133
6.2.1. Measurements Of XY Squareness Using Ballbar	133
6.2.2. Results Of Squareness Tests	135
6.2.3. Analysis Of Squareness Tests	136
6.3. Volumetric Tests At Ambient Temperature (22 °C).....	138

6.3.1. Results At Ambient Temperature	140
6.3.2. Analysis Of Results At Ambient Temperature	141
6.4. Measurements Over Volume At Controlled Temperature.....	143
6.4.1. Results At Controlled Temperature	150
6.4.2. Analysis Of Results At Controlled Temperature	154
6.5. Summary.....	157
Chapter 7	159
Conclusion	159
7.1. Conclusions.....	159
7.2. Suggestions For Further Work.....	160
Appendix A Effect Of Sphericity.....	162
Appendix B CMM Error Map At Ambient.....	167
Appendix C Ballbar Data	177
References.....	185

List Of Illustrations

Figure 1-1 DEA Iota 1102 Coordinate Measuring Machine	5
Figure 1-2 Compensation Procedure Flow	14
Figure 2-1 Abbe Principle Without Error [Based On Slocum 1999].....	18
Figure 2-2 Abbe Principle With Error [Based On Slocum 1999].....	18
Figure 2-3 FICA Column Type CMM.....	22
Figure 2-4 Iota P Bridge Type CMM	22
Figure 2-5 Cantilever Type CMM [Ni 1995]	23
Figure 2-6 Gantry Type CMM [Ni 1995].....	23
Figure 2-7 Industrial Measuring Robot [Turner 2003]	24
Figure 2-8 OSIS Integration Model [IACMM 2003]	27
Figure 2-9 Ball Plate Used In Round Robin Testing [Caskey 1997].....	41
Figure 2-10 Errors In CMMs [Kunzmann 1995].....	50
Figure 3-1 Moving Bridge CMM	59
Figure 3-2 Six Degrees Of Freedom Error Motion.....	60
Figure 3-3 Optics To Measure Linearity Of Scales	66
Figure 3-4 Optics To Measure Angular Errors	67
Figure 3-5 Laser Used To Measure Errors	67
Figure 3-6 Error Map Measurements.....	69
Figure 3-7 X Axis Linearity Errors.....	74

Figure 3-8 X Axis Straightness Errors.....	75
Figure 3-9 Y Axis Linearity Errors.....	76
Figure 3-10 Y Axis Straightness Errors.....	77
Figure 3-11 Z Axis Linearity Errors	78
Figure 3-12 Z Axis Straightness Errors	79
Figure 3-13 X Axis Rotational Errors About Y	80
Figure 3-14 X Axis Rotational Errors About Z	81
Figure 3-15 Y Axis Rotational Errors About X.....	82
Figure 3-16 Y Axis Rotational Errors About Z	83
Figure 3-17 Z Axis Rotational Errors About X	84
Figure 3-18 Z Axis Rotational Errors About Y	85
Figure 4-1 Principle Of Triangulation Using Synchronised Scanning [Hymarc].....	104
Figure 4-2 Hymarc 45C Field Of View [Hymarc].....	105
Figure 4-3 Incremental Trunnion [Hymarc]	106
Figure 4-4 Digitizer Mounted On Trunnion [Hymarc].....	106
Figure 4-5 Digitizer Alignment	107
Figure 4-6 Optical Vernier [Hymarc]	109
Figure 4-7 Ball Tower Calibration Sphere [Hymarc]	112
Figure 5-1 Laser Digitizer At $\gamma = 0^\circ$	117
Figure 6-1 Ballbar Position For Squareness Tests	134
Figure 6-2 B89 Test Positions [ASME 1997].....	139
Figure 6-3 Digitizer W Aligned With X Axis, $\gamma = -60^\circ$	140

Figure 6-4 Results Of Initial Test	145
Figure 6-5 Volume Measurements At Ambient.....	146
Figure 6-6 Results At 20 °C	147
Figure 6-7 Results At 25 °C.....	148
Figure 6-8 Results At 30 °C.....	149
Figure A 1 Side View Of Oblate Sphere	164
Figure A 2 Oblate Sphere	166
Figure A 3 Prolate Sphere.....	166
Figure C 1 Ballbar Sphere Data (1)	178
Figure C 2 Ballbar Sphere Data (2)	179
Figure C 3 Ballbar Sphere Data (3)	180
Figure C 4 Ballbar Sphere Data (4)	181
Figure C 5 Ballbar Lengths At 20 °C.....	182
Figure C 6 Detailed Sphere Data, Uncompensated	183
Figure C 7 Detailed Sphere Data, Compensated	184

List Of Tables

Table 1 Coordinate System Nomenclature	xvii
Table 2 Acronyms.....	xviii
Table 3 Types And Structures Of CMM.....	21
Table 4 Comparison Of CMM Performance Standards.....	36
Table 5 Measuring Methods For Error Components	45
Table 6 21 Geometric Component Errors Of The CMM.....	61
Table 7 Squareness Error Versus Temperature	73
Table 8 X Carriage Error Map At 20 °C	86
Table 9 Y Carriage Error Map At 20 °C	88
Table 10 Z Carriage Error Map At 20 °C.....	89
Table 11 X Carriage Error Map At 25 °C	91
Table 12 Y Carriage Error Map At 25 °C	93
Table 13 Z Carriage Error Map At 25 °C.....	94
Table 14 X Carriage Error Map At 30 °C	96
Table 15 Y Carriage Error Map At 30 °C	98
Table 16 Z Carriage Error Map At 30 °C.....	99
Table 17 Hymarc Hyscan 45C Specifications	103
Table 18 Pose Factors For Data Correction	114

Table 19 Summary Of Controlled Temperature Results	151
Table 20 Summary Of Results Per ASME B89.....	152
Table 21 Length At Standard Temperature	154
Table 22 Grade 200 Ball Tolerance	163

List Of Symbols

Table 1 Coordinate System Nomenclature

D, E, F	Uncorrected readings from the axis linear scales on the CMM.
U, V, W	Coordinates of the laser digitizer.
X, Y, Z	Coordinates in the world (machine) reference frame.
α, β, γ	Euler angles describing the pose alignment of the laser digitizer.
${}^B_A[HTM]$	The 4x4 homogeneous transformation matrix that maps numbers from the A coordinate system into the B coordinate system.
${}^H \begin{bmatrix} X \\ Y \\ Z \\ 1 \end{bmatrix}$	Position data expressed in terms of the H coordinate system, i.e. based at the origin of the specified coordinate system.
H	Origin based at the CMM home position.
L	Origin based at the laser digitizer coordinate origin.
P	Origin based at the mount location of the laser digitizer, a reference frame moving with the ram of the CMM, used to apply pose corrections to the data.
R	Origin based at a reference sphere.
D_0, E_0, F_0	CMM coordinates when the laser digitizer origin is aligned with the reference sphere

List Of Abbreviations

Table 2 Acronyms

Abbreviations and Acronyms

3D	Three Dimensional
A2LA	American Association for Laboratory Accreditation
ACMC	Association for Coordinate Metrology Canada
ANOVA	Analysis of Variance (statistical technique)
a-s	$\text{arc-second} = \frac{1}{3600} \text{ angular degree}$
ASME	American Society of Mechanical Engineers
ASPE	American Society for Precision Engineering
CAD	Computer Aided Design
CAD/CAM	Computer Aided Design/Computer Aided Manufacture
CCD	Charge Coupled Device
CIRP	International Institution for Production Engineering Research
CMM	Coordinate Measuring Machine
CNC	Computer Numerical Control
CSME	Canadian Society of Mechanical Engineers
DMSL	Dimensional Modelling Systems Laboratory
FMS	Flexible Manufacturing System

Abbreviations and Acronyms

HSV	Hymarc Optical Vernier
HTM	Homogeneous Transformation Matrix
ICP	Iterative Closest Point
IDW	International Dimensional Workshop
IEEE	Institute of Electrical and Electronics Engineers
ISO	International Standards Organisation
LED	Light Emitting Diode
MAA	Metrology Automation Association
NIST	National Institute of Standards and Technology
OSIS	Optical Sensor Interface Standard
PDE	Partial Differential Equations
RH	Relative Humidity
SME	Society of Manufacturing Engineers
VDI/VDE	Verein Deutscher Ingenieure/Verband Der Elektrotechnik Elektronik Informationstechnik

Chapter 1

Introduction

The research described in this thesis is aimed at developing an accurate method of measuring coordinate data with a 3D laser digitizer mounted on a coordinate measuring machine. General equations are developed for software compensation of a two component system consisting of an end effector measuring transducer and a transport mechanism for positioning the transducer. The initial equation development and validation with crossed ballbars was presented at the 2002 CSME conference [Harris 2002-1]. Later that year a paper, including validation over the CMM working volume, was presented at the ASPE conference [Harris 2002-2]. In 2003, the equations were presented as an accuracy enhancement to the development of an open architecture control for coordinate measuring machines [Chang 2003]. The completed work, incorporating the technique for thermal error compensation, has been published in the International Journal of Machine Tools and Manufacture [Harris 2004].

The main research contributions of the thesis are explicit integration of laser digitizer pose compensation with the CMM error map, including quasi-static thermal compensation and introduction of an optical ballbar evaluation method.

1.1. Background

The coordinate measuring machine (CMM) with direct computer control and motorised drives on the axes is a relatively new device. According to Bosch [1995], what may be the first mechanical coordinate measuring machine was built by Brown & Sharpe in 1875 for the Herreshoff Company in Bristol, Rhode Island, the world's best known builder of boats and racing yachts. The first measuring machine that falls into the category of what today we think of as a manually operated coordinate measuring machine was developed in 1959 by Ferranti Ltd. in Dalkeith, Scotland. It was developed as a companion product to their numerically controlled machine tools, as a result of the need for faster and more flexible measuring when machining became more automated. Originally hard probes were the only probes available to use with a CMM. The measurement operation could not be assisted by putting motor drives on the axes because the probes could not be positioned with great accuracy and the probes were likely to break or the machine itself could become damaged. The development of motorised direct computer controlled machines occurred after the development of a compliant probe. Touch trigger probes were invented in 1972 to solve one specific inspection problem, the fuel lines used on the Olympus engine of the Concorde SST. Touch trigger probes work by providing an open switch signal when touched against a component and this signal is used to record the axis position readouts at the instant of touch. Today electromechanical touch trigger probes are widely used. A DEA Iota 1102 CMM is shown with a touch probe in Figure 1-1.

Scanning technology was initially developed during the mid- to late 1970s. Beginning in the late 1980s, microprocessor-based controllers and firmware were introduced. At about this time, the RS-232 connection between the CMM and host computer changed to Ethernet, and sampling rates increased to 200 Hz. Today, more PC-like controllers and 500+ Hz sampling speeds have made high-speed data manipulation possible. An Ethernet connection between the CMM and the host computer can transfer information at 100 MB/sec or faster. Because of these advances, as well as the widespread use of finite element and modal analysis in coordinate measuring, CMMs can now gather thousands of data points per second using advanced sensor technology.

In the early 1980's, North American automakers were feeling the effects of increased competition from their Japanese counterparts. Of particular concern to U.S. manufacturers was a perceived quality gap between U.S.-built cars and Japanese-made vehicles, which was driving more consumers to purchase imported cars. These trends spawned a renewed emphasis on quality in North American automotive production, at the same time that rapid advances were occurring in personal computers, lasers, cameras and image processing. When these areas came together to produce a new technology known as machine vision, U.S. automakers soon recognised its potential for use in improving vehicle quality.

One of the earliest automotive applications for the technology was the use of laser-triangulation machine vision sensors and specialised algorithms to perform automatic dimensional measurements aimed at quality control. The power of laser-based dimensional measurement lies in its combination of speed and non-contact measurement

capability. Because a large number of measurements can be performed quickly and simultaneously without touching the car body, laser measurement systems can be placed "in process" to measure 100% of production.

The original automotive application for laser measurement was dimensional verification of fully built, unpainted, "body-in-white" automobile body structural assemblies. Each completed body-in-white passed through a measurement station to check if it was dimensionally correct. Rejected assemblies were repaired or scrapped, while acceptable assemblies continued through the process. The objective is to control the length of a car to within 1 mm.

Today, in-process laser measurement systems are used for much more than just quality inspection. Because they can measure every part that is produced, in-process measurement systems are proving to be invaluable tools for root cause determination and process improvement. Over the past two decades, the scope of laser measurement in automotive manufacturing has grown beyond standalone, end-of-line stations to encompass nearly every processing centre within the automotive assembly line. Hymarc developed its first 3D scanning system for military applications in 1987 and introduced the first commercial HYSCAN system in the early 1990's.

1.2. Coordinate Measuring Machines

A coordinate measuring machine (CMM), such as the one shown in Figure 1-1, measures three dimensional (3D) points. Its use has changed the way of measuring objects from a comparison to a calculation. Instead of comparing the test object to a ruler

or reference standard, the first CMMs simply had a digital readout to provide the centre location of a hard probe. Using the two readouts, the length measurement could be manually calculated. This means the CMM provides differential gauging which has some advantages over comparative measurements. Measurement of size is done without regard to position, so the staging or positioning of the test object does not affect the measurement. With the addition of computers and software, the functionality of a CMM is enhanced. These functions include geometric feature development, CMM automation and part programming, geometric error correction and data storage for analysis or transmission throughout a network.

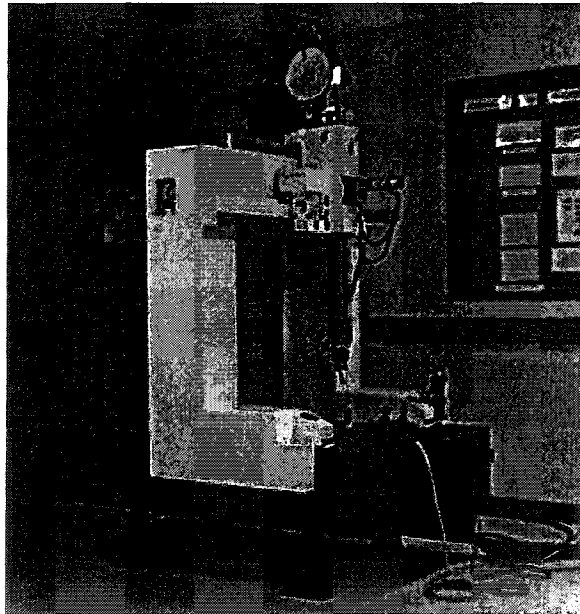


Figure 1-1 DEA Iota 1102 Coordinate Measuring Machine

1.3. Lasers For Measurement

Customer requirements for measuring small or fragile parts are pushing traditional touch-probe equipment to the limit. Soft materials, such as the silicone elastomer keypads used on cell phones, would be deformed if measured with a touch probe. An emerging trend in dimensional inspection of manufactured parts is the use of coordinate measuring machines equipped with non-contact laser digitizers instead of traditional contact probes.

Laser triangulation sensors have a stand-off (distance from the sensor to the part) and use a low power laser diode as a source of light. The light is projected onto the test object at an angle, and the position of the reflected light on a strip detector is used to calculate the distance to the object using triangulation. More information is included in section 2.3.2 Laser Digitizers Based On Triangulation and section 4.1 Laser Digitizer.

The laser digitizer offers the advantages of no contact deflection force and data collection rates of thousands of points per second. Currently, however, the accuracy of such a system is limited by the lack of an integrated CMM/laser digitizer geometric error compensation system, and the absence of a standard evaluation method. As a result, there is no correction of the laser digitizer point coordinates to compensate for the varying geometric errors encountered at different locations within the CMM volume.

1.4. Accuracy

For many years, the research community has focussed attention on improving aspects of accuracy in manufacturing. Higher accuracy in manufacturing results in the following:

- 1) Quality control improvement by reduction of rework and rate of rejection of produced parts,
- 2) More automatic assembly as opposed to fitting,
- 3) Improvement of component life against wear and fatigue, and
- 4) Increase of interchangeability of components [McKeown 1987].

Accuracy is pertinent in particular to both the machining and inspection stages. To achieve better accuracy at the machining stage improved design concepts and working conditions have been studied and introduced to the machining process. Coordinate Measuring Machines (CMMs) are normally incorporated to perform the quality control task in the production line. CMMs should be five to ten times more accurate than the machine tools in the same production line [Sartori 1995] [Scarr 1967] [ISO10360 2000]. Therefore, correction of errors occurring in their results is imperative to the level of accuracy of the entire integrated manufacturing system. The factors affecting the accuracy of both the machine tool and the CMM are almost similar. The differences in the accuracy issues between the two modules are dependent on the nature of the process carried out by each of them. A clear example is the thermal error resulting from the cutting process in a machine tool, which does not apply to the CMM case [Bryan 1990].

Before CMMs were incorporated in the production line, part inspection was done manually and separately. This inspection includes measurements for part dimensions, form, surface characteristics and position of geometrical elements. The incorporation of CMMs in the production line allowed for a complete metrological description of the workpiece in a fully co-ordinated manner. It also accomplished a major step in bringing up the quality control aspect of a production line to the automated level [Kunzmann 1988] [Peggs 1989]. CMMs find applications in different industries from tiny parts to complete vehicles [Danzer 1987]. Current research interests aim at the investigation of standards and protocols to exchange information between CMMs and other parts of the manufacturing system. Industrial dimensional metrology is currently just awakening to the need for uncertainty analysis as our understanding of the technology improves. Standards on this subject have only recently been published [ISO 14253, Part 3 2002].

Accuracy of the CMM can be evaluated without access to a primary length standard, which would require temperature stabilisation and be difficult to maintain to the required level. The technique used is called auto-calibration and uses the fact that an arbitrary length can be measured in several locations. It doesn't matter what the length is, as long as it is stable over a short period of time. An example or analogy may clarify the situation, and highlight the differences between repeatability (grouping or measurement uncertainty) and accuracy. Let's assume you are an excellent marksman and a friend comes to you with a new rifle asking, "Are the sights aligned accurately?"

Your repeatability is known to be excellent. With any given rifle, you can put 20 shots into a target and the grouping of holes can be covered with a dime. There is very little uncertainty that when you shoot you put the bullet in the same place every time.

However, you can't measure the accuracy of this particular rifle because you don't have access to a true calibration standard. You have no idea how much this calibre of bullet will be affected by wind or how much the bullet will drop at 100 yards. The question is "Where should the grouping of bullet holes be?" The solution is to do what is called an auto-calibration or self-calibration. By holding the rifle in many positions, you can eliminate the effect of misaligned sights and determine the answer of where the bullets should go.

You hold the gun upright and the bullet lands three inches to the left of the bullseye at the 8 o'clock position. You hold the gun on its right side, and the bullet lands two inches high. You hold the gun upside down and the bullet hole is three inches to the right at the 4 o'clock position. Finally, you hold the gun on its left side and the bullet lands four inches low at the 6 o'clock position.

You can now answer the accuracy question in two steps. The first step is to answer the question, "What is the true sight position? or Where should the bullets go?" It is given by the centre of all the holes in the target. When the gun was held in many various positions the problem with the sight misalignment is averaged out. For this calibre, the answer is one inch low. What is the uncertainty of this true sight position? Since your shooting ability (when holding the gun upright every time) produces a group

that can be covered by a dime, the uncertainty in the true sight position can be covered with a dime. The second step is to answer the important original question, "Are the sights aligned accurately?" This answer is given by the distance from the ideal sight position (one inch low) to where the four bullets actually landed on the target. On the first shot, the bullet hole was three inches left (but not low) of the true sight position. The second shot (two inches high of the bullseye) was three inches high of the true sight position. On average, ignoring whether the bullet was high or left, the bullets landed three inches away from where they should have. The sights have a three inch rms accuracy error (or inaccuracy).

The CMM has very good repeatability due to feedback from the glass scales on the axes. It will go to the same spot every time it is commanded. It is not easy to know where in real space that repeatable spot is, because instead of sight misalignment the CMM has geometric error (that varies by location). When evaluating a CMM's performance using self-calibration, the calibration unknown is the ballbar length instead of "where should the bullets land". Similar to turning the gun around four times to get different positions to average out and eliminate sight misalignment, the ballbar is measured at 20 different positions throughout the CMM's working volume to average out and eliminate the effect of geometric error.

The true length of the ballbar is estimated to be the mean of the length measurements at the 20 positions. An indication of the accuracy is the deviation (expressed as rms accuracy error to be independent of direction) of measured length from the true length at the various positions used. The B89 standard uses only one position,

the worst case position, to determine CMM accuracy. When evaluating the improvement of the compensation algorithm, since an improvement throughout the working volume is desired, it was appropriate to include all the measurements.

The improvement in accuracy was through the use of compensation. The rms accuracy error is a measure of how well the compensation rule has done.

1.5. Error Mapping And Compensation

The availability of computing power within CMM controllers has led to error compensation of reported coordinates ever since Hocken won the F. W. Taylor medal from CIRP in 1979 for his original development of software compensation [Hocken 1977].

Measuring machines or precision machine tools are built with a great amount of accuracy control and fitted with very precise guideways, high accuracy ballscrews, linear scales, air bearings, etc. With the use of error compensation, machine designers can concentrate on making the machines repeatable and reduce the effort on making the machines mechanically accurate. The accuracy is instead achieved by software.

1.6. Thermal Effects

Temperature influences upon production processes and measurement accuracy have been for many years a great concern for researchers. In a CIRP keynote paper, J. B.

Bryan drew attention to the problem of thermal errors [Bryan 1968]. CIRP members are disappointed by the fact that "CMM manufacturers as well as users do not pay enough attention to temperature influences." They also claim: "the limits of length measurement accuracy are determined by the accuracy of temperature measurements" [Kunzmann 1988]. Experts believe that 40–70% of the error in precision parts arises from thermal error. In spite of evidence regarding the importance of the problem, even up until the early 1990s, not much had changed in the industry [Bryan 1990].

Also, there is a trend to put the CMM on the factory floor where it can perform inline inspection. This improves the speed of measurement and feedback to the machine operators and managers, but increases the range of operating temperature where accuracy is required. The measuring equipment is no longer located in a temperature controlled quality lab.

1.7. Justification

There is a need for accuracy in the data used for both reverse engineering and quality analysis. Semiconductor devices continue to get smaller and faster, with more computing power in less expensive packages. Pushed by shrinking computer chips, mechanical devices also continue to shrink: Computer-aided fuel injection allows more precise control over fuel flow, which in turn creates a need for more precisely machined fuel injectors; pacemakers, once cigarette packet-sized boxes carried outside the body, are now so small they're embedded in the body.

The Metrology Automation Association made their first survey of CMM sales in 2000 [MAA 2000] and found that sales were \$252.6 million, including 2, 415 new units shipped. Sales for bridge style coordinate measuring machines topped the list of machine types sold, with 85% of the market. Two years later [MAA 2002], in an economic downturn, sales were \$135.4 million, with 1, 243 units shipped. This indicates that retrofit additions are more likely than new equipment purchases as industry tries to fully utilise existing equipment.

1.8. Scope Of Thesis

The research work undertaken herein ultimately aims to develop a comprehensive error compensation technique that can be effectively integrated into a laser digitizer equipped CMM. The errors to be compensated are the geometric component errors of the machine structure and their effect on the mounting pose of the laser digitizer. The quasi-static changes in geometric component errors due to thermal effects at temperatures other than 20 °C are also included.

As shown in Figure 1-2 four things are required for error compensation: 1) an error map, 2) digitizer alignment calibration, 3) the measured point data and 4) the equation to compensate the point data.

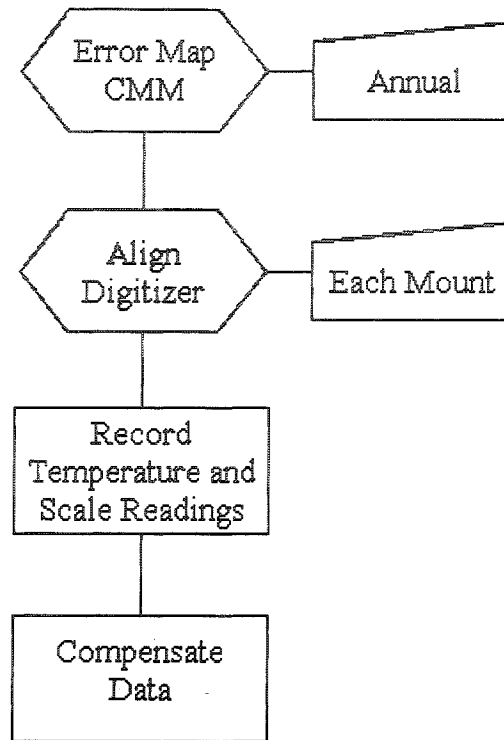


Figure 1-2 Compensation Procedure Flow

Error mapping of a CMM is well known. This thesis develops the digitizer alignment relative to the error map, and develops the necessary equations to compensate the measured point data, and proposes a standard evaluation method.

The methods developed have been experimentally verified and can be incorporated into a new CMM design, or added to a retrofit CMM controller.

1.9. Outline

The rest of the thesis is organised as follows. Chapter 2 is a literature review of CMMs, laser digitizers, the need for accuracy, error compensation and the effects of thermal variations. Chapter 3 is a review of the error map for a bridge type CMM, and

measurement at three temperatures of the CMM used for testing and verification. This measurement procedure is only needed once. Chapter 4 describes laser digitizers and the alignment calibration technique used for each pose of the digitizer. The contribution is the development of the relationship between the origin of the digitizer coordinate system and the CMM home position. This key piece of information is needed to use the CMM error map. Chapter 5 provides a mathematical contribution to the enhanced accuracy of digitizers. It develops the compensation equation for position errors of the digitizer and adds a new error compensation term for the pose attitude. The interpolation of error maps at various temperatures develops a compensation technique to account for all the known errors. The equation developed in this chapter is used for every data point collected by the laser digitizer. Chapter 6 gives test results and analysis, including the introduction of a system evaluation method based on an optical ballbar. Chapter 7 provides conclusions.

Chapter 2

Literature Review

2.1. Metrology

In his book, Scarr [1967] gives an historical perspective of measurement. The Pyramid at Giza was built in 2700 BC and has sides that are 756 feet long and equal to within 8 inches, and square to within 3.5 arc-seconds. In the 18th century, there was chaos in Europe regarding units of length, a multitude of measurement systems were in use. The metric system was initiated in 1827 but it wasn't until after the Second World War that it became possible to produce monochromatic light of sufficient purity to consider its adoption as an international standard to replace the platinum bar used as the meter standard. In 1960, the length of a meter was defined in terms of the wavelength of the orange radiation of the isotope Krypton 86. Scarr [1967] doesn't define "precision engineering" but sees it as a continuously changing target.

McKeown [1987] defines precision engineering as manufacturing to tolerances smaller than 1 part in 10,000. Precision engineering finds applications in fields like metrology and advanced manufacturing.

Schafrik [1999] discusses evolving technological capabilities, and says precision machining was manufacturing to tolerances of less than 10 μm in 1980 and to tolerances of less than 1 μm in 1990.

According to Slocum [1999], there are three basic definitions to remember with respect to how well a machine tool can position its axes: accuracy, repeatability (precision), and resolution. Accuracy is the maximum translational or rotational error between any two points in the machine work volume. Repeatability (precision) is the error between a number of successive attempts to move the machine to the same position, or the ability of the machine to make the same motion over and over. Resolution is the smallest unit measured by the machine.

The Abbe principle is known as the first principle in metrology [Zhang 1989]. In the late 1800s, Dr. Ernst Abbe noted "If errors in parallax are to be avoided, the measuring system must be placed coaxial with the axis along which displacement is to be measured on the workpiece." [Slocum 1999]. The Abbe principle can be visualised by comparing the measurement and reading points made with a micrometer which is free of Abbe errors since the object contact points are in line with the gauge (Figure 2-1) and a dial calliper where the object contact points are offset from the gauge (Figure 2-2). The Abbe offset error results from the 'angular' or 'tilt' motion of the probe relative to the test object; the angular error results in an error in the displacement measurement. In medium and large machines the Abbe offset errors are often the errors of greatest magnitude. Thermal gradients which cause machine bending (see Figure 2-10) increase Abbe error.

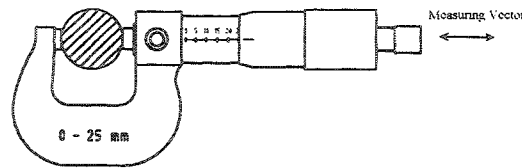


Figure 2-1 Abbe Principle Without Error [Based On Slocum 1999]

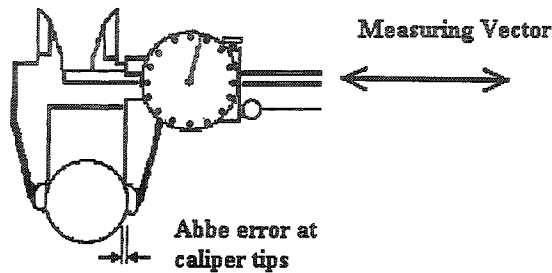


Figure 2-2 Abbe Principle With Error [Based On Slocum 1999]

2.2. Coordinate Measuring Machines

CMMs are presently used for a wide range of measurement tasks. This is because of its ability to carry out measurements under different environment conditions (shop floor) with high speed and accuracy. CMMs also offer flexibility over fixed gauging as they can be programmed to measure a wide range of shapes.

The basic function of coordinate metrology consists of the measurement of the actual shape of a work piece, its comparison with the desired shape and the evaluation of the basic parameters such as size, form, location, and orientation. CMMs basically perform a point-to-point sampling. The shape of the work piece is obtained by probing

the surface at discrete measuring points. The parameters cannot be evaluated directly from the measured coordinates. Therefore, an analytical model of the work piece is built using basic geometrical elements (lines, circles, planes etc.). From the analytical model, the various metrological parameters can be measured with a high degree of accuracy.

Before CMMs were incorporated in the production line, part inspection was done manually and separately. This inspection includes measurements for part dimensions, form, surface characteristics and position of geometrical elements. The incorporation of CMMs in the production line allowed for a complete metrological description of the workpiece in a fully co-ordinated manner. It also provided a major advance in bringing up the production line to the automated flexible manufacturing system (FMS) level [Kunzmann 1988] [Peggs 1989]. Kunzmann [1988] describes the future factory as including CMMs with automatic part handling. Also according to Kunzmann [1988], the market growth in CMMs utilisation as a part of the FMS is 10 to 15% per year. This is specifically for the 3D CMMs. This shows the value of 3D CMMs for industry as the most important measuring machines of today. CMMs find applications in different industries from tiny parts to complete vehicles [Danzer 1987].

2.2.1. CMM Types And Structures

There are four types of CMMs, if they are to be divided according to their mechanical system configuration. Table 3 shows the different types, applications and specifications. The selection of the CMM is dependent on the type of product to be handled. In some cases a 3D CMM is completed by a rotary table or a fourth axis. This

increases the flexibility of the CMM without a significant loss in accuracy [Kunzmann 1988]. Balsamo [1995] provides another division of CMM types based on the sequence order of their base. He reports the existence of an intrinsic axis order in a CMM that is referred to as a CMM kinematic sequence. This is based on the fact that typically CMMs are made up of four rigid bodies, three carriages, and a base. These components are linked together in a sequence from the workpiece to the probe. This concept is used in modelling CMMs.

Table 3 Types And Structures Of CMM

CMM Type	Specifications	Applications
1. Column	<ul style="list-style-type: none"> - High accuracy - Convenient access for the operator. 	<ul style="list-style-type: none"> - Universal applications - Small measuring volumes
2. Cantilever	<ul style="list-style-type: none"> - Lower accuracy compared to type 1. - Has relatively low movable masses. - Very Fast. - Allows excellent access to the measuring area 	<ul style="list-style-type: none"> - Large measuring ranges. - Called a measuring robot.
3. Bridge	<ul style="list-style-type: none"> - Most frequently used machine. - High accuracy. - Limited access to the measuring volume. <p style="margin-left: 40px;">This can be solved using an automatic feeder.</p>	<ul style="list-style-type: none"> - Medium and small size measuring volumes. (1 m³)
4. Gantry	<ul style="list-style-type: none"> - Reasonable accuracy. 	<ul style="list-style-type: none"> - Very large parts handling. (Up to 10 m Horizontally)

An example of the column structure is the FICA CMM (see Figure 2-3).

Examples of the bridge structure are the DEA Iota P (see Figure 2-4) and DEA Iota 1102 CMM (see Figure 1-1).

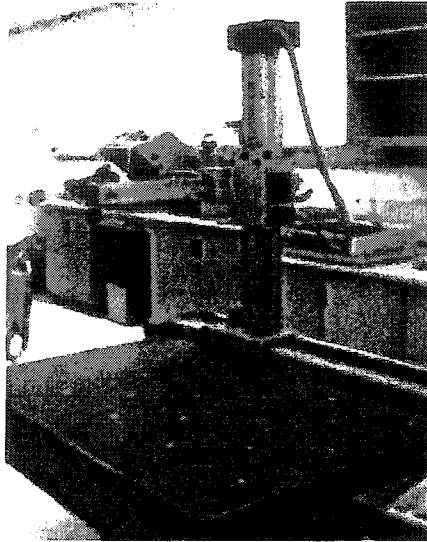


Figure 2-3 FICA Column Type CMM

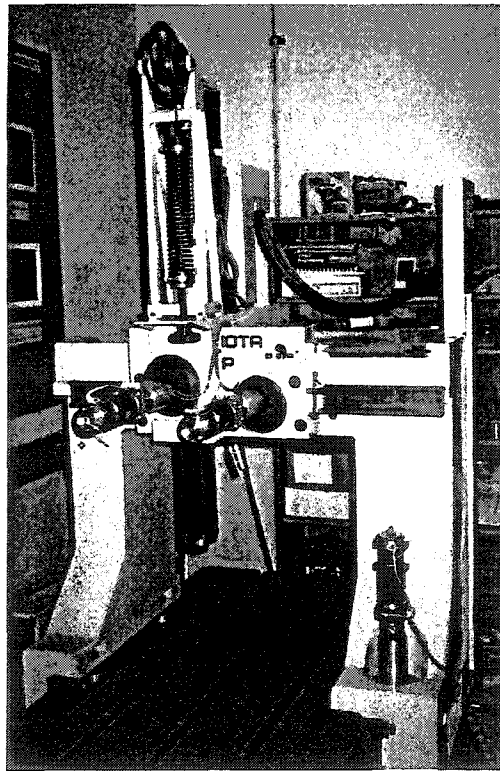


Figure 2-4 Iota P Bridge Type CMM

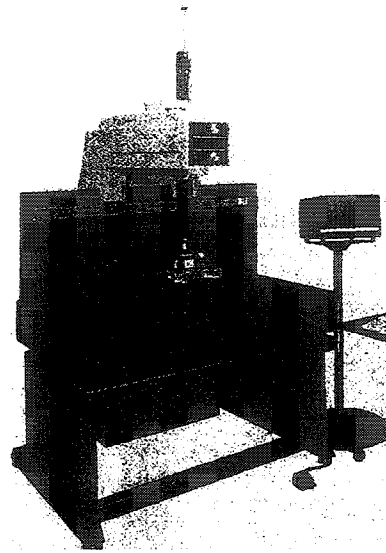


Figure 2-5 Cantilever Type CMM [Ni 1995]

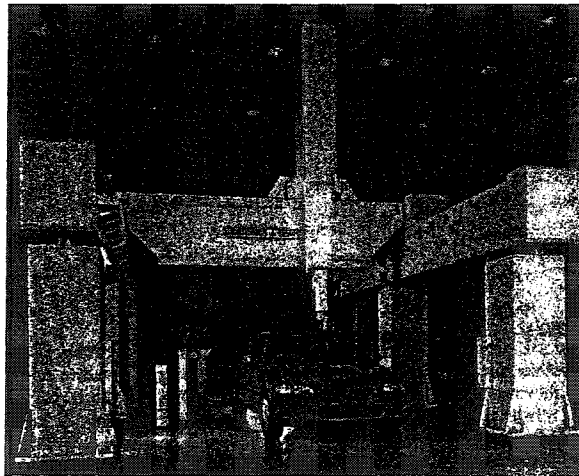


Figure 2-6 Gantry Type CMM [Ni 1995]

Although the cantilever structure is called a measuring robot, there is also interest in using industrial robots for measuring purposes. At AUDI Ingolstadt

(Germany) four RX130L robots measure both Audi A4 and A3 bodies offline in order to detect statistical trends at specific diagnostic points [Turner 2003]. (See Figure 2-7.)

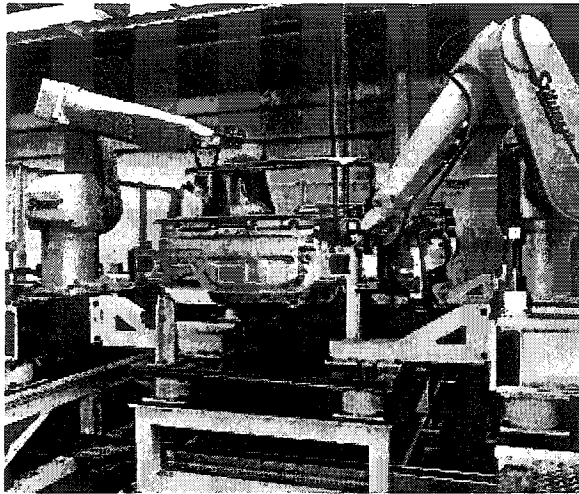


Figure 2-7 Industrial Measuring Robot [Turner 2003]

2.3. Probing

2.3.1. Touch Probes

CMMs utilise commercially available touch trigger probes. This is beneficial in the automation of the measurement process because touch trigger probes are self-guiding feedback control sensors for part search and measurement data collection. Using a touch trigger probe for measurements and sensing is a standard practice in industry. A touch trigger probe is a digital device that changes a signal state upon physical establishment or loss of contact with another object. It consists of a probe stylus connected to a deflection sensor that switches between the “1” and “0” states. Upon receipt of a change of signal

of the probe from "1" to "0" the controller can activate an interrupt routine to read the coordinates of the null origin of the probe. In a CMM, all axes position coordinates are read simultaneously.

Several probe path generation algorithms can be traced in the literature. Guidance of the probe can be accomplished using incremental velocity rotation on a "serpentine" path or by estimating the tangent to the part surface on a "saw-tooth" path. Advantages of one path over the other and related mathematics can be found in Jie-Chi [1982]. It is to be mentioned that the probing process contains random and systematic errors in the order of micrometers. Nawara and Kowalski [1984] studied the static and dynamic forces affecting the probe. Moreover, they reported some results regarding the effect of speed of probing and data transfer from the probe on the results collected. The probe was modelled and the deflections were calculated and compensated for in the tests conducted. Results reported suggest more deflection to occur than calculated due to dynamic forces.

2.3.2. Laser Digitizers Based On Triangulation

Laser scanning probes are ideal for non-contact measurement of soft materials. These probes use the principle of triangulation to measure variations in distance between the probe and the work piece. A beam of laser light is focussed on the surface being inspected. The light that is reflected from the surface is collected by a sensitive detector, such as a charge coupled device (CCD) camera, inside the probe. The location on the

CCD of the spot of reflected light indicates the angle of reflection and is used to infer the distance between the work piece and the probe.

A triangulation sensor estimates an object's distance based on a reflected ray of light, which becomes a spot on the CCD camera or other detector. Jalkio [1999] summarised the object properties that cause error in spot detection as:

- 1) Reflectivity variation
- 2) Surface microstructure
- 3) Specular reflections (a surface property)
- 4) Volumetric scattering
- 5) Step height changes
- 6) Steeply sloped and highly curved surfaces.

Feng [2001] and Xi [2001] did experiments characterising the error caused by angle of the laser beam to the normal of the scanned surface. They defined "incident angle" to be in the scan plane and "projected angle " to be perpendicular to the scan plane. They found a systematic error with a linear relationship to scan depth and each of the angles.

The International Association of CMM Manufacturers has started a working group to develop an Optical Sensor Interface Standard (OSIS). OSIS is an industry initiative with the aspiration to promote development and usage of optical metrology in combination with 3D coordinate measuring machines [IACMM 2003]. Complexity and high integration costs are the main reasons that prevent large-scale usage of optical sensors in combination with CMMs. The absence of available sensors and absence of

applicable standards for integrating those into CMM systems cause financial and technical risks for both suppliers and their customers. The OSIS integration model (see Figure 2-8) shows the principal function blocks of a coordinate measuring machine with an integrated optical sensor. This is neither a pure physical nor a pure logical system layout but a mixture of both to show what interfaces exist.

The primary differences between a touch trigger probe equipped CMM and a laser digitizer equipped CMM is that the touch trigger probe error compensation is directly implemented in the motion controller, but the laser digitizer is not similarly integrated. Furthermore, whereas touch trigger probes collect a single point at a time, a laser digitizer scans a curve in a plane. This introduces a new requirement to extend the touch trigger probe error compensation procedure to explicitly include the scan plane orientation information.

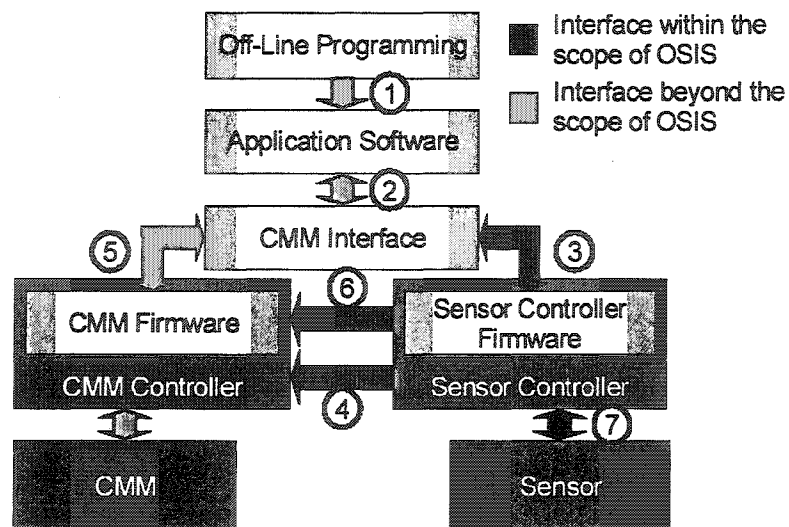


Figure 2-8 OSIS Integration Model [IACMM 2003]

2.4. Accuracy And Precision Machining

There are many similarities between CMMs and machining centres. As such there is much literature which is applicable to improving the accuracy of both. The cutting process and the inspection stage are closely tied in accuracy requirements. To improve the cutting process accuracy, five-axis machining centres have been introduced to industry. Some of the major advantages of five-axis machining are the higher accuracy in cutting, higher metal removal rates, ability to handle complex surfaces using standard tools and the improved surface finish.

To evaluate the results of processed parts according to high precision standards, an inspection station is often located at another section of the production line. This inspection station contains a standard piece of equipment in today's factory, which is the CMM. Precision engineering links CMMs and cutting centres in the accuracy issue as a common interest. The error types and sources occurring in both and the solutions developed by the research community can be exchangeable to a certain limit. An example of these limits is errors such as those due to temperature changes. In CMMs, no cutting process heat is involved and minimum internal heat is generated. This is the kind of difference that has to be considered when exchanging studies between the two modules [Bryan 1990].

2.5. Sources Of Errors

Scarr [1967] divides errors into two categories, controllable and random.

Controllable errors are such things as:

- 1) Calibration errors.
- 2) Ambient conditions.
- 3) Stylus pressure.
- 4) Parallax in reading measuring instruments.

Random errors can be detected by the fact that repeated measurement of a workpiece would produce results that deviate slightly from one another. These are best evaluated by statistical means and application of the least squares principle.

2.5.1. Errors In CMMs

Measurement inaccuracy occurs when an error exists in the relative position between the measured point and the probe [Eman 1987]. In other words, measurement error is the difference between the true value and the observed value of a variable [Shen 1991].

Every error affecting a CMM has a systematic and a random component [Kunzmann 1983] [Shen 1991]. An example of systematic errors is link geometry related errors that are time invariant and repeatable. Therefore, they are considered to be part of the systematic error component. This part can be calculated using error models developed for the machine [Eman 1987] [Duffie 1985] [Treib 1987].

An example of the random error component is link motion related error because it is non-repeatable. This is known in some literature as the precision error [Shen 1991]. Eman *et al.* [1987] suggested the use of average values of the random error to calculate the CMM accuracy. Nawara and Kowalski [1987] analysed the random component of a CMM position error. They suggested statistical methods to obtain the random error and calculate their distribution and standard deviation. They also demonstrated experimentally the inverse proportional relation between the random error component and the number of data points collected for a circular profile. The use of statistical methods to handle the random error component is also reported by Shen [1991].

Errors can be generated by different sources. Some researchers reported a reduction in measurement accuracy by the increase of measuring speed [Knapp 1988] [Nawara 1984]. Others developed methods to calculate the uncertainty in the use of a Homogeneous Transformation Matrix (HTM) [Shen 1991]. Errors, in general, can be divided into categories based on different criteria [Lau 1984].

The following sections list errors divided according to the difference in physical cause [Weekers 1995].

2.5.1.1. Quasi Static Errors

These are defined as errors of relative position that are varying slowly in time and are related to the structure of the machine. These errors contribute to more than 70% of the machine errors [Eman 1987]. They include:

1) Geometric error

This error is inherent in the manufacture of the machine and can be found by the measurement of squareness, straightness, flatness, and angular motion errors. A practical way of performing these measurements can be found in the literature [Kunzmann 1995] and Table 5. This error is caused mainly by the structural elements. Sources of geometric errors are:

- A) Accuracy of components (Manufacturing errors).
- B) Accuracy of components adjustment and alignment (Maintenance and installation).
- C) Measuring system errors.

Knapp [1983] demonstrated that a CMM could be tested using a circular profile for geometric errors. The recorded data can be analysed and some logical combinations can be used to find the main sources of geometric errors in the structure of the machine. The geometric error affects the machine repeatability and kinematic accuracy. It also is the direct measured error produced partially by other sources such as the thermal error.

2) Stiffness error

This error can originate from the following sources:

- A) Assumption of infinite stiffness, which is not valid in all cases. This error has been investigated and a finite stiffness of some machine components has been reported. This causes a limitation and an error to the modelling methodology of that machines error [Teeuwsen 1989] [Ferreira 1986] [Weekers 1995].
- B) Weight of components in the structure, especially moving ones.
- C) Configuration of components.

3) Kinematic error

This is the error appearing in the ability of the CMM to reach the exact specified position by the controller. It is related to the commanded motion of the machine. Nawara *et al.* [1989] studied kinematic error modelling and calculation in a CMM. They presented results showing the effect of change of position and measured profile on kinematic errors. They also discussed the effect of both systematic and random components of kinematic errors. Position of machine slides, gears, ball screws, couplers, motors, and controllers contribute to this error. In addition, hysteresis or backlash in these elements affect this error and consequently make it a function of motion direction [Srivastava 1995].

4) Thermal error

Thermal errors are explained further in section 2.10 Thermal Errors. They are a major cause of error [Scarr 1967] and because of their great importance there is a large base of literature specifically on this issue. In machining centres, thermal errors account for 60 to 70% of error [Bryan 1990].

2.5.1.2. Dynamic Errors

This is the collection of errors that causes dynamic instability of the CMM [Weekers 1995]. It is caused by factors like excessive play or preload in the joints and gears, structural flexibility, and external excitation forces. Medium to high frequency vibrations of relatively high amplitudes are typically the signs of this error group. These vibrations are often at well-defined frequencies [Lau 1984]. This group includes the following error types and sources:

1) Acceleration errors

Acceleration errors are those which are due to part movement and consequently develop forces on the structure that can lead to deformation. These have a greater effect on accuracy when the sensor is far away from the axes scales.

2) Vibration errors

This can be of two types: self induced and forced. Nijs *et al.* [1988] suggested that the amplitude of vibrations by CMMs in response to excitations has to be low because substantial amplitude of resonance vibrations can cause severe loss of accuracy. He proposed a method based on the Lagrange energy equation and Guyan reduction to estimate the dynamic behaviour of a CMM machine and henceforth optimise its dynamic response before constructing the prototype. On the other hand, he did not propose any solution to the problem, only a method for analysis prior to construction.

3) Control errors

Effects of errors related to the controller show mainly as quasi-static errors when measured, although the cause is classified as dynamic. An unstable controller design or changes in the CMM parameters (e.g., payload, speed of operation, extra hysteresis, etc.) which are not accounted for by the controller can cause such errors.

4) Distributed force errors

This source includes forces exerted by the measuring system on the measured piece. Deformation resulting from these forces contributes to the total error of the machine [Zhang 1991].

5) CMM structural property errors

These include: mass distribution, component stiffness, and damping characteristics.

2.5.1.3. Software Induced Errors

This is caused by software packages. One example of a software error is a simple "bug" or programmer error. Another error could be a loss of accuracy due to the fixed memory size of numbers stored inside the computer; numbers should be normalised from measured coordinates before feature calculations are performed. These errors can be detected using what is known as the "black box test". Peggs and McKeown [1989] concluded that the black box testing technique is the only practical method of evaluating the performance of geometrical element assessment software. They found when testing

software, available in the market for CMMs, that some results were not satisfactory in one or more aspects.

2.6. CMM Calibration Standards

Calibration is knowing the error behaviour of a measuring instrument for all types of configurations of the instrument and all cases of application intended. Calibration is the method metrologists use to investigate measuring aspects of instrument precision. It is based on the idea of a reference workpiece of sufficient stability. Each time measurements are taken, possibly in different orientations and positions, the same geometry of that workpiece is observed. The literature includes many reports on calibration tests and methods of operating CMMs.

Today, there are three primary standards used to verify the accuracy of measuring machine performance: ASME B89.4.1 [1997], VDI/VDE 2617 [1989], and ISO 10360 [2000].

Table 4 Comparison Of CMM Performance Standards

	B89.4.1	VDI/VDE 2617	ISO 10360
No. of Tests	5	3	1 for volumetric length 1 for probe uncertainty
Specification	Single Number a mm/b mm	Formula $U3 = a + b \frac{L}{1000}$	Formula $E = A + \frac{L}{K}$ R = R
	a = maximum error measured at any position. b = length of ball-bar used.	a = basic error. bL = error dependent on length of ballbar used.	A = systemic uncertainty (mm) L = length measurement uncertainty (mm) K = length constant R = Probe uncertainty.
Test Environment	Non-specific	Manufacturer Specific	Manufacturer Specific

	B89.4.1	VDI/VDE 2617	ISO 10360
Standard-Specific Tests	Tests for Multiple probe tips. Laser diagonal measurements. Duplex performance. Heavy workpiece performance. Rotary Tables.	Block Method. Ball Plates. Ring Gauges. Rotary Tables.	Numerous extensions in committee draft form being balloted upon.

2.6.1. ASME B89

The ASME B89.4.1 standard [1997] uses five tests to evaluate length-measuring performance. B89 specifications use a single number to represent a performance range.

The basic test of CMM performance under the B89 standard includes five measurements:

- 1) Multiple measurements of the position of a fixed ball. The range is the repeatability of the machine.
- 2) Measurements with a step gauge or laser in each axial direction. This is the linear accuracy of the machine.
- 3) Measurements of a ballbar at multiple positions and orientations in the machine working volume. This is the volumetric performance of the machine.
- 4) Measurement of the ballbar in four diagonal positions in vertical planes. In each position, the ballbar is measured with two right angle probe offsets and the difference of measured lengths is determined. The differences are compared with an offset probe performance specification. The test is sensitive to Z axis probe offset errors. This is important when using the probe at right angles to the Z axis, such as with indexing probes.
- 5) Measurement of length of a short gauge block in four orientations. The measurement is compared with a bi-directional accuracy measuring capability specification. This test is sensitive to probe qualification errors.

B89 volumetric performance is specified as "a" mm/"b" mm, the number after the slash being the length of the ballbar that was measured. This means that the range of measured lengths with the ballbar in many positions is no greater than "a" millimetres.

2.6.2. VDI/VDE 2617

VDI/VDE 2617 [1989] uses three tests. Measurements made on a calibrated step gauge, or an equivalent set of gauge blocks. The gauge is measured in three types of

positions: axial (U1), planar (U2), and volumetric (U3). Differences between the measured lengths and the calibrated lengths of the gauge are compared in the formula

$U = a + b \times \frac{L}{1000}$. The "a" term is a value representing the error made when measuring

something of zero length. The "b" and "L" terms divided by 1,000 represent the increase in error based on the length being measured. The formula represents a line that for zero measured length is the "a" value, and goes up by a slope defined by the "b" term.

2.6.3. ISO 10360 And ISO 14253

At the heart of the ISO 10360 standard [2000] is the reliance on certified artefacts that by definition reproduce known values of a determined quantity. The artefacts utilised by the standard may include a series of gauge blocks, step gauges and a precision sphere.

It is recommended that the longest standard be at least 66% of the longest measuring volume diagonal and that the shortest be no longer than 30 mm. The artefact used should not have a length uncertainty of greater than 20% of the CMM manufacturer's stated volumetric length uncertainty.

To verify the CMM's volumetric length measuring uncertainty a series of gauge blocks or a step gauge is utilised. The user selects 7 different locations (position and direction) within the machine measuring volume for the test. For each location five material standards (lengths) are measured, three times each, for a total of 105 measurements. All 105 measurement results (100%) must be within the stated tolerance specified by the manufacturer.

The measurement approach is the same as for the VDI/VDE standard, but the formula is changed to $E = a + L/k$ where "k" is the "b" value for the VDI/VDE formula divided into 1,000. There are no individual axial and planar specifications; they are included in the volumetric "E" specification.

There are two general uncertainties associated with the ISO standard; the first is the volumetric length measurement uncertainty (E) and the second is the probing uncertainty (R).

To verify the CMMs probing uncertainty a precision sphere is utilised. The sphere is required to be between 10 mm and 50 mm in diameter with certification for form and diameter. The test consists of measuring 25 equally spaced points on the sphere's hemisphere. R is computed by adding the absolute values of the minimum and maximum deviation from the radial form. This result is typically reported in micrometers (μm). All 25 probed points (100%) must be used in the calculation.

ISO 14253 [1998] establishes the rules for quantifying the uncertainty when determining the characteristics of a specific measuring equipment, taking into account the uncertainty of measurement. The CMM shall be operated using the procedures given in the manufacturer's operating manual when conducting the tests. Specific areas in this manual to be adhered to are, for example: machine start up/warm up cycles and probing system qualification.

Kunzmann and Waldele [1988] concluded that the most important element in CMM calibration conception is the theoretical model of the mechanical system. This model describes the interaction between the parts of the system and is the base for error

propagation computation and for the overall accuracy description of the task. Calibration of a CMM with a rotary table can be found in the work of Kunzmann and Waldele [1988]. Zhang *et al.* [1991] developed a calibration method using a ballbar and a laser interferometer. They aimed to develop an approach that is inexpensive and simple enough to be used on a shop floor.

2.6.4. Other

Ball plate evaluations have been used in round robin testing in Europe [Kunzmann 1995], and North America [Caskey 1997] to determine the consistency of calibration of various CMMs.

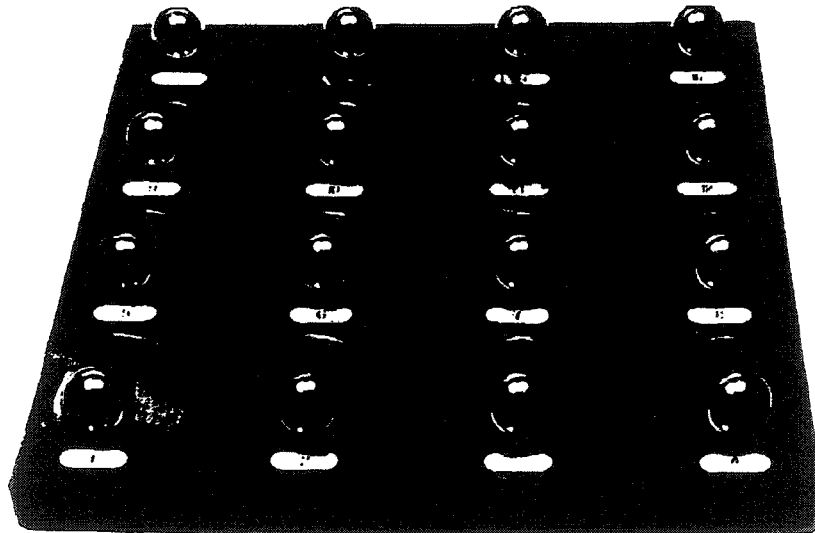


Figure 2-9 Ball Plate Used In Round Robin Testing [Caskey 1997]

Ball plates are very popular in CMM calibration as a workpiece. The centrelines of the balls are coordinates that have to be measured by the CMM in different orientations. Gauge blocks and end bars are also used for CMM calibration.

Peggs [1989] described different ways of utilising step gauges in CMM calibration using laser interferometers. In addition, he elaborated on the calibration of one, two and three-dimensional artefacts and its importance and uses. Kunzmann *et al.* [1995] presented a comparison of calibration between commercially available CMMs using ball plates. He also discussed a methodology to follow in calibration and error analysis to find the sources. A state of the art formula for uncertainty in measurement calculation was also given in his study based on ball plate measurements. This formula is $u = 0.8\mu\text{m} + 1.1 \times 10^{-6}L$ where L is the distance in metres between arbitrary ball centres of the plate and u is the uncertainty of arbitrary distances between ball centres.

2.7. Integration With CAD/CAM

On a system with scanning capability, the CMM probing path usually must be generated manually. For example, a digitizer CMM will need at a minimum a start point, direction to scan and a stop point [Millett 1999]. Following the measurement of a profile, the actual data collected must be compared to the nominal geometry to determine the actual profile value and the deviations of each point to the nominal. Due to the limited field of view of a digitizer, several passes may be required to collect data over the entire profile surface. Each scan piece needs to be as accurate as possible to provide a composite measurement.

Ainsworth *et al.* [2000] say that registration, which establishes the relation between the CMM coordinate frame and that of the CAD model, poses considerable difficulties because free-form objects generally do not possess clearly identifiable

reference features. The most popular method of refining a given registration is the iterative closest point (ICP) algorithm [Besl 1992]. It is based on two overlapping data sets and various extensions to the algorithm have been suggested to extend its applicability [Eggert 1998] [Turk 1994]. The available measurement packages, such as Imageware [EDS 2000], prescribe the registration procedure to be performed on the basis of adequately compensated measurement data. However, since accurate compensation requires accurate registration as prerequisite, considerable errors may be introduced at this stage.

2.8. Measurement And Modelling Of Errors

Error identification techniques in CMMs and machining centres have been widely addressed in the literature. There are few references dealing with laser digitizers.

Typically, the linear, straightness, and angular errors of a CMM are obtained using a laser interferometer. All CMM axes are initially located at a home position that can repeatedly be returned to. At this position, the error terms are set to zero. Optics appropriate to the error term being measured are attached at the sensor mounting location, and the axis is translated in regular steps. At each step, the CMM scale positions, and the laser interferometer error measurement, are recorded. Roll errors are obtained using digital levels. Squareness errors are obtained using a ballbar. All of this information is recorded within the CMM motion controller using an error map similar to that shown in Appendix B. Okafor and Ertekin [2001] give a good description of the procedure. In all cases, the measured angles are plane angles, and a small angle assumption is made.

During operation, the scale position is used with the error information to correct the actual probe mounting location in three-dimensional space.

This technique is often used with contact probes, which are well integrated with the CMM controller. The error compensation is extended to the actual probe tip position. As a result, much improved part coordinate data is obtained during inspection. For the laboratory CMM, the geometric error was reduced from 200 μm to 20 μm over the working volume [Spence 2000].

2.8.1. CMM Modelling And Error Description

Modelling a CMM is important to establish a generalised framework that facilitates a systematic approach to the analysis of errors and the subsequent assessment of their influence on the overall accuracy of a multi-axis machine. Modelling leads to relating the sources of error in the individual motion and structural components to the error between the tool and workpiece. Analytical and empirical models are generally difficult to obtain because of the large number of influencing variables and complex inter-dependencies. Therefore, they have to be built over restricted domains, which are increased by periodic updating [Ferreira 1986].

The most powerful modelling method under accuracy aspects is the one that assumes that the components of the CMM are rigid bodies. The position error of a carriage can be described by three displacement errors and three rotational errors parallel to the axes and about the axes respectively. These six errors can be measured separately for each of the three carriages, as they are independent of the others. A total of 18 path

dependent errors and three squareness errors can be measured and treated in the model. A rotary table addition would add six more errors to be measured [Kunzmann 1995].

Table 5 summarises the methods suggested in the literature to obtain the different machine error components experimentally [Kunzmann 1988] [Zhang 1985].

Table 5 Measuring Methods For Error Components

Error Component	Measuring Method
Rectangularity	Straightness measurement in two rectangular lines, test bodies.
Straightness	Reversal method with straight edge.
Positioning	Laser interferometer or Capacitive probe.
Squareness	Along diagonals displacement errors.
Pitch, Yaw	Laser interferometer with angular reflector
Roll of X and Y axes	Level
Roll of Z axis	Straightness measurement in two parallel distant lines.

An inexpensive, multi-purpose, and quick method is required for CMM calibration and machine accuracy inspection. Kunzmann *et al.* [1995] described the ideal method for CMM calibration and inspection as having the following properties:

1. Traceability according to standards for stable reference objects.
2. Accuracy which is similar to the CMM global standards.
3. A uniform approach in concept, allowing the use of the same hardware and software for calibration and inspection.
4. Quality parameters should be the same for all inspection, periodic tests, and calibrations to allow for the deduction of application measurement uncertainty.
5. Compatibility with existing standards.
6. Affordability by CMM users.

In general, calibration methods of CMMs can be categorised into three groups:

- A. Methods based on measuring the 21 source errors. These methods require the use of expensive instruments including laser interferometers.
- B. Methods based on measuring certain artefacts, which are used as references for calibration. These methods do not give the source errors and so can not be used for compensation. This is in addition to the cost of building the accurate artefacts.
- C. Methods based on kinematic references (e.g., the magnetic ballbar). These also have the problem of not defining the source errors and are not very useful for compensation.

Choosing any of the methods above would involve a compromise that has to be calculated by the user.

For some time, the research community has been concentrating on a measuring standard to evaluate machining and measuring accuracy. This is useful in the precision evaluation of both the machining centre and the CMM performing the inspection on the

workpiece. Inspection works with methods similar to those used for CMM calibration [Kunzmann 1995]. Inspection methods include the use of gauge blocks, ball plates, and ballbars, which are the same standards used for calibration. Iwata *et al.* [1982] listed some of the CMM disadvantages in measuring functional items like cam profiles and waviness. He suggested a modular-type measuring system for the evaluation of the machining accuracy using "the part family" concept to classify the required measurements. The rotary table was a major part in his suggested module. Other investigations on these types of errors have been reported in the literature [Nawara 1981] [Kunzmann 1983].

Since CMMs are used in contouring mode, where two or more axes move simultaneously, positioning accuracy is not enough as an acceptance test of a CMM [Knapp 1988]. In general, volumetric accuracy is described by systematic deviations in the relative location of the probe for two arbitrary positions of the machine carriages. A considerable amount of geometrical and thermal quantities has to be measured to determine the volumetric accuracy of a CMM. Teeuwsen *et al.* [1989] summarise the specifications according to which measurements should be carried out:

- 1) Spacing between measured positions should be sufficiently small. This is to obtain information about the periodic terms in the measuring system.
- 2) The measured positions have to be approached from two opposite directions. This is necessary to find the backlash effects. This is only applicable when the position is measured using an encoder on the drive motor shaft. When the position is measured

using a linear scale directly mounted on the CMM structure, the position read is independent of direction of approach.

- 3) Multiple measurements have to be carried out to obtain good estimation of the measurements, especially in the case where random vibrations occur.

They also suggest a method to perform automated and fast inspection of a CMM employing laser interferometers. A laser interferometer can also be incorporated in the feedback loop of the CMM.

This method has already been applied to CMM modelling in the literature and link geometry and motion errors have been identified [Zhang 1985]. Other modelling methods which compare the different types of errors inherent in a CMM can be found in the literature. These methods include:

- 1) The application of analytic geometry to arrive at an expression for the geometric errors.
- 2) Vector representation utilisation to obtain an expression for the error vector.
- 3) Error matrices calculation where the error vector components at different locations in the machine working volume are stored for various loading and thermal conditions [Zhang 1985].

Nevertheless, the first method described provides a simple error model formulation for an arbitrary machine configuration. The other methods also lead to an error model, but lack formalism. Other modelling methods are reported in the literature. Belforte *et al.* [1987] presented a general model of a CMM based on parametric functions and a simulation program of the model. This model is based on a combination of

assumptions and hypotheses. The simulation output is an estimation of the CMM reading that is used to calculate the machine error and compensate for it.

The rigid body assumption method based on the HTM includes assumptions, which impose restrictions on the model accuracy, according to some researchers [Teeuwsen 1989] [Ferreira 1986]. These assumptions are: 1) rigid body kinematics, 2) approximation of differential errors (e.g., $\cos \theta \approx 1$, $\sin \theta \approx \theta$, when θ is small), 3) first and second orders terms of the error equations are considered only and higher order terms are neglected, and 4) linear temperature effects on the machine [Teeuwsen 1989].

Teeuwsen *et al.* [1989] incorporated a set of five stiffness parameters in the HTM based model to describe the static deformation effect on the CMM. This is a counter-measure to the first assumption above. They suggested the elimination of the stiffness parameters only if suitable measurements are performed. They also proved that for a specific machine these parameters are not negligible. On the other hand, some machines do have components with stiffness parameters that can be considered rigid [Zhang 1985]. Moreover, to account for the fourth assumption above, they introduced another set of thermal parameters to the mathematical model [Teeuwsen 1989]. In all cases, the model has to be reasonably simplified by means of suitable assumptions. This results in having to compromise between cost and accuracy required (i.e., the less complicated the model the faster its calculation. However, the trade-off is typically with accuracy [Balsamo 1990].

2.8.2. Use Of Homogeneous Transformation Matrix

This methodology is based on the Homogeneous Transformation Matrices (HTM) and the rigid body kinematics assumption [Paul 1982] [Craig 1989].

Modelling techniques can also be divided into direct modelling techniques like the HTM kinematic model or indirect modelling techniques like the linear regression estimation. Although both models provide good tools for relating the error between the tool and the workpiece to the axes of motion, the later (indirect techniques) have more limitations and require more computation time.

Srivastava *et al* [1995] used the HTM model combined with the small angle approach to model geometrical and thermal errors of a five axes milling machine. A compensation strategy using neural networks was based later on this methodology [Veldhuis 1995].

2.9. Error Reduction

Improvement in the accuracy of a machine can be achieved by two means. One of them is error avoidance, or eliminating the source of error, and is a design problem controlled by the structure and manufacture of the machine. The other method of error reduction is error compensation, which involves defining a model of the error and cancelling the effects of the predicted error. This is done by software and control schemes.

Using environmentally controlled rooms for measuring equipment can minimise thermal effects. The standard conditions are 20 °C, 760 mm Hg barometric pressure, and 10 mm Hg water vapour pressure (55 % RH) [Scarr 1967].

2.9.1. Changes To CMM Structure

According to Kunzmann [1988], better quality control in the manufacture of a machine reduced the geometric errors significantly. Use of improved gears and ball screws reduced their contribution to kinematic errors. Work has been done on minimising thermally caused errors by careful selection of the materials used for the CMM structure. By implementing a thermally symmetrical configuration, a structure is capable of thermal expansion without developing a bending (Abbe error) deformation [Ogura 1995].

In general, error avoidance can be achieved by the following measures:

- 1) Improvement of structure design.
- 2) Improvement of heat distribution by circulation of thermally conditioned fluids (for machining centres).
- 3) Improvement in external heat sources by placing the machine in a thermally controlled environment. [Weck 1995]

2.9.2. Software Compensation Of Measurements

As for the design problem, according to Kunzmann and Waldele [1988] the treatment of all measured errors can be of two types: 1) improvement of the accuracy by numerical error correction, and 2) computation of measurement uncertainty. Other issues

affecting the machine accuracy such as the trade-off between accuracy and speed in measurement modules has also been addressed in the literature [Weekers 1995]. Yonezawa *et al.* [1990] simulated and designed a high precision table to demonstrate this principle.

Because of the fact that position measurement (based on only distance information) is more accurate than that based on distance and angle information, methods of position measurement by means of laser interferometers based on distance data only are proposed in the literature. Nakamura *et al.* [1991] developed a coordinate measuring system based on this idea. Although their system gives more accurate figures than the regular available ones, it still needs more investigation to be error proof and applicable.

Weekers and Schellekens [1995] developed a method to assess the dynamic errors in a CMM due to carriage motion. The method includes measuring the major joint deflections due to accelerations with position sensors. The influence of these errors on the probe position is calculated by means of a kinematic model of the machine.

Laser interferometers are popular for assessing and calibrating the accuracy of machine tools and CMMs. A calibration method using a laser interferometer is reported by Lingard *et al.* [1991]. This method is quick and minimises thermal effects due to the handling of standard parts. A typical CMM should have specifications that can be summarised by the following: [Weekers 1995]

- 1) High manufacturing and adjusting accuracy.
- 2) High component stiffness and low mass.
- 3) Temperature conditioned environment and small internal heat sources.
- 4) Vibration isolation and small movements during probing.

Software compensation for CMM errors is not a replacement for design consideration related to errors, especially the thermal error [Bryan 1990] [Balsamo 1990]. This is because for software correction to be effective, the following points have to be considered:

- 1) It is impossible to get a perfect model or a completely general one.
- 2) Correction can be achieved for a small range of error; the larger correction comes from machine proper design.

If first order errors are large, second order errors also grow. These are commonly ignored for simplicity, but can be significant. Nevertheless, compensation for errors gains its importance because design and operating specifications are either difficult to implement or contradicting. Moreover, dynamic errors are random and not systematic, so they are not easy to calculate and account for.

Compensation for error correction has the following advantages [Teeuwssen 1989]:

- 1) Cost reduction of error correction and avoidance.
- 2) Increase in machine accuracy to its level of resolution.

Another advantage of numerical correction of errors is that it is based on the models developed for describing the machine errors so it indirectly represents a test of the value of these models.

2.10. Thermal Errors

Thermal error effects in machining and measuring accuracy is one of the most addressed problems in precision engineering and machining accuracy literature. For many years, thermal effects have been the largest single source of dimensional errors and equipment non-repeatability. Thermal error variation has a complex non-linear nature, which makes it difficult to handle. Bryan [1990] divided the overall thermal problem into two major categories:

- 1) The effect of uniform temperatures other than 20 °C.
- 2) The effect of non-uniform temperatures.

Thermal error effect on the CMM accuracy has been widely addressed [Peggs 1989] [Danzer 1987] [Lau 1984] [Srivastava 1995] [Zhang 1985]. This error is considered as a component in the random part of the total error. It shows as a difference in the readings of the CMM, or a geometrical size difference in the workpiece for the case of machining. The thermal error has a clear importance. According to Bryan [1990], all the systematic solutions suggested for the thermal error problem fall into three categories:

- 1) Control of heat flows into the system.
- 2) Redesign of the frame and scale to reduce their sensitivity to heat flows.
- 3) Compensation through controlled relative motions among the frame or scale.

The most widely used sensors in measuring temperature variation are thermocouples. Veldhuis [1995] used type E thermocouples to measure temperature changes in a five axes machine, based on recommendations by Attia and Kops [1993]. The main qualities of type E thermocouples are its low thermal conductivity and having the highest output level, and hence greater noise immunity.

Focusing on thermal errors, attempts to compensate for errors by software are presented by Zhang *et al.* [1985] and Balsamo *et al.* [1990]. Zhang used an error matrix model to obtain thermal errors in different points of the work volume. In addition, the HTM model was used to compensate for geometric errors. A simple thermal model was developed and a factor called "effective coefficient of expansion" was used to find the error and compensate for it. Bryan [1990] discusses this coefficient in detail.

2.11. Summary

The CMM is a ubiquitous measurement tool. Traditional CMM structures are well documented and there are several methods of determining the errors associated with them. The effects of thermal errors are also well documented, and recognised as one of the main difficulties in obtaining accurate measurements.

The use of a laser digitizer is beneficial in several applications where non-contact measurement is required or where large quantities of measured points are needed.

The ICP method of combining data with registration problems is appropriate for scans of pictures or sculptures, but higher data collection accuracy is needed for combining several scans to be used for quality assurance or reverse engineering.

Chapter 3

CMM Error Mapping

For any structure of CMM, such as moving bridge or horizontal arm, it is possible to create a geometric model of the CMM showing the relationship of each axis carriage to the end position of the measurement transducer [Sartori 1995].

A traditional coordinate measuring machine has three carriages mounted in orthogonal directions, providing a Cartesian coordinate system. The case presented here is a moving bridge XYZ kinematic CMM. (See Figure 3-1.) The X carriage is a bridge mounted on the table, the Y carriage is mounted on the bridge and the Z carriage is mounted on the ram.

3.1. Geometric Component Errors

Geometric component errors, also called parametric errors, are the fundamental error motions of the machine described relative to some coordinate system. The ASME B5.54 standard [1992] defines parametric errors as "... any of the geometrical error terms of a machine. These include, for example, angular errors, straightness errors, spindle errors, and alignment errors such as parallelism and squareness." Parametric errors are often referred to as geometric or kinematic errors. Each axis or carriage has six inherent error sources, position in three dimensions and rotations about three axes. (See Figure 3-2.) Each joint (linear axis) on a machine is intended to have a single degree of

controlled freedom. In actuality there are 5 additional unintended freedoms that exist for each axis as well as the error of the controlled freedom. These 6 unwanted error motions can be caused by many sources: imperfections in the axis mechanical components, feedback sensor error, thermal expansion, etc. The notation used is given in Figure 3-2 and Table 6. The angular error motions are often called roll, pitch, and yaw but the use of this terminology is not consistent between different authors and has been avoided in this thesis unless the specific axis of rotation has been also specified. The sign, or direction, of angular errors is defined to obey the right hand rule. This means that if your right hand is wrapped around the axis, with your thumb pointing in the positive direction of the axis, your fingers curl in the direction of positive angles. Squareness errors between the axes are also considered geometric component errors.

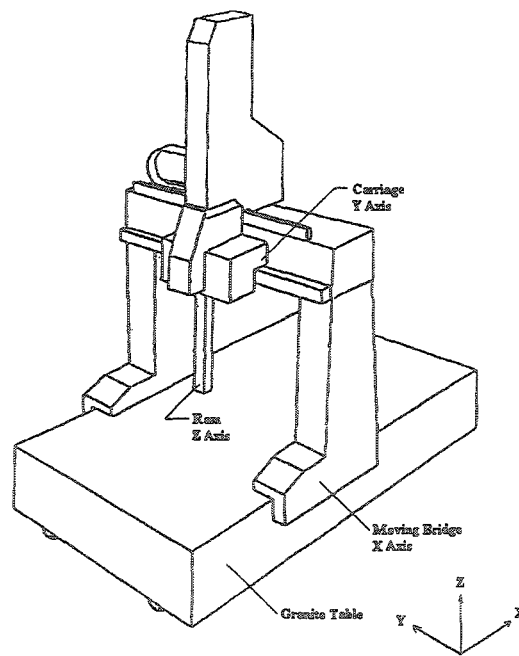


Figure 3-1 Moving Bridge CMM

Although the principles developed are general, the CMM discussed in this thesis is a moving bridge structure with an X-Y-Z kinematic chain. Experiments were done using a DEA model Iota 1102. The Iota 1102 has a working volume of X 900 mm, Y 600 mm, and Z 550 mm. The machine is equipped with an Omni-Tech OTC-5000 controller [Omni-Tech].

3.2. CMM Error Measurement

Any measured position has error associated with it,

$$[Pa] = [Pm] + [E] \dots\dots\dots (1)$$

where $[Pa] = [Xa \ Ya \ Za]^T$ is the actual or true position, $[Pm] = [Xm \ Ym \ Zm]^T$ is the measured position, and $[E] = [e_x \ e_y \ e_z]^T$ is the error.

To implement position error compensation on a three-axis machine, it is necessary to measure 21 geometric component errors, often called parametric errors, to calibrate its volumetric error. [Kunzmann 1995][Schultschick 1977]

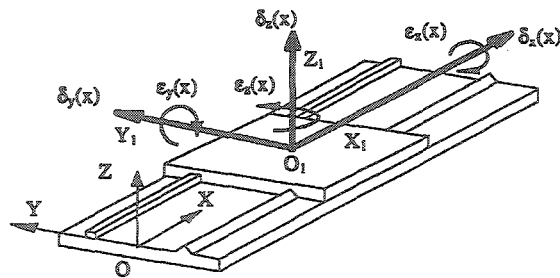


Figure 3-2 Six Degrees Of Freedom Error Motion

The kinematic error measurement technique used in section 3.2 is laser interferometry. Typically, the linear, straightness, and angular errors of a CMM are obtained using a laser interferometer. All CMM axes are initially located at a home position that can repeatably be returned to. At this position, the error terms are set to zero. Optics appropriate to the error term being measured are attached at the sensor mounting location, and the axis is translated in regular steps. At each step, the CMM scale positions, and the laser interferometer error measurement, are recorded. Roll errors, $\epsilon_x(x)$ and $\epsilon_y(y)$, are obtained using digital levels. Squareness errors are obtained using a ballbar. All of this information is recorded within the CMM motion controller. A good description of the procedure is given by Okafor and Ertekin [Okafor 2000-1] [Okafor 2000-2].

Other methods have been developed to obtain the 21 geometric component errors with other measurements [Chen 2001].

Table 6 21 Geometric Component Errors Of The CMM

<u>21 Geometric Component Errors of the CMM</u>	
$\delta_x(x)$	Position error in X direction along the X carriage (Linear or scale error)
$\delta_y(x)$	Position error in Y direction along the X carriage (Straightness error)
$\delta_z(x)$	Position error in Z direction along the X carriage (Straightness error)
$\epsilon_x(x)$	Rotation about the X axis along the X carriage (roll)
$\epsilon_y(x)$	Rotation about the Y axis along the X carriage (pitch)

<u>21 Geometric Component Errors of the CMM</u>	
$\epsilon_z(x)$	Rotation about the Z axis along the X carriage (yaw)
$\delta_x(y)$	Position error in X direction along the Y carriage (Straightness error)
$\delta_y(y)$	Position error in Y direction along the Y carriage (Linear or scale error)
$\delta_z(y)$	Position error in Z direction along the Y carriage (Straightness error)
$\epsilon_x(y)$	Rotation about the X axis along the Y carriage (pitch)
$\epsilon_y(y)$	Rotation about the Y axis along the Y carriage (roll)
$\epsilon_z(y)$	Rotation about the Z axis along the Y carriage (yaw)
$\delta_x(z)$	Position error in X direction along the Z carriage (Straightness error)
$\delta_y(z)$	Position error in Y direction along the Z carriage (Straightness error)
$\delta_z(z)$	Position error in Z direction along the Z carriage (Linear or scale error)
$\epsilon_x(z)$	Rotation about the X axis along the Z carriage (pitch)
$\epsilon_y(z)$	Rotation about the Y axis along the Z carriage (yaw)
$\epsilon_z(z)$	Rotation about the Z axis along the Z carriage (roll)
S_{XY}	Squareness error between the X and Y axes. Defined as 90° - the angle between the machine carriage axes.
S_{YZ}	Squareness error between the Y and Z axes
S_{ZX}	Squareness error between the Z and X axes

In all cases the measured angles are plane angles, and a small angle assumption is made:

$$\cos \theta \approx 1 \text{ and } \sin \theta \approx \theta.$$

3.2.1. Storing Error Measurements

There are several methods of storing corrections in computer memory. They are known as:

- 1) A volumetric error lattice for a large number of points spread throughout the workzone,
- 2) An error table or kinematic error map where errors are a function of axis position, or
- 3) A coefficient table where error functions are given in an analytic form [Sartori 1995] [Hocken 1977].

In this dissertation a kinematic error map is used with errors recorded every 25 mm along each axis. A sample error map is given in Appendix B.

During operation with a touch probe, the scale position is used with the error information to correct the actual probe mounting location in three-dimensional space. Because contact probes are well integrated with the CMM controller, this error compensation is extended to the actual probe tip position. As a result, much improved part coordinate data is obtained during inspection. For the laboratory CMM, the geometric error with a touch probe was reduced from 200 μm to 20 μm over the working volume [Spence 2000] when using a Denavit-Hartenberg model of the CMM. This work is different from a touch probe system in that it addresses the orientation of the plane of the transducer. By addressing the needs of an independent line scan system, it extends the concept beyond a hard point into the "field of view" space of a laser digitizer system. (See Figure 4-1 and Figure 4-2.) The new development is based on the error map of the CMM and includes the effect of a separate coordinate system for the sensor.

During operation with a laser digitizer, the scale position is obtained by a separate computer, which does not incorporate the error map nor the pose compensation described in chapter 5. The error compensation method described in this work involves post processing the digitizer data using scale readings, temperature readings, and the error map.

3.3. Error Measurement

An error map of the machine was measured using an HP/Renishaw laser interferometer and the technique previously mentioned [Okafor 2000-1] [Okafor 2000-2].

The laser interferometer system consists of four main units: (1) an HP laser head (see Figure 3-5) which uses a low-powered (1 mW) class II HeNe laser beam with a nominal wavelength of 0.633 μm and contains the detector; (2) a Renishaw linear optics kit including linear interferometer (see Figure 3-3) and retroreflector; (3) a weather station to measure air temperature, air humidity, air pressure and material temperature; and (4) an HP measurement display. The resolution for linear measurements was 0.1 μm . During set-up, the laser beam was aligned to the carriage motion to prevent dead path and cosine errors. Full beam strength was achieved over the entire axis travel during the measurements.

To obtain accurate results, laser interferometer readings must be corrected for the effects of air temperature, air humidity and air pressure on the refractive index of the medium (air), and the subsequent effect on the wavelength of the laser beam. This is automatically done in the HP Measurement Display unit using the information from the

attached weather station [Kneppers 1999]. Background information on the wavelength in air can be found in [Edlén 1966] [Birch 1993]. Because of the complicated dependencies of the refractive index of air on the composition and state of the air, assessing the uncertainty in measurements of length due to varying and correlated atmospheric temperature, pressure, and humidity conditions is complex. From [Kneppers 1999], the formula used by HP is

$$N = 0.3836391 \cdot P \cdot \left[\frac{1 + 10^6 \cdot P \cdot (0.817 - 0.0133 \cdot T)}{1 + 0.0036610 \cdot T} \right] - 3.033 \cdot 10^{-3} \cdot H \cdot e^{(0.057627 \cdot T)}$$

where N is $(n - 1) \cdot 10^6$ where n is the refractive index, P is the air pressure in mm Hg, T is the temperature in °C, and H is the relative humidity in percent.

For uncorrelated inputs, the combined uncertainty for $N = f(x_1, x_2, \dots, x_n)$ is calculated using: [ISO GUM 1995, equation 10].

$$\begin{aligned} u_N^2 &= \sum_{i=1}^n \left(\frac{\partial f}{\partial x_i} \right)^2 \cdot u_i^2 \\ &= (0.97 \cdot 10^{-6})^2 \cdot u_T^2 + (-0.38 \cdot 10^{-6})^2 \cdot u_P^2 + (0.01 \cdot 10^{-6})^2 \cdot u_H^2 \end{aligned}$$

where u_N is the uncertainty in N , u_i is the uncertainty in x_i , and u_N was evaluated at $T = 20$ °C, $P = 760$ mm Hg, and $H = 50$ % RH. From Kneppers [1999], a 1 PPM error in a measurement of length will result from a 1 °C change in air temperature, a 2.5 mm Hg change in air pressure, or an 80 % change in relative humidity (e.g., from 50% RH to 10% RH). During the experimental calibration procedure, this magnitude of air temperature and air pressure change, and a 10 % change in relative humidity (e.g., from

50% RH to 45% RH) is possible, and hence a reasonable estimate of the total laser interferometer calibration uncertainty is 2.5 PPM. The laser interferometer that was used includes a "weather station" that compensates for humidity, temperature, and barometric pressure. For interferometers, keeping the weather station calibration is an important issue. The company that loaned the interferometer (Omni-Tech) is ISO 17025 certified by the American Association for Laboratory Accreditation (A2LA) (the US equivalent of the Standards Council of Canada) through Mitutoyo to perform CMM calibrations, and hence they keep their equipment calibrated. The manufacturer's specification for system accuracy with atmospheric compensation is 0.2 PPM.

For the measurement of angular errors, the linear interferometer optics were replaced by angular interferometer optics. (See Figure 3-4 and Figure 3-5.) The resolution for the angular measurements was 0.1 arc-second.

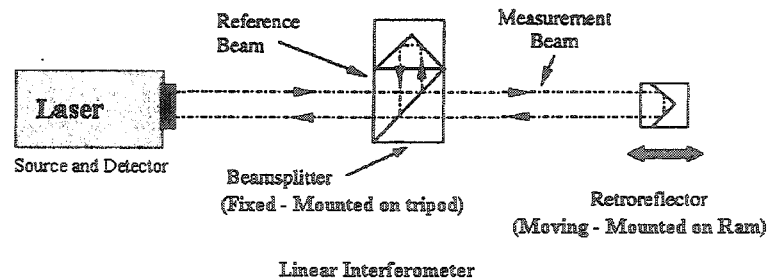


Figure 3-3 Optics To Measure Linearity Of Scales

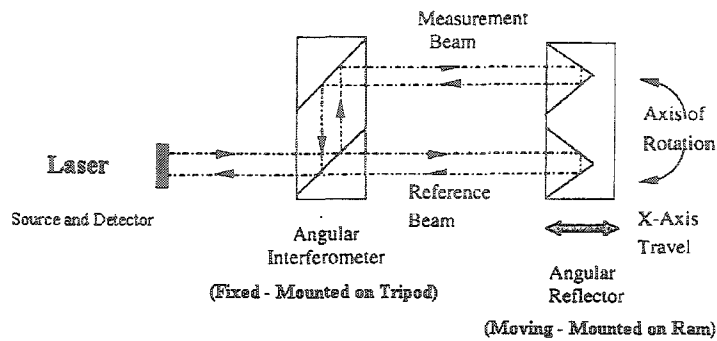


Figure 3-4 Optics To Measure Angular Errors

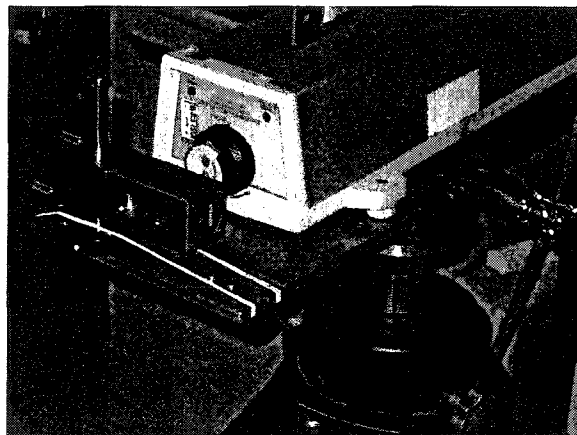


Figure 3-5 Laser Used To Measure Errors

Measurement of the Z axis errors require a turning mirror in the laser path, since the granite table prevents the interferometer laser beam from being lined up with the axis travel direction.

The initial set of error map testing was performed at an ambient temperature of 22 °C by a commercial CMM service contractor and is given in Appendix B. It may be noted that the roll error $\epsilon_i(i)$ was not measured and is recorded as 0 at all positions along

the scale i . This is typical in industry, and was the error map used for compensation. The assumption is that the planar angles measured are the solid angles of rotation and the two measured angles are sufficient to characterise the errors of the machine. To validate this assumption, a trial error map was made converting the two planar angle measurements into three solid angle values using five degrees of freedom. The compensated sphere centres using the modified error map were within $1 \mu\text{m}$ on a spatial basis ($S = \sqrt{X^2 + Y^2 + Z^2}$) for the 40 spheres measured in section 6.3.

3.4. CMM Error Map At Specific Temperatures

Every error affecting a CMM has a systematic and a random component. Bryan [1990] listed the thermal error components that contribute to its development as follows:

- 1) Uniform temperature changes.
- 2) Temperature gradients.
- 3) Machine structure and heat sources distribution.
- 4) Materials of components of the machine and their thermal properties.
- 5) Temperature distribution of the machine influenced by:
 - A) External sources: which is the environment effect including room temperature variation, exposure to sunlight, and use of a coolant in machining.
 - B) Internal sources: which result from the drives and internal heat sources like motors, amplifiers, circuitry, and slide friction.

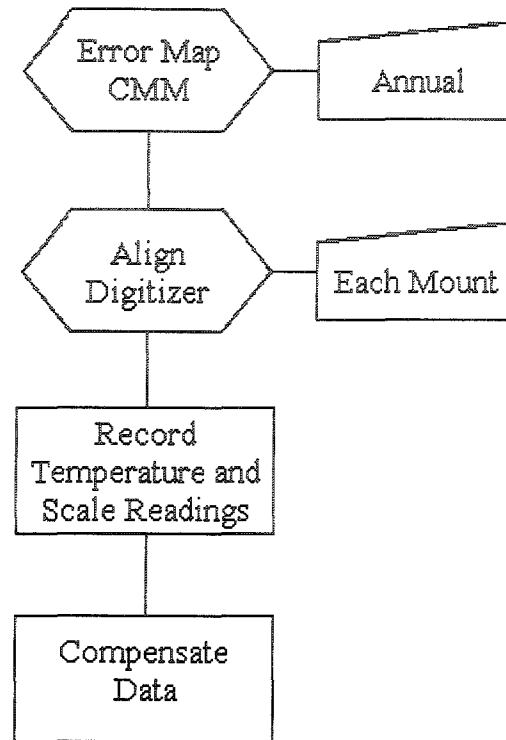


Figure 3-6 Error Map Measurements

This thesis examines the systematic error effect of uniform temperatures other than 20°C. For our experiments, circulating the air around the CMM reduced the effects of temperature gradients. The heat sources of a CMM are minimal when compared to the spindle of a milling machine. The laboratory had insulating panels on the window to eliminate exposure to sunlight.

The CMM was equipped with 11 type-E thermocouples to monitor the temperature, three on each axis scale and the top and bottom of the granite table. The geometric component errors of the CMM were measured and recorded at 20, 25 and 30°C. Care was taken to maintain the CMM at a constant temperature during the error recording and subsequent measurements. Temperature control in the laboratory was

implemented using two 1500-watt heaters and an industrial temperature controller accurate to 0.1 °C. The air was circulated with two 18-inch diameter fans. Measurements at ambient were taken using the nominal heating and ventilation system of the building which was set to 22 °C. To ensure that the heaters were effectively in control of the 20 °C temperature, the building supply air was reduced to 17 °C for the weeks of those tests.

The CMM errors were stored as data tables for each of the three temperatures. The results are given in graphical form in Figure 3-7 to Figure 3-18 and Table 7. The largest source of angular error was the XY squareness error of 170 arc-seconds. The largest source of positional error was the linear expansion of the axis scales.

Position errors are shown in Figure 3-7 to Figure 3-12. Angular errors are shown in Figure 3-13 to Figure 3-18. The error table is based on the average of these three or five readings made with the laser interferometer at each 25 mm along the axis. Figure 3-7 shows the linear or scale error, $\delta_x(X)$, of the X axis at three temperatures. At 20 °C, it can be seen that a majority of the error could be caused by a stretched scale, the error at the end of the scale (900 mm) is 43 μm . The scale is mounted on a stainless steel bar that has an expansion coefficient of 12 $\mu\text{m}/\text{m}^\circ\text{C}$. At 25 °C the expansion at 900 mm would be 54 μm and at 30 °C the expansion of 900 mm is 108 μm giving scale errors of 97 μm and 151 μm respectively. These values are slightly larger than the observed values of 77 μm and 141 μm . Figure 3-8 shows the straightness error, $\delta_y(X)$ and $\delta_z(X)$, of the X axis at 25 °C. Straightness measurement requires special optics, which were only available for the set of error calibrations done at 22 °C. The small values

measured, less than 2 μm , were assumed constant at all temperatures between 20 and 30°C. The small values also justify the typical industry practice of assuming straightness errors are negligible except on very large gantry CMMs.

Figure 3-9 shows the linear or scale error, $\delta_Y(Y)$, of the Y axis at three temperatures. It also shows a predominantly "stretched" Renishaw tape scale, with an error of 52 μm at 20°C at the maximum carriage movement of 550 mm. With thermal expansion of the steel bridge, this should become 85 μm at 25°C and 118 μm at 30°C. The measured values were 77 μm at 25°C and 106 μm at 30°C, and are in good agreement with these calculations. Figure 3-10 shows the straightness error, $\delta_X(Y)$ and $\delta_Z(Y)$, of the Y axis at 25°C. The values of $\delta_X(Y)$ straightness are less than 11 μm and the values of $\delta_Z(Y)$ straightness are less than 2 μm . Again, the small values measured were assumed constant at all temperatures between 20 and 30°C.

Figure 3-11 shows the linear or scale error, $\delta_Z(Z)$, of the Z axis at three temperatures. Because the Z axis has negative dimensions, the "stretched" error has 20°C as the top curve, whereas it was the bottom curve for the X and Y axes. An error of 11 μm at 20°C at the maximum carriage movement of 500 mm, with thermal expansion of the steel ram, should become 41 μm at 25°C and 71 μm at 30°C. The measured values were 27 μm at 25°C and 47 μm at 30°C, which is slightly less than predicted. Figure 3-12 shows the straightness error, $\delta_X(Z)$ and $\delta_Y(Z)$, of the Z carriage at 25°C,

the values of straightness errors are less than $2 \mu\text{m}$, and are assumed constant for all temperatures between 20 and 30°C .

By excluding straightness, twelve of the 21 geometric component errors were measured at 20 and 30°C . Eighteen of the 21 geometric component errors were measured at 25°C . As was done in section 3.3, the angular roll error $\epsilon_i(i)$ of each axis i was not measured and assumed to be represented by the two measured angular errors.

The pitch angular errors, $\epsilon_y(X)$, of the X carriage versus temperature are given in Figure 3-13. They show a slight twisting of the carriage which is mostly independent of temperature, and has a maximum value of 15.8 arc-seconds. The yaw angular errors, $\epsilon_z(X)$, of the X axis versus temperature are given in Figure 3-14. The values are small, less than 2.4 arc-seconds and not well correlated to temperature.

The angular errors of the Y carriage are given in Figure 3-15 and Figure 3-16. The $\epsilon_x(Y)$ error shows a small, less than 5.8 arc-seconds, of temperature-independent twisting of the carriage. The $\epsilon_z(Y)$ error is less than 2.2 arc-seconds at all temperatures. The angular errors of the Z carriage are given in Figure 3-17 and Figure 3-18. The errors are less than 4.2 arc-seconds at all temperatures.

The squareness errors are given in Table 7. It can be seen that the CMM used in the experiments has a predominant XY squareness error, which is independent of temperature. The YZ and ZX squareness errors show slight temperature variation, which is likely caused by the differential expansion of the granite base.

Table 7 Squareness Error Versus Temperature

Temperature	20 °C	25 °C	30 °C
S _{XY}	-173 arc-seconds	-178 arc-seconds	-172 arc-seconds
S _{YZ}	-19 arc-seconds	-4 arc-seconds	-20 arc-seconds
S _{ZX}	21 arc-seconds	42 arc-seconds	1 arc-second

X Axis Linear Error Measurement

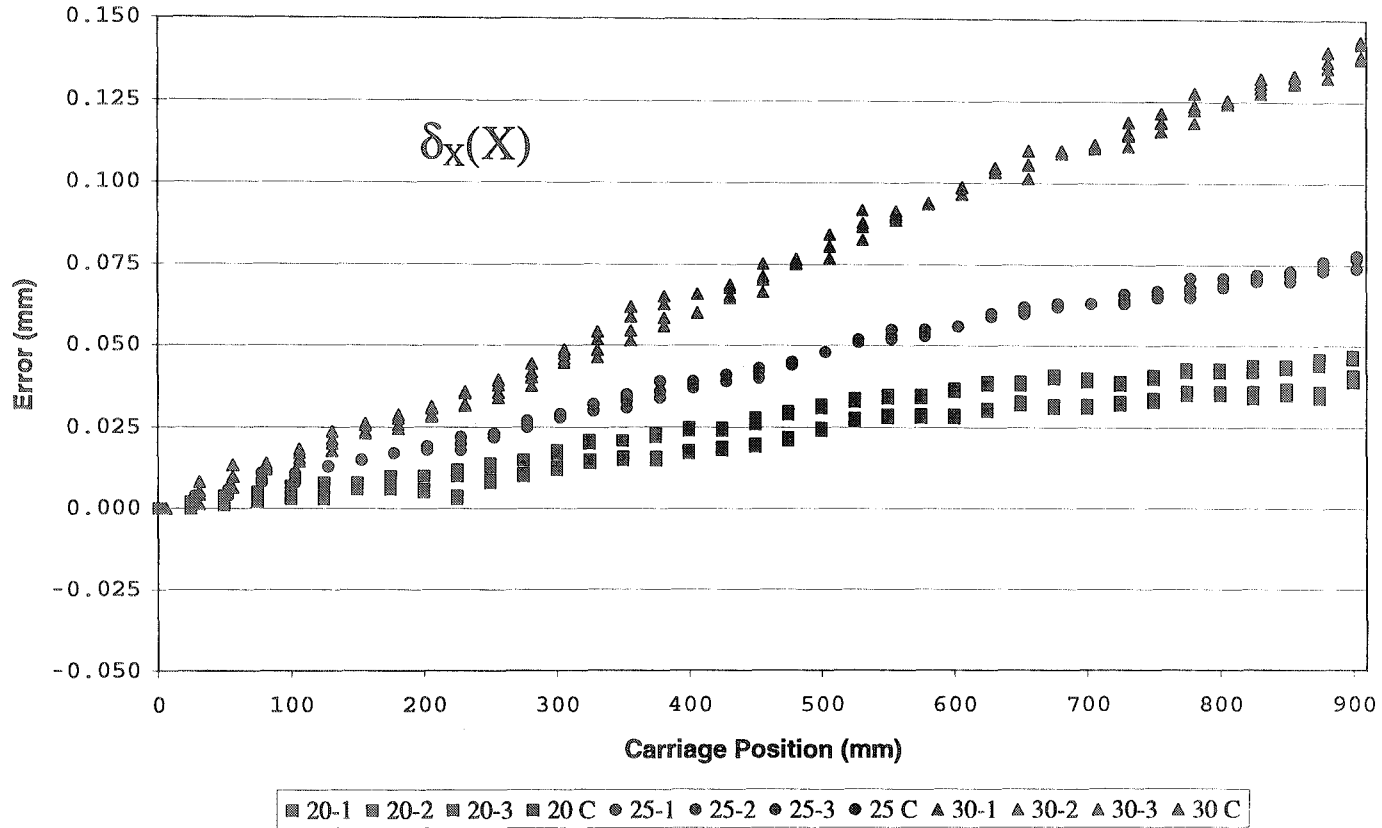


Figure 3-7 X Axis Linearity Errors

X Axis Straightness Errors (25 °C)

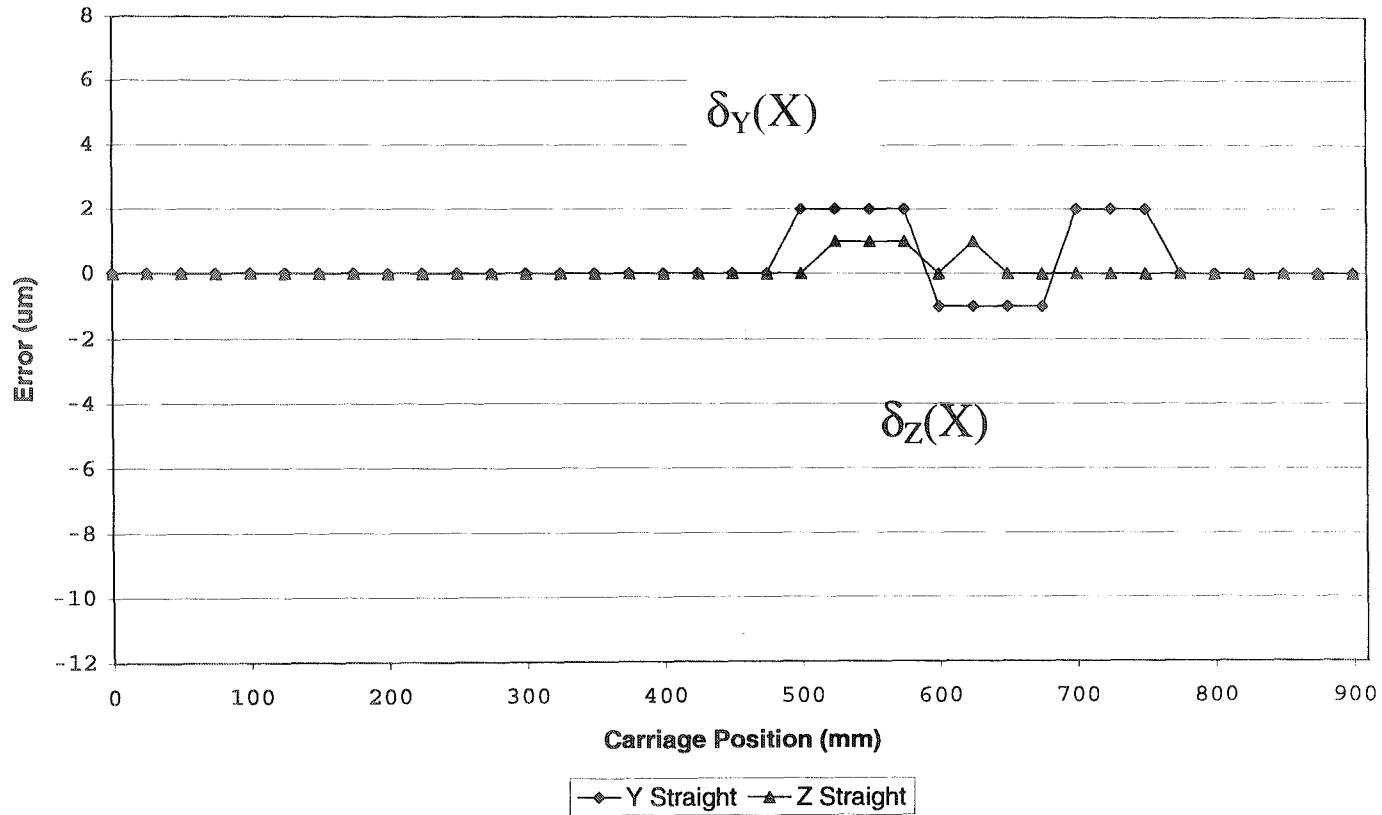


Figure 3-8 X Axis Straightness Errors

Y Axis Linear Error Measurement

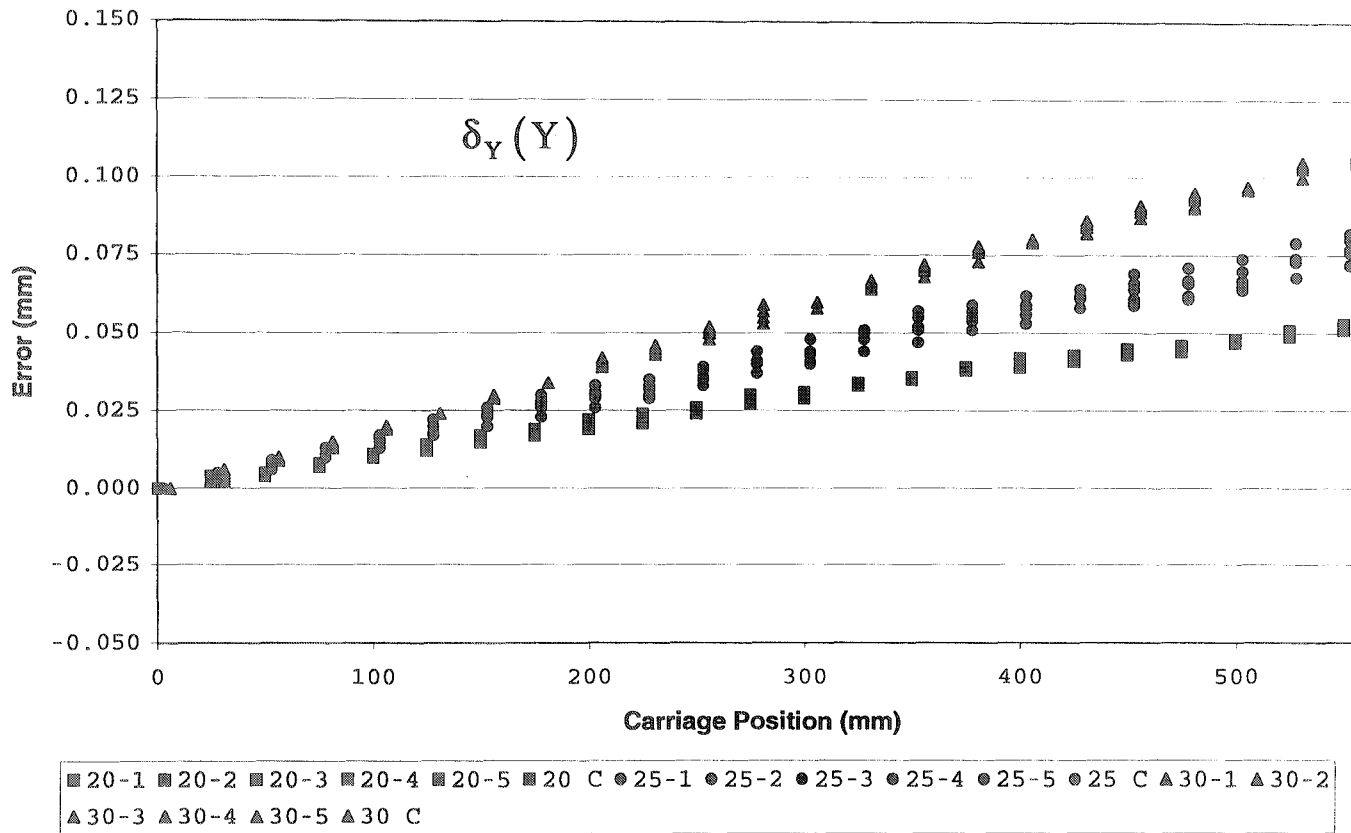


Figure 3-9 Y Axis Linearity Errors

Y Axis Straightness Errors (25 °C)

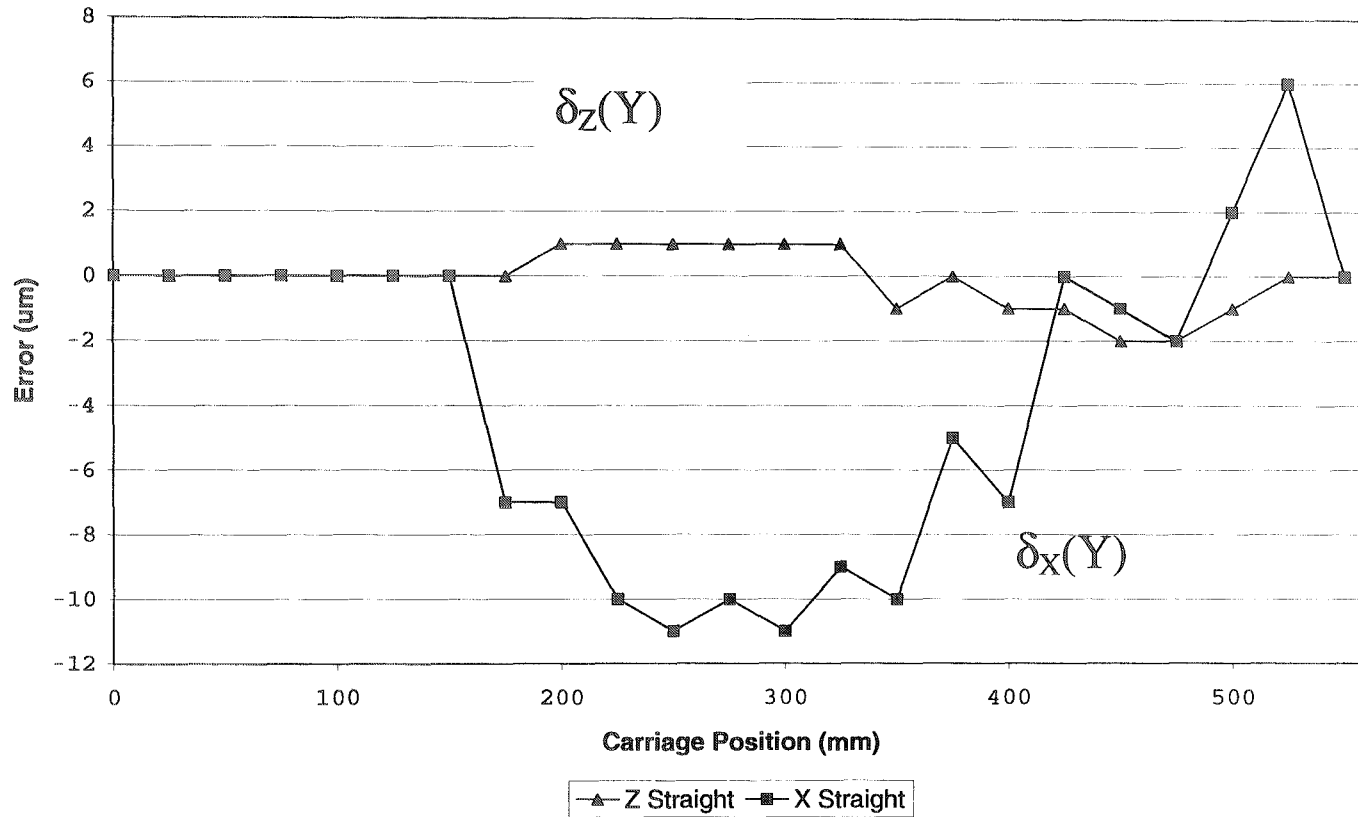


Figure 3-10 Y Axis Straightness Errors

Z Axis Linear Error Measurement

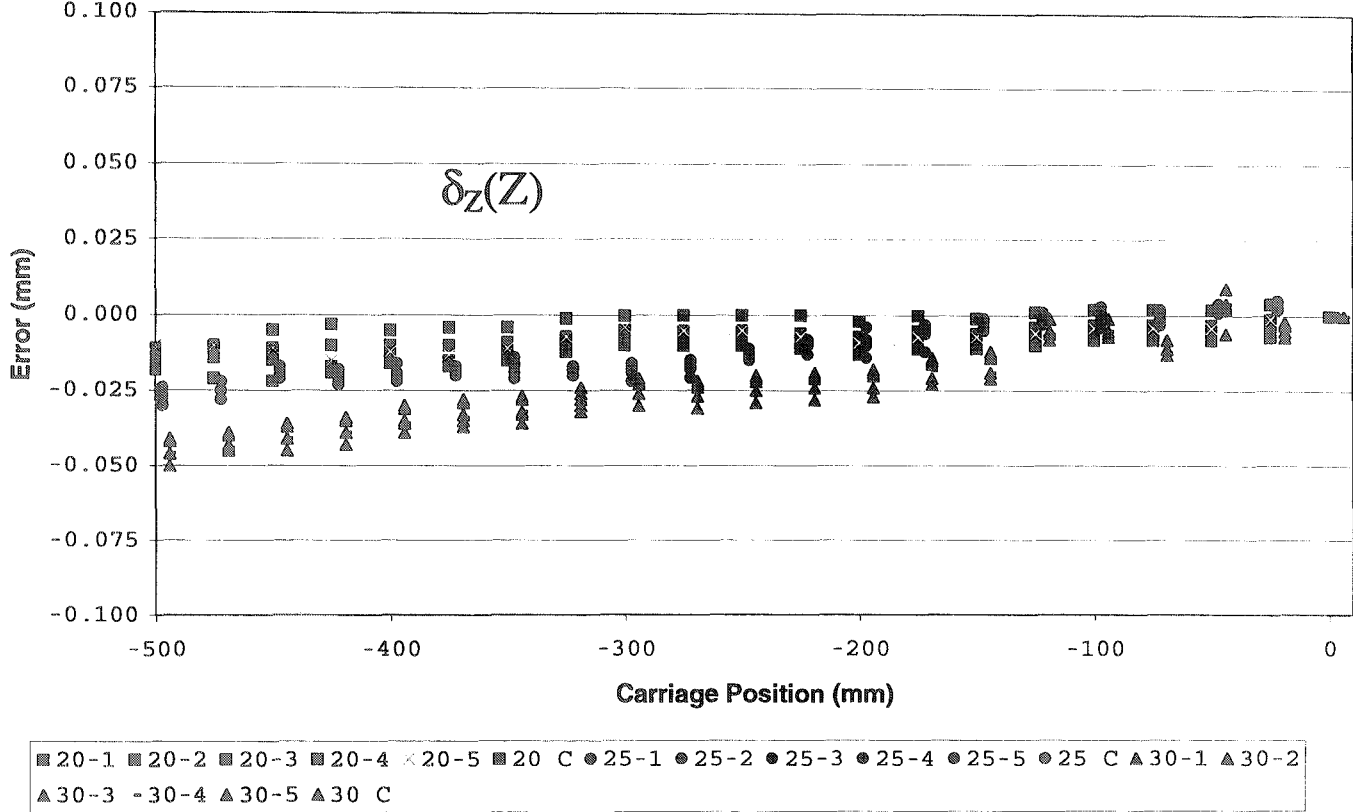


Figure 3-11 Z Axis Linearity Errors

Z Axis Straightness Errors (25 °C)

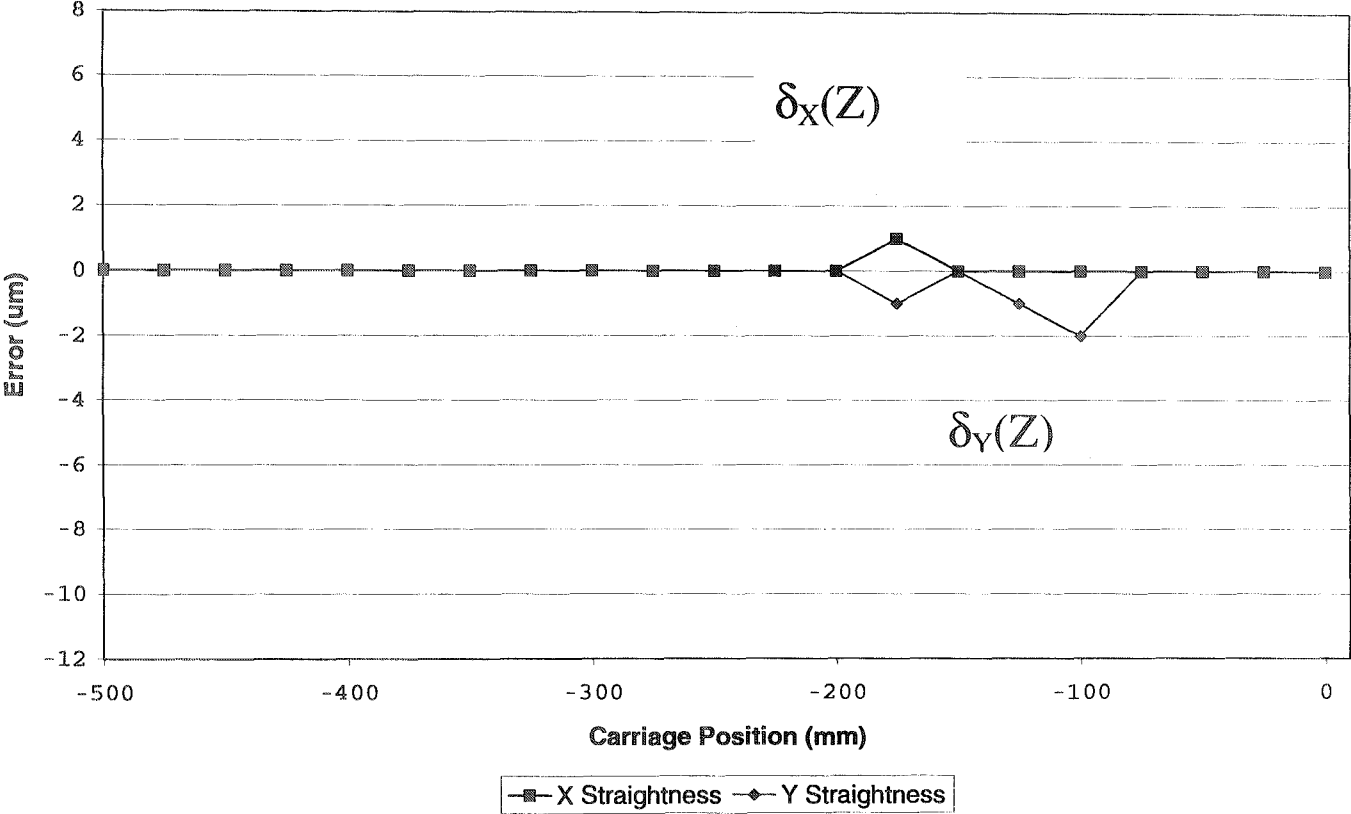


Figure 3-12 Z Axis Straightness Errors

X Carriage Rotation About Y Measurement

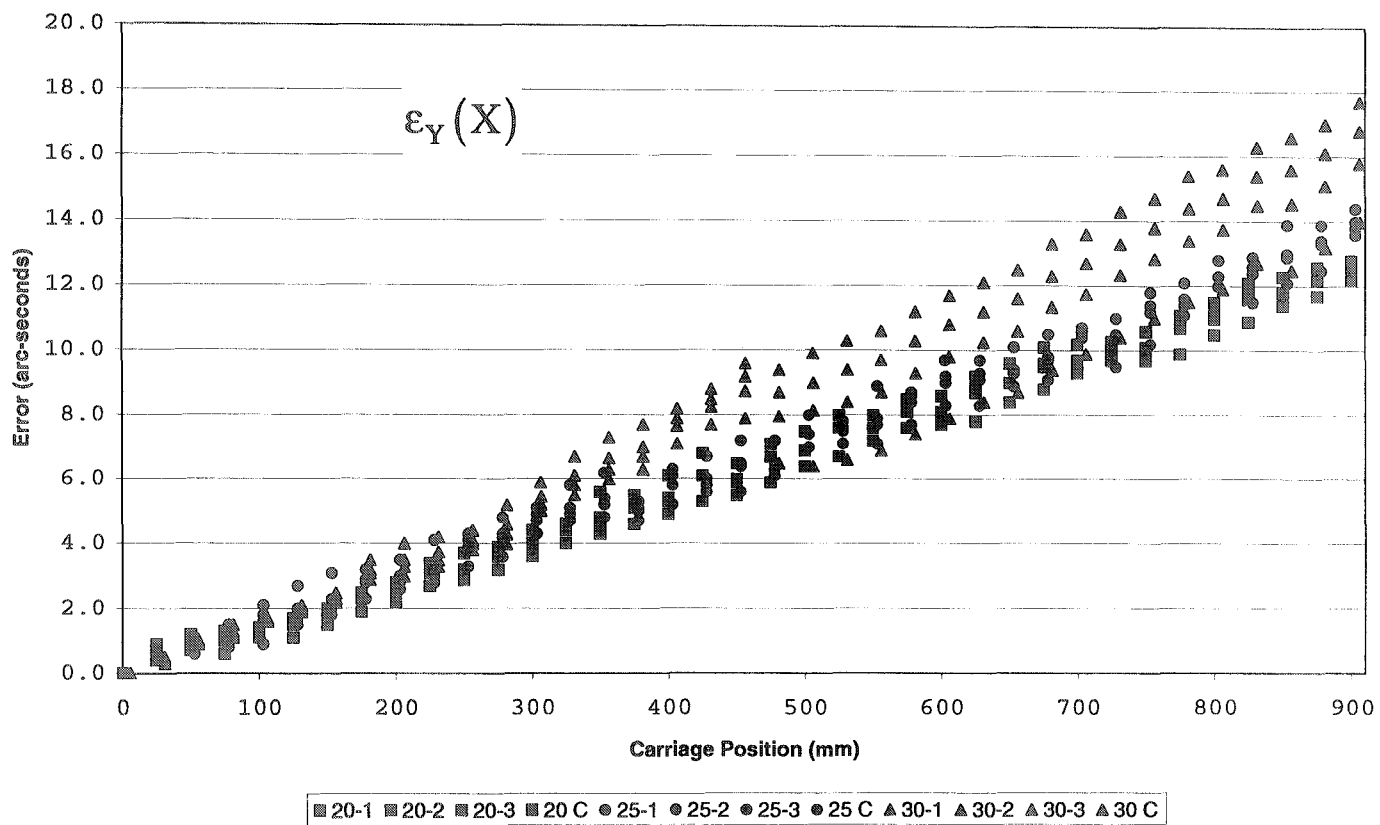


Figure 3-13 X Axis Rotational Errors About Y

X Carriage Rotation About Z Measurement

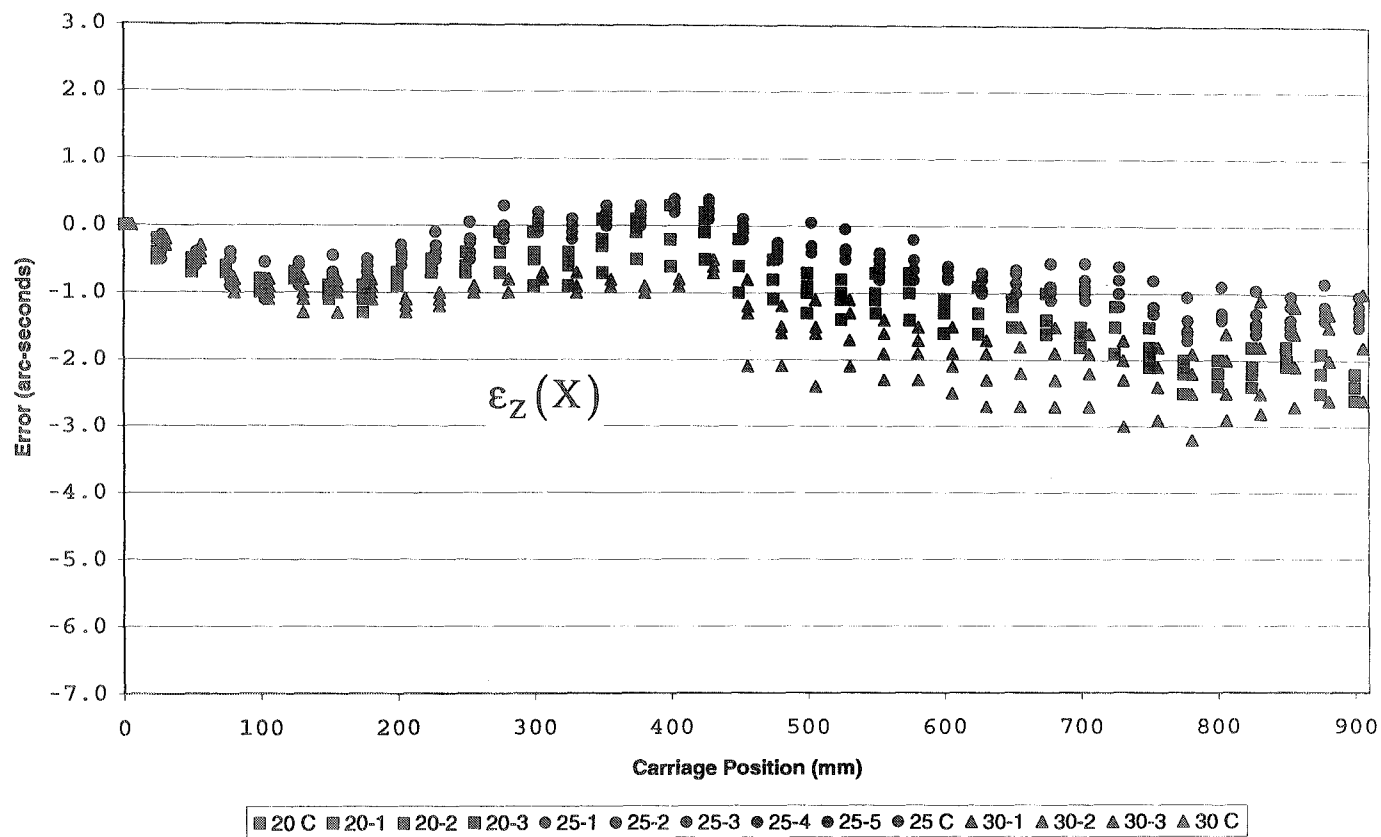


Figure 3-14 X Axis Rotational Errors About Z

Y Carriage Rotation About X Measurement

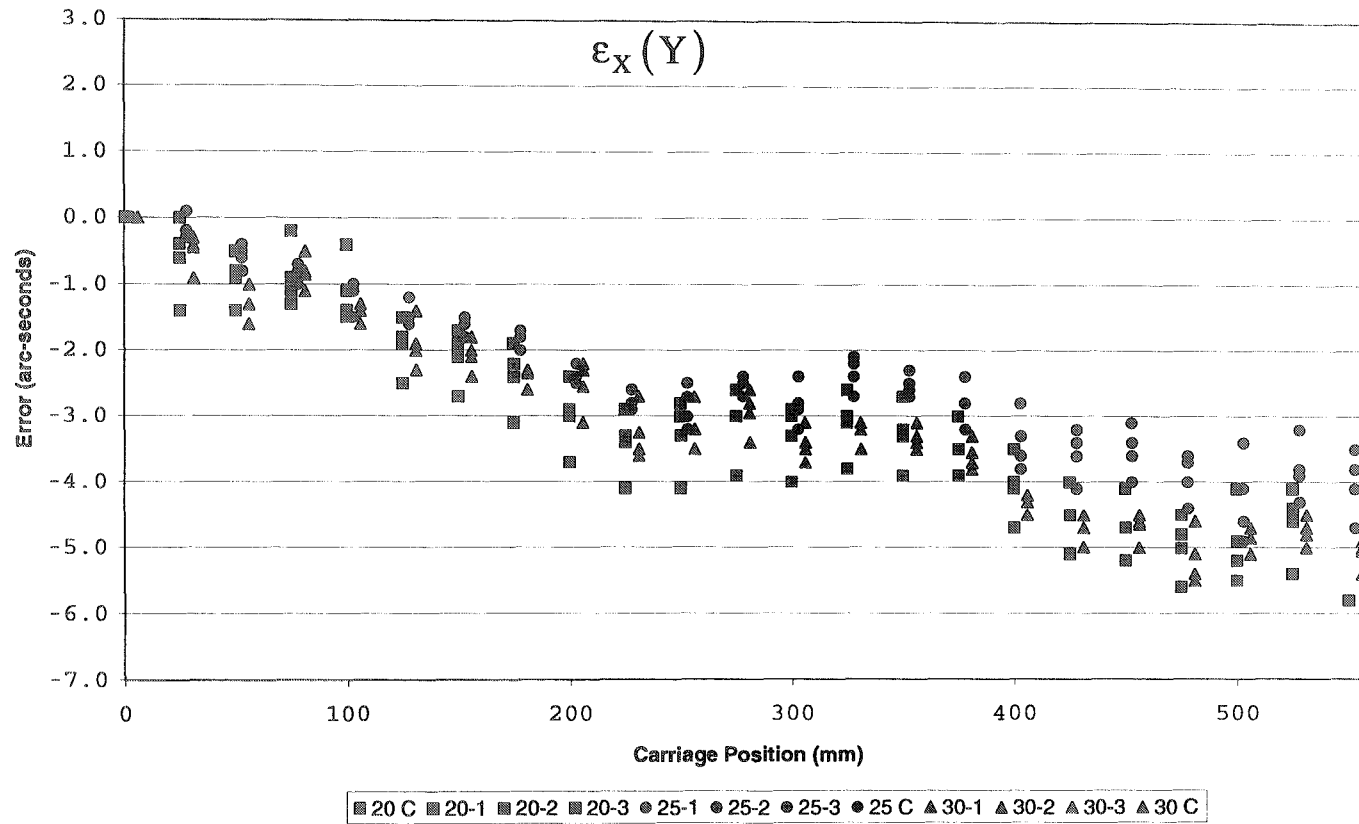


Figure 3-15 Y Axis Rotational Errors About X

Y Carriage Rotation About Z Measurement

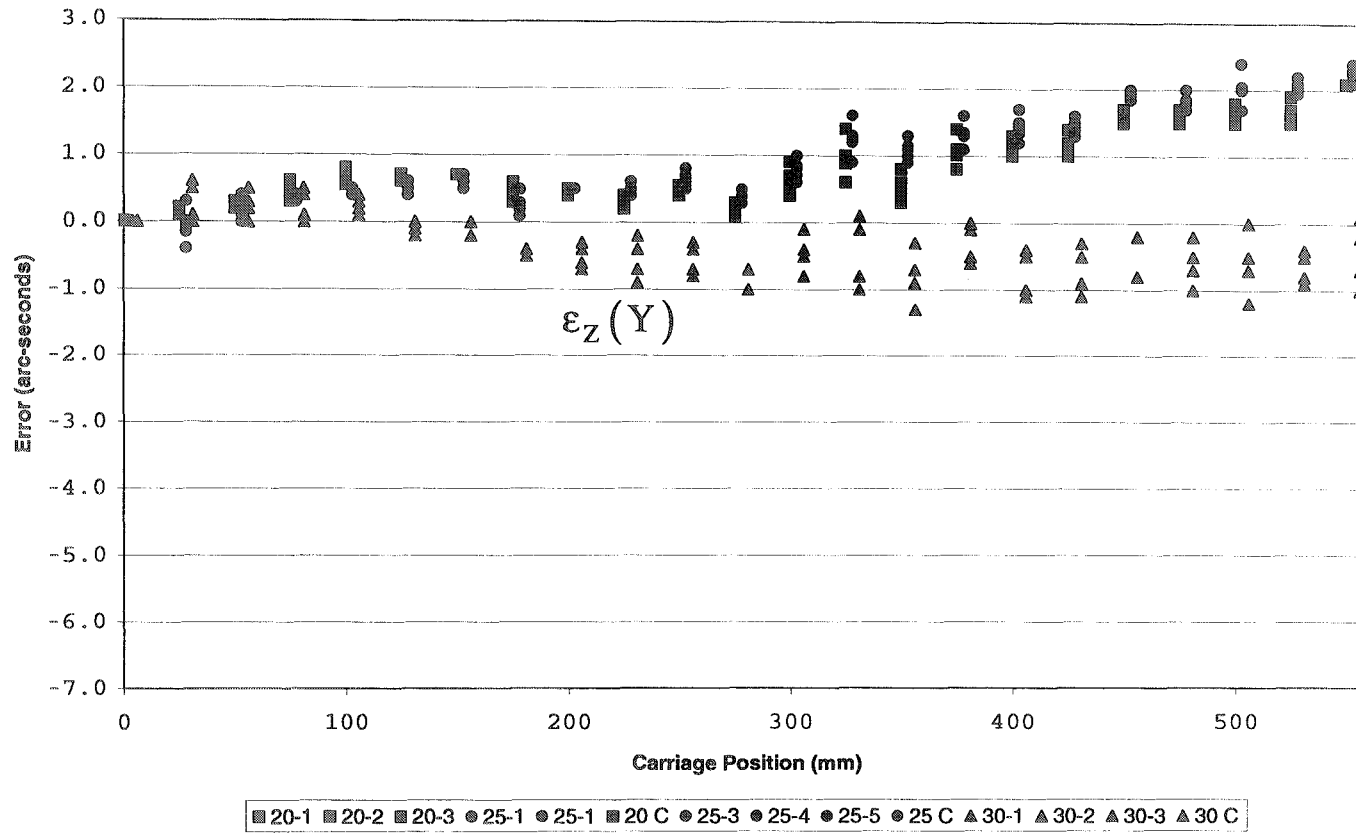


Figure 3-16 Y Axis Rotational Errors About Z

Z Carriage Rotation About X Measurement

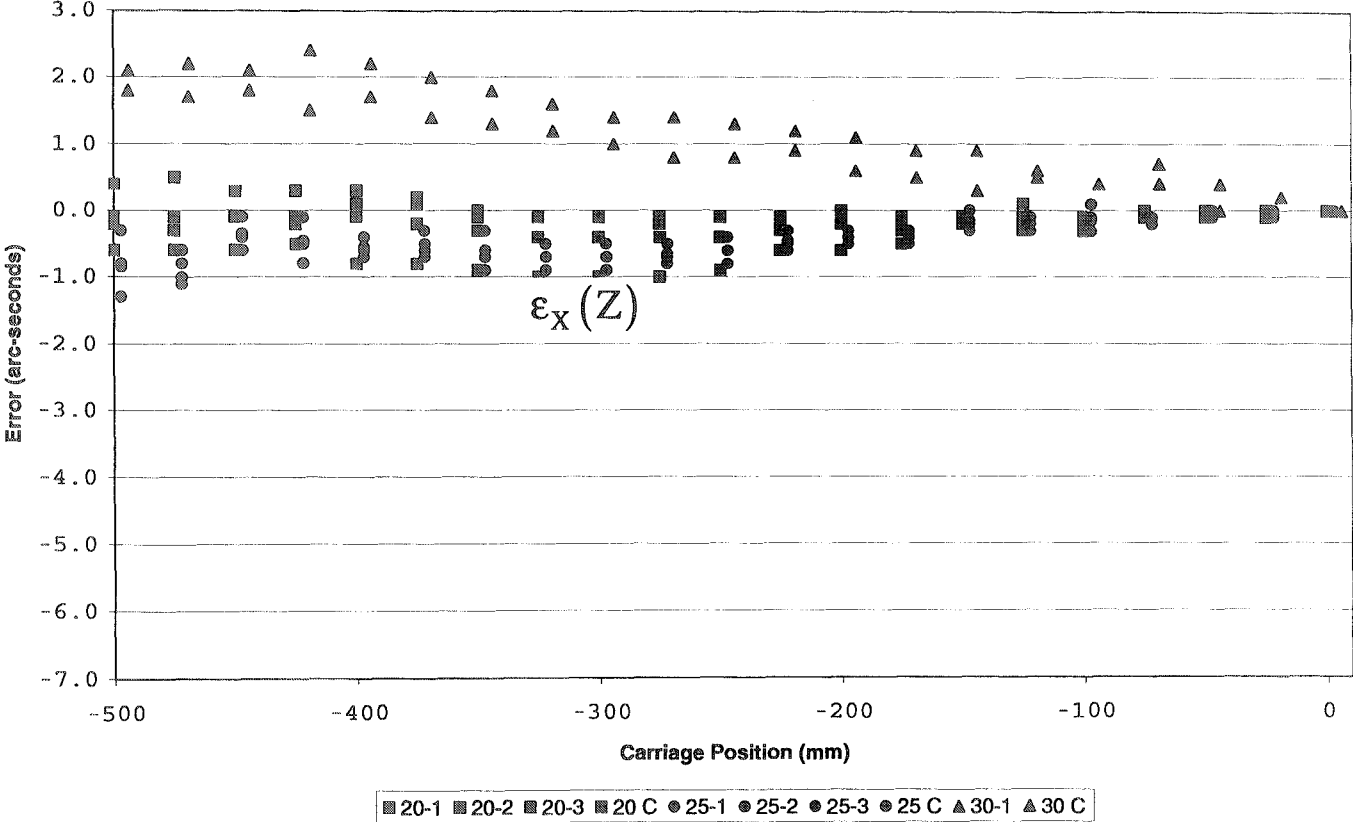


Figure 3-17 Z Axis Rotational Errors About X

Z Carriage Rotation About Y Measurement

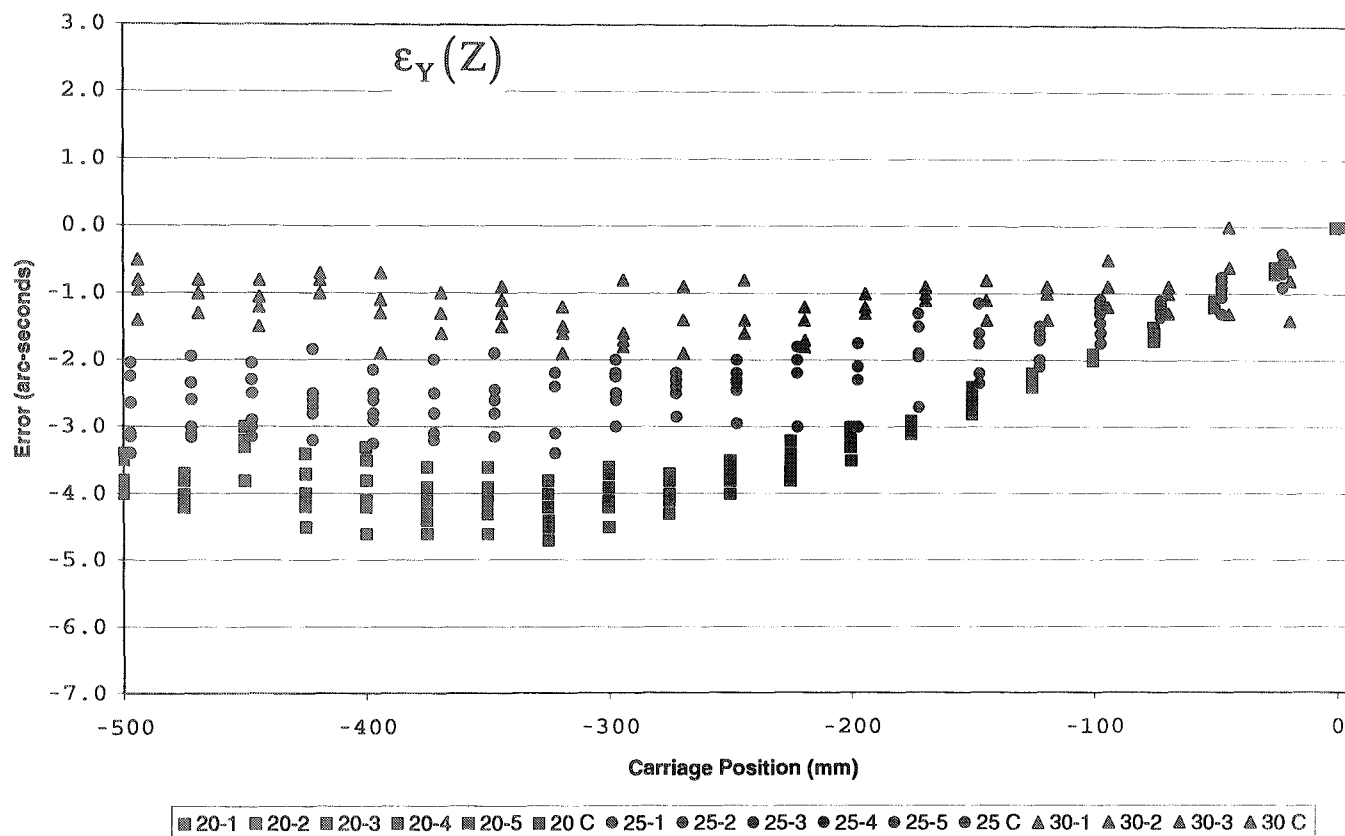


Figure 3-18 Z Axis Rotational Errors About Y

3.5. Error Map At 20 °C

Table 8 X Carriage Error Map At 20 °C

X (mm)	$\delta_x(X)$ (μm)	$\delta_y(X)$ (μm)	$\delta_z(X)$ (μm)	$\varepsilon_x(X)$ (a-s)	$\varepsilon_y(X)$ (a-s)	$\varepsilon_z(X)$ (a-s)
0	0	0	0	0	0	0
25	2	0	0	0	0.57	-0.37
50	4.5	0	0	0	1.03	-0.63
75	6.1	0	0	0	1	-0.67
100	8.9	0	0	0	1.23	-0.9
125	10.7	0	0	0	1.5	-0.73
150	12.9	0	0	0	1.67	-1
175	14.8	0	0	0	2.3	-1.1
200	15.9	0	0	0	2.5	-0.77
225	16.2	0	0	0	3.1	-0.63
250	20.8	0	0	0	3.2	-0.6
275	23.9	0	0	0	3.63	-0.4
300	27.2	0	0	0	3.97	-0.47
325	30.6	0	0	0	4.37	-0.6
350	32.3	0	0	0	4.8	-0.27
375	34.2	0	0	0	5.13	-0.13

X (mm)	$\delta_x(X)$ (μm)	$\delta_y(X)$ (μm)	$\delta_z(X)$ (μm)	$\epsilon_x(X)$ (a-s)	$\epsilon_y(X)$ (a-s)	$\epsilon_z(X)$ (a-s)
400	37.2	0	0	0	5.43	-0.17
425	38.7	0	0	0	6.07	-0.07
450	41.4	0	0	0	5.97	-0.6
475	44.5	0	0	0	6.7	-0.8
500	48.3	2	0	0	6.93	-0.97
525	51.7	2	1	0	7.57	-1.07
550	53.6	2	1	0	7.6	-1.03
575	54.7	2	1	0	8.1	-0.97
600	56.6	-1	0	0	8.07	-1.3
625	59.4	-1	1	0	8.67	-1.27
650	61.7	-1	0	0	9	-1.23
675	63.1	-1	0	0	9.5	-1.4
700	63.4	2	0	0	9.7	-1.6
725	64.7	2	0	0	10.03	-1.53
750	67.1	2	0	0	10.1	-1.83
775	70.1	0	0	0	10.67	-2.2
800	70.9	0	0	0	11.03	-2.2
825	72	0	0	0	11.6	-2.13
850	73.9	0	0	0	11.83	-1.97

X (mm)	$\delta_x(X)$ (μm)	$\delta_y(X)$ (μm)	$\delta_z(X)$ (μm)	$\epsilon_x(X)$ (a-s)	$\epsilon_y(X)$ (a-s)	$\epsilon_z(X)$ (a-s)
875	75	0	0	0	12.17	-2.2
900	79.4	0	0	0	12.57	-2.4

Table 9 Y Carriage Error Map At 20 °C

Y (mm)	$\delta_x(Y)$ (μm)	$\delta_y(Y)$ (μm)	$\delta_z(Y)$ (μm)	$\epsilon_x(Y)$ (a-s)	$\epsilon_y(Y)$ (a-s)	$\epsilon_z(Y)$ (a-s)
0	0	0	0	0	0	0
25	0	3	0	-0.6	0	0.15
50	0	4.7	0	-0.9	0	0.25
75	0	7.6	0	-0.87	0	0.45
100	0	10.7	0	-1.1	0	0.675
125	0	12.8	0	-1.93	0	0.65
150	0	15.8	0	-2.1	0	0.7
175	-7	18.3	0	-2.4	0	0.45
200	-7	20.5	1	-3	0	0.45
225	-10	22.5	1	-3.43	0	0.3
250	-11	24.6	1	-3.3	0	0.475
275	-10	28.7	1	-3.03	0	0.2
300	-11	29.8	1	-3.3	0	0.65

Y (mm)	δ_x (Y) (μm)	δ_y (Y) (μm)	δ_z (Y) (μm)	ϵ_x (Y) (a-s)	ϵ_y (Y) (a-s)	ϵ_z (Y) (a-s)
325	-9	33.4	1	-3.13	0	1
350	-10	35.5	-1	-3.27	0	0.55
375	-5	38.3	0	-3.47	0	1.1
400	-7	40.3	-1	-4.07	0	1.15
425	0	41.8	-1	-4.53	0	1.2
450	-1	43.7	-2	-4.67	0	1.6
475	-2	45.2	-2	-4.97	0	1.6
500	2	47.7	-1	-4.93	0	1.65
525	6	50.1	0	-4.63	0	1.7
550	0	51.8	0	-5.85	0	2.1

Table 10 Z Carriage Error Map At 20°C

Z (mm)	δ_x (Z) (μm)	δ_y (Z) (μm)	δ_z (Z) (μm)	ϵ_x (Z) (a-s)	ϵ_y (Z) (a-s)	ϵ_z (Z) (a-s)
-500	0	0	-11.3	-2.3	-3.05	0
-475	0	0	-11.3	-2.25	-3.15	0
-450	0	0	-11.3	-1.95	-3.25	0
-425	0	0	-10	-1.5	-3.97	0
-400	0	0	-10.4	-0.13	-3.83	0

Z (mm)	$\delta_x(Z)$ (μm)	$\delta_y(Z)$ (μm)	$\delta_z(Z)$ (μm)	$\epsilon_x(Z)$ (a-s)	$\epsilon_y(Z)$ (a-s)	$\epsilon_z(Z)$ (a-s)
-375	0	0	-9.7	-0.17	-4.13	0
-350	0	0	-9.4	-0.33	-4.07	0
-325	0	0	-6.7	-0.4	-4.23	0
-300	0	0	-5	-0.4	-3.9	0
-275	0	0	-4.9	-0.43	-3.97	0
-250	0	0	-4.9	-0.37	-3.67	0
-225	0	0	-5.6	-0.3	-3.53	0
-200	0	0	-7.2	-0.23	-3.17	0
-175	1	-1	-5.5	-0.27	-2.97	0
-150	0	0	-5.8	-0.17	-2.53	0
-125	0	-1	-4.1	-0.13	-2.3	0
-100	0	-2	-3	-0.17	-1.97	0
-75	0	0	-3.1	-0.07	-1.57	0
-50	0	0	-2.7	-0.07	-1.2	0
-25	0	0	-1.3	-0.03	-0.67	0
0	0	0	0	0	0	0

3.6. Error Map At 25°C

Table 11 X Carriage Error Map At 25°C

X (mm)	$\delta_x(X)$ (μm)	$\delta_y(X)$ (μm)	$\delta_z(X)$ (μm)	$\epsilon_x(X)$ (a-s)	$\epsilon_y(X)$ (a-s)	$\epsilon_z(X)$ (a-s)
0	0.0	0.0	0.0	0	0.0	0.0
25	2.9	0.0	0.0	0	1.1	-0.7
50	5.3	0.0	0.0	0	2.2	-1.2
75	9.0	0.0	0.0	0	3.0	-1.4
100	9.6	0.0	0.0	0	4.3	-1.6
125	13.0	0.0	0.0	0	5.2	-1.3
150	15.0	0.0	0.0	0	6.1	-1.3
175	17.0	0.0	0.0	0	7.2	-1.2
200	18.3	0.0	0.0	0	8.3	-0.7
225	19.9	0.0	0.0	0	9.1	-0.5
250	22.7	0.0	0.0	0	10.1	-0.2
275	25.9	0.0	0.0	0	11.2	0.5
300	28.8	0.0	0.0	0	12.3	0.8
325	31.6	0.0	0.0	0	13.1	0.7
350	33.2	0.0	0.0	0	14.0	1.3
375	36.2	0.0	0.0	0	14.8	1.5

X (mm)	$\delta_x(X)$ (μm)	$\delta_y(X)$ (μm)	$\delta_z(X)$ (μm)	$\epsilon_x(X)$ (a-s)	$\epsilon_y(X)$ (a-s)	$\epsilon_z(X)$ (a-s)
400	37.9	0.0	0.0	0	15.8	1.8
425	39.4	0.0	0.0	0	16.6	2.1
450	41.9	0.0	0.0	0	17.5	1.7
475	44.7	0.0	0.0	0	18.6	1.3
500	48.0	2.0	0.0	0	19.2	1.8
525	51.3	2.0	1.0	0	20.3	1.9
550	53.3	2.0	1.0	0	20.9	1.3
575	54.1	2.0	1.0	0	22.1	1.4
600	56.1	-1.0	0.0	0	22.8	1.4
625	59.3	-1.0	1.0	0	23.7	1.2
650	60.9	-1.0	0.0	0	24.7	1.6
675	62.3	-1.0	0.0	0	25.5	1.6
700	63.1	2.0	0.0	0	26.6	1.9
725	64.2	2.0	0.0	0	27.5	1.8
750	66.1	2.0	0.0	0	29.0	1.7
775	67.8	0.0	0.0	0	30.0	1.1
800	69.2	0.0	0.0	0	30.9	1.8
825	71.1	0.0	0.0	0	31.8	1.7
850	71.7	0.0	0.0	0	33.4	1.9

X (mm)	$\delta_x(X)$ (μm)	$\delta_y(X)$ (μm)	$\delta_z(X)$ (μm)	$\epsilon_x(X)$ (a-s)	$\epsilon_y(X)$ (a-s)	$\epsilon_z(X)$ (a-s)
875	74.3	0.0	0.0	0	34.0	2.5
900	76.6	0.0	0.0	0	34.7	2.9

Table 12 Y Carriage Error Map At 25 °C

Y (mm)	$\delta_x(Y)$ (μm)	$\delta_y(Y)$ (μm)	$\delta_z(Y)$ (μm)	$\epsilon_x(Y)$ (a-s)	$\epsilon_y(Y)$ (a-s)	$\epsilon_z(Y)$ (a-s)
0	0.0	0.0	0.0	0.0	0	0.0
25	0.0	3.7	0.0	-0.3	0	0.3
50	0.0	7.2	0.0	-0.7	0	0.3
75	0.0	11.4	0.0	-0.9	0	0.4
100	0.0	15.0	0.0	-1.1	0	0.5
125	0.0	18.3	0.0	-1.6	0	0.2
150	0.0	22.9	0.0	-1.7	0	0.1
175	-7.0	26.6	0.0	-1.9	0	-0.4
200	-7.0	29.3	1.0	-2.4	0	-0.3
225	-10.0	32.3	1.0	-2.8	0	-0.2
250	-11.0	36.1	1.0	-2.8	0	-0.3
275	-10.0	40.5	1.0	-2.6	0	-0.5
300	-11.0	43.7	1.0	-2.8	0	-0.2

Y (mm)	$\delta_x(Y)$ (μm)	$\delta_y(Y)$ (μm)	$\delta_z(Y)$ (μm)	$\epsilon_x(Y)$ (a-s)	$\epsilon_y(Y)$ (a-s)	$\epsilon_z(Y)$ (a-s)
325	-9.0	47.7	1.0	-2.5	0	0.0
350	-10.0	52.0	-1.0	-2.5	0	-0.3
375	-5.0	55.1	0.0	-2.8	0	-0.1
400	-7.0	57.5	-1.0	-3.3	0	-0.3
425	0.0	60.7	-1.0	-3.7	0	-0.4
450	-1.0	64.0	-2.0	-3.6	0	-0.2
475	-2.0	66.6	-2.0	-4.0	0	-0.2
500	2.0	69.5	-1.0	-4.2	0	0.0
525	6.0	73.5	0.0	-3.8	0	-0.1
550	0.0	76.7	0.0	-4.1	0	0.1

Table 13 Z Carriage Error Map At 25 °C

Z (mm)	$\delta_x(Z)$ (μm)	$\delta_y(Z)$ (μm)	$\delta_z(Z)$ (μm)	$\epsilon_x(Z)$ (a-s)	$\epsilon_y(Z)$ (a-s)	$\epsilon_z(Z)$ (a-s)
-500	0.0	0.0	-26.8	-2.3	-3.1	0
-475	0.0	0.0	-24.8	-2.3	-3.2	0
-450	0.0	0.0	-18.4	-2.0	-3.1	0
-425	0.0	0.0	-18.6	-1.5	-3.2	0
-400	0.0	0.0	-18.7	-1.4	-3.8	0

Z (mm)	$\delta_x(Z)$ (μm)	$\delta_y(Z)$ (μm)	$\delta_z(Z)$ (μm)	$\epsilon_x(Z)$ (a-s)	$\epsilon_y(Z)$ (a-s)	$\epsilon_z(Z)$ (a-s)
-375	0.0	0.0	-17.0	-1.1	-3.8	0
-350	0.0	0.0	-17.3	-0.9	-3.9	0
-325	0.0	0.0	-16.9	-2.0	-3.8	0
-300	0.0	0.0	-18.8	-2.8	-3.6	0
-275	0.0	0.0	-17.5	-2.7	-3.5	0
-250	0.0	0.0	-11.9	-3.1	-3.5	0
-225	0.0	0.0	-7.9	-0.3	-3.1	0
-200	0.0	0.0	-7.7	-0.5	-2.8	0
-175	1.0	-1.0	-4.4	-0.3	-2.6	0
-150	0.0	0.0	-3.5	-0.3	-2.2	0
-125	0.0	-1.0	-1.4	-0.3	-2.0	0
-100	0.0	-2.0	-0.5	-0.1	-1.6	0
-75	0.0	0.0	-0.5	-0.2	-1.4	0
-50	0.0	0.0	3.3	-0.1	-1.0	0
-25	0.0	0.0	4.0	-0.2	-0.7	0
0	0.0	0.0	0.0	0.0	0.0	0

3.7. Error Map At 30 °C

Table 14 X Carriage Error Map At 30 °C

X (mm)	$\delta_x(X)$ (μm)	$\delta_y(X)$ (μm)	$\delta_z(X)$ (μm)	$\varepsilon_x(X)$ (a-s)	$\varepsilon_y(X)$ (a-s)	$\varepsilon_z(X)$ (a-s)
0	0.0	0.0	0.0	0	0.0	0.0
25	4.8	0.0	0.0	0	0.4	-0.3
50	9.9	0.0	0.0	0	1.0	-0.4
75	12.9	0.0	0.0	0	1.3	-0.9
100	16.4	0.0	0.0	0	1.7	-1.0
125	20.8	0.0	0.0	0	2.0	-1.1
150	24.6	0.0	0.0	0	2.4	-1.0
175	26.7	0.0	0.0	0	3.2	-1.0
200	29.8	0.0	0.0	0	3.5	-1.2
225	33.7	0.0	0.0	0	3.8	-1.1
250	36.7	0.0	0.0	0	4.1	-1.0
275	41.0	0.0	0.0	0	4.6	-0.9
300	46.7	0.0	0.0	0	5.5	-0.8
325	50.2	0.0	0.0	0	6.1	-0.9
350	56.7	0.0	0.0	0	6.7	-0.9
375	60.7	0.0	0.0	0	7.0	-1.0

X (mm)	$\delta_x(X)$ (μm)	$\delta_y(X)$ (μm)	$\delta_z(X)$ (μm)	$\epsilon_x(X)$ (a-s)	$\epsilon_y(X)$ (a-s)	$\epsilon_z(X)$ (a-s)
400	63.0	0.0	0.0	0	7.7	-0.9
425	66.7	0.0	0.0	0	8.3	-0.6
450	70.9	0.0	0.0	0	8.8	-1.4
475	76.0	0.0	0.0	0	8.0	-1.6
500	80.7	2.0	0.0	0	8.2	-1.7
525	87.2	2.0	1.0	0	8.4	-1.6
550	90.0	2.0	1.0	0	8.7	-1.8
575	93.7	2.0	1.0	0	9.3	-1.9
600	97.7	-1.0	0.0	0	9.8	-2.0
625	104.0	-1.0	1.0	0	10.3	-2.2
650	105.7	-1.0	0.0	0	10.6	-2.1
675	109.6	-1.0	0.0	0	11.4	-2.1
700	111.3	2.0	0.0	0	11.8	-2.1
725	115.1	2.0	0.0	0	12.4	-2.3
750	118.7	2.0	0.0	0	12.9	-2.3
775	123.2	0.0	0.0	0	13.4	-2.5
800	125.1	0.0	0.0	0	13.8	-2.3
825	130.1	0.0	0.0	0	14.5	-2.1
850	132.0	0.0	0.0	0	14.6	-1.9

X (mm)	$\delta_x(X)$ (μm)	$\delta_y(X)$ (μm)	$\delta_z(X)$ (μm)	$\epsilon_x(X)$ (a-s)	$\epsilon_y(X)$ (a-s)	$\epsilon_z(X)$ (a-s)
875	136.4	0.0	0.0	0	15.1	-1.9
900	140.9	0.0	0.0	0	15.8	-2.0

Table 15 Y Carriage Error Map At 30°C

Y (mm)	$\delta_x(Y)$ (μm)	$\delta_y(Y)$ (μm)	$\delta_z(Y)$ (μm)	$\epsilon_x(Y)$ (a-s)	$\epsilon_y(Y)$ (a-s)	$\epsilon_z(Y)$ (a-s)
0	0.0	0.0	0.0	0.0	0	0.0
25	0.0	1.9	0.0	-0.5	0	0.3
50	0.0	9.6	0.0	-1.3	0	0.3
75	0.0	14.1	0.0	-1.0	0	0.3
100	0.0	19.6	0.0	-1.4	0	0.3
125	0.0	23.9	0.0	-1.9	0	-0.1
150	0.0	29.3	0.0	-2.1	0	-0.1
175	-7.0	34.0	0.0	-2.3	0	-0.5
200	-7.0	39.9	1.0	-2.7	0	-0.5
225	-10.0	43.8	1.0	-3.2	0	-0.6
250	-11.0	49.4	1.0	-3.1	0	-0.6
275	-10.0	54.8	1.0	-3.0	0	-0.9
300	-11.0	58.9	1.0	-3.3	0	-0.5

Y (mm)	$\delta_x(Y)$ (μm)	$\delta_y(Y)$ (μm)	$\delta_z(Y)$ (μm)	$\epsilon_x(Y)$ (a-s)	$\epsilon_y(Y)$ (a-s)	$\epsilon_z(Y)$ (a-s)
325	-9.0	64.8	1.0	-3.1	0	-0.5
350	-10.0	69.5	-1.0	-3.3	0	-0.8
375	-5.0	74.9	0.0	-3.5	0	-0.3
400	-7.0	79.5	-1.0	-4.3	0	-0.8
425	0.0	83.6	-1.0	-4.6	0	-0.7
450	-1.0	88.2	-2.0	-4.6	0	-0.5
475	-2.0	92.3	-2.0	-5.0	0	-0.6
500	2.0	96.7	-1.0	-4.9	0	-0.6
525	6.0	101.9	0.0	-4.7	0	-0.7
550	0.0	106.3	0.0	-5.1	0	-0.5

Table 16 Z Carriage Error Map At 30°C

Z (mm)	$\delta_x(Z)$ (μm)	$\delta_y(Z)$ (μm)	$\delta_z(Z)$ (μm)	$\epsilon_x(Z)$ (a-s)	$\epsilon_y(Z)$ (a-s)	$\epsilon_z(Z)$ (a-s)
-500	0.0	0.0	-46.2	2.0	-0.8	0
-475	0.0	0.0	-43.7	2.0	-0.8	0
-450	0.0	0.0	-41.1	2.0	-0.8	0
-425	0.0	0.0	-38.9	2.0	-0.8	0
-400	0.0	0.0	-35.3	2.0	-1.1	0

Z (mm)	$\delta_x(Z)$ (μm)	$\delta_y(Z)$ (μm)	$\delta_z(Z)$ (μm)	$\varepsilon_x(Z)$ (a-s)	$\varepsilon_y(Z)$ (a-s)	$\varepsilon_z(Z)$ (a-s)
-375	0.0	0.0	-33.1	1.7	-1.3	0
-350	0.0	0.0	-31.7	1.6	-1.3	0
-325	0.0	0.0	-28.0	1.4	-1.5	0
-300	0.0	0.0	-23.2	1.2	-1.6	0
-275	0.0	0.0	-24.4	1.1	-1.4	0
-250	0.0	0.0	-22.0	1.1	-1.4	0
-225	0.0	0.0	-20.8	1.1	-1.4	0
-200	0.0	0.0	-20.0	0.9	-1.3	0
-175	1.0	-1.0	-16.4	0.7	-1.0	0
-150	0.0	0.0	-14.3	0.6	-1.1	0
-125	0.0	-1.0	-0.9	0.6	-1.0	0
-100	0.0	-2.0	-0.6	0.4	-0.9	0
-75	0.0	0.0	-7.7	0.6	-1.0	0
-50	0.0	0.0	9.2	0.2	-0.6	0
-25	0.0	0.0	-2.4	0.2	-0.5	0
0	0.0	0.0	0.0	0.0	0.0	0

Chapter 4

Laser Digitizer

Active 3-D position sensing systems, such as laser digitizers, obtain the object coordinates from external information such as scanning angles and reflected beam patterns. Passive systems require well-defined features such as targets and edges, which are affected by ambient light. Therefore, they have difficulty with sculptured surfaces and unstructured environments. Active systems provide their own illumination so they can easily measure surfaces in most environments regardless of the ambient light conditions. In most applications, measurements on surfaces are all required to completely describe an object.

4.1. Laser Digitizer

Laser sensors work by projecting a strip of light on a part's surface to make a virtual copy of an existing part or shape. This virtual 3-D copy consists of a cloud of measured points, each with its own XYZ coordinate in space; the point cloud is used to perform inspections or develop CAD models.

The Hyscan 45C laser digitizer is a single-axis range camera that operates by optical triangulation. A laser beam is projected onto a double-sided scanning mirror that provides synchronisation between projection and detection. (See Figure 4-1.) The projected beam of laser light is directed by the scanning mirror onto the test object and

swept across the scene through an angle of about 30°. The return beam reflects off of the object surface for points lying in the swept plane and is measured by the CCD linear position sensor. From the position of the beam on the CCD and the orientation of the scanning mirror the Hyscan system computes the $[U \ V]$ coordinates of a point on the object surface. As the mirror is rotated about its centre, the laser beam sweeps out a line along the surface being scanned. Data is collected at up to 1024 discrete points along this scan line, yielding a surface profile of the object. If the digitizer is stationary, all acquired data will lie in a plane called the scan plane. The field of view is a region within the scan plane for which surface sample data is generated. The Hyscan 45C is mounted on the CMM, which is used as a translation device, and data is acquired with the camera in motion. The Hyscan system continuously monitors the scales on each CMM axis to determine the position of the camera head at the time at which each data point is acquired. Hyscan system software combines translation device scale data with range measurements to generate 3-D sample points in a fixed reference coordinate system. The system also records the two dimensional position in the scan plane and the CMM scale reading, D for the X axis scale, E for the Y axis and F for the Z axis. The system software incorporates digitizer alignment calibration, but does not provide error compensation for the changes cause by geometric component errors or thermal variations

The laser beam emitted by the Hyscan 45C sweeps out a planar region referred to as the scan plane. The rectangular subregion of the scan plane in which the camera acquires data is called the field of view. (See Figure 4-2.) The nominal accuracy at the

3σ level specified for the Hyscan 45C is $25\ \mu\text{m}$. Based on a working knowledge of this technology the error is assumed to have a normal distribution.

Table 17 Hymarc Hyscan 45C Specifications

Mirror Scanning Rate	3.3 Hz sinusoidal
Scanning Angle	30°
Data Density	1024 Points per Scan Line
Scan Direction	Forward, Reverse or Bi-directional
Stand-off	140 mm
Scan Width	60 mm
Depth of View	60 mm
Point Measurement Accuracy	$\pm 25\ \mu\text{m}$ ($3\ \sigma$ limit)
Probing Uncertainty	$\pm 9\ \mu\text{m}$ ($1\ \sigma$ limit)

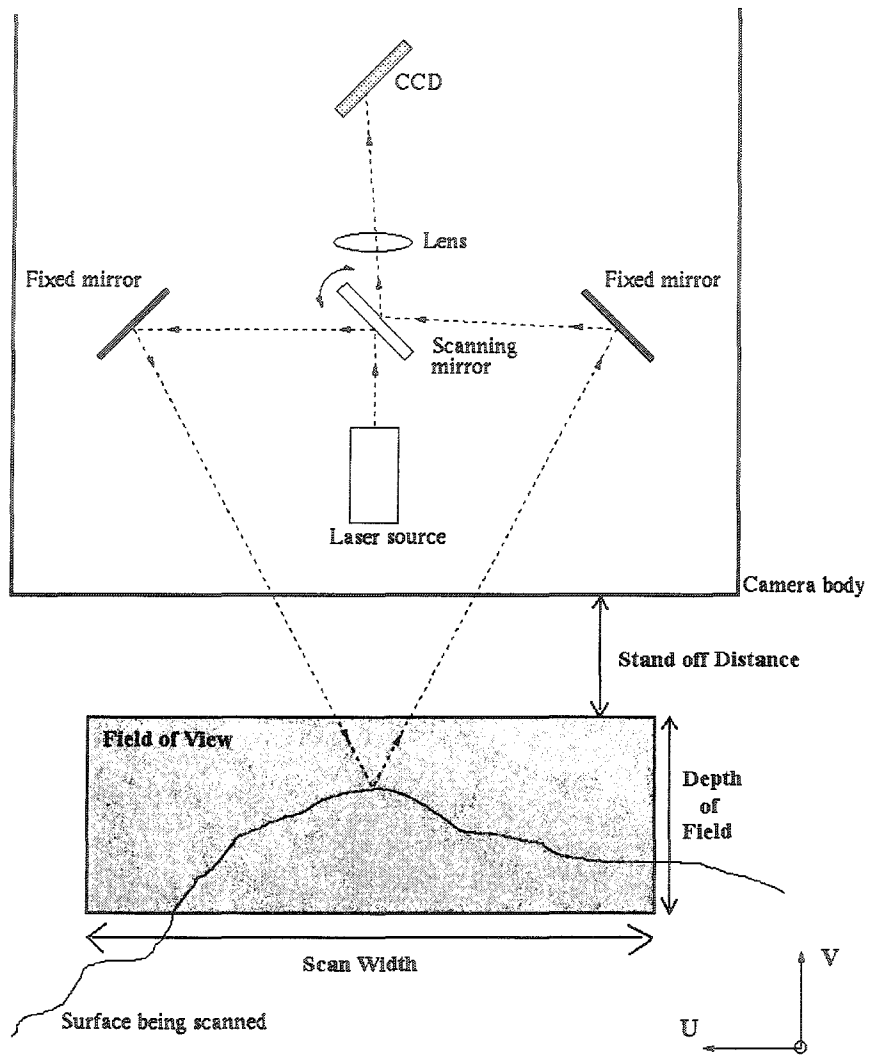


Figure 4-1 Principle Of Triangulation Using Synchronised Scanning [Hymarc]

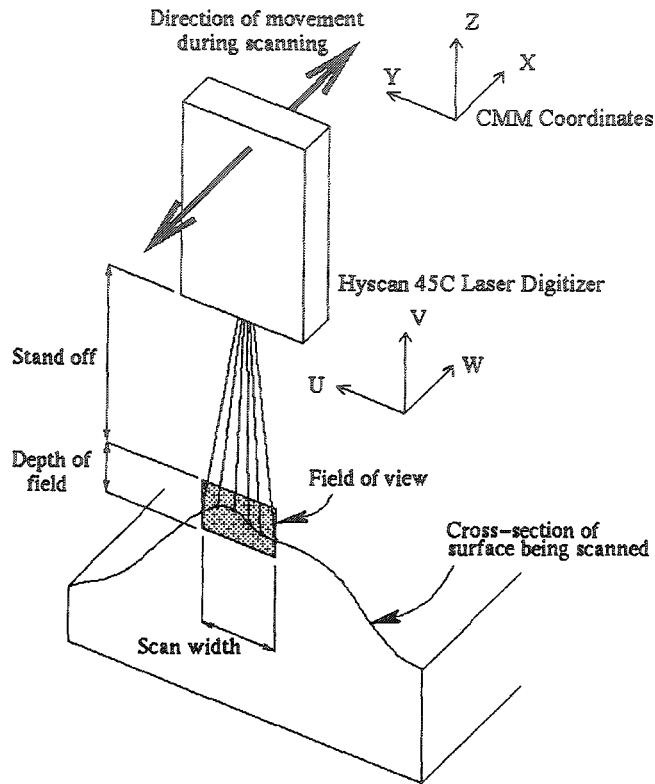


Figure 4-2 Hymarc 45C Field Of View [Hymarc]

4.2. Digitizer Mount

The Hyscan 45C digitizer is attached to the ram of the CMM via an incremental trunnion providing two rotary degrees of freedom. (See Figure 4-3.) This joint, often referred to as the "wrist", is manually operated and indexed, meaning that it provides a discrete number of repeatable configurations. The trunnion allows the camera to be mounted on the end of the ram with the camera W axis aligned in either positive or negative X or Y direction. The camera can rotate about the W axis in 15° increments.

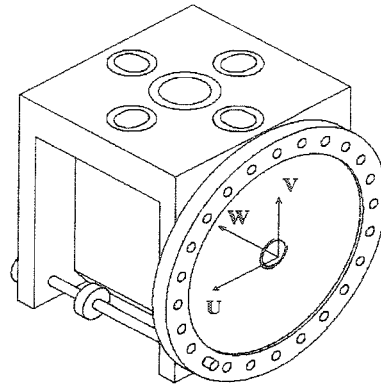


Figure 4-3 Incremental Trunnion [Hymarc]

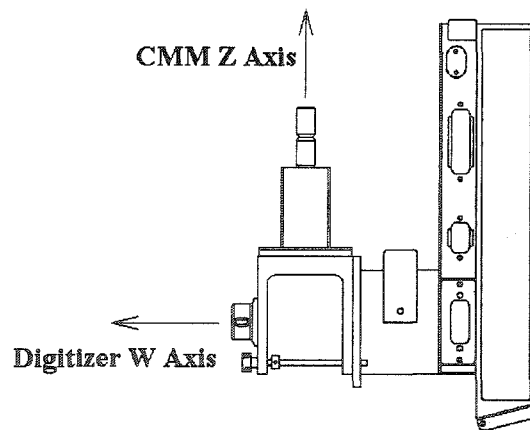


Figure 4-4 Digitizer Mounted On Trunnion [Hymarc]

4.3. Euler Angle Method Of Digitizer Alignment Calibration For Pose Attitude

Each time the digitizer is mounted on the ram of the CMM the local U-V-W coordinate system of the laser digitizer needs to be aligned with the global X-Y-Z coordinates of the CMM.

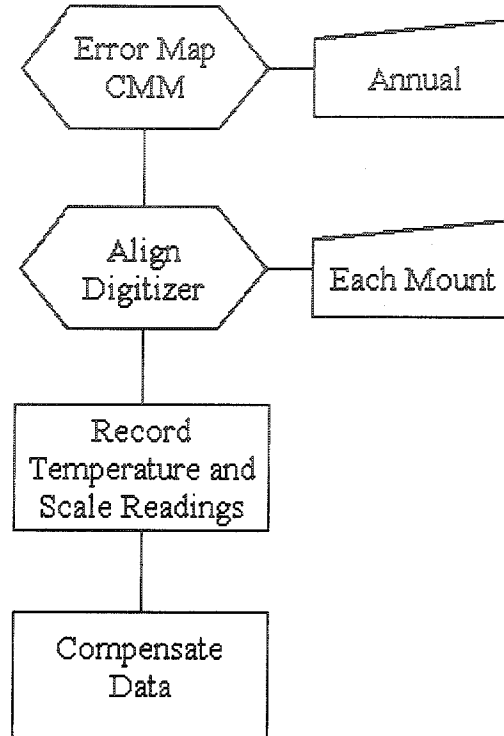


Figure 4-5 Digitizer Alignment

Because the laser digitizer is mounted so that it can rotate collinear with its W axis, it is convenient to describe its pose attitude in terms of Euler angles [Zeid 2000]. The Euler angles are the parameters of a sequence of three rotations used to define the orientation of the digitizer coordinate system with respect to the CMM coordinate system. The three rotations are to some extent arbitrary. The initial rotation can be taken about any of the coordinate axes. Each rotation is based on a previously rotated axis and there are twelve possible combinations of rotation sequences that can be chosen. The rotation matrix selected to describe the pose of the digitizer is the E3-1-3-sequence $[R] = \text{Rotate}(Z'', \gamma) \cdot \text{Rotate}(X', \beta) \cdot \text{Rotate}(Z, \alpha)$. The rotation axis of the mount for the

digitizer camera is the W axis, and is equivalent to the Z" axis. The Euler rotation matrix [R] is developed and given as [E₃₋₁₋₃] in equation 7 and equation 8.

In this method, three angles α, β and γ describe the angular position of a device. Each angle gives the rotation about a specific axis, and is measured from the result of the previous rotation.

The following equation for a rotation of θ about an arbitrary axis [u v w]^T is used to develop the digitizer alignment rotation matrix [R].

$$R(uvw, \theta) = \begin{bmatrix} \cos \theta + u^2 \cdot (1 - \cos \theta) & -w \cdot \sin \theta + u \cdot v \cdot (1 - \cos \theta) & v \cdot \sin \theta + u \cdot w \cdot (1 - \cos \theta) \\ w \cdot \sin \theta + u \cdot v \cdot (1 - \cos \theta) & \cos \theta + v^2 \cdot (1 - \cos \theta) & -u \cdot \sin \theta + v \cdot w \cdot (1 - \cos \theta) \\ -v \cdot \sin \theta + u \cdot w \cdot (1 - \cos \theta) & u \cdot \sin \theta + (1 - \cos \theta) & \cos \theta + w^2 \cdot (1 - \cos \theta) \end{bmatrix} \dots \dots \dots (2)$$

This work has chosen the first angle α to be a rotation about the global Z axis.

After the rotation about the Z axis, one obtains a new X' Y' Z' coordinate system.

$$\begin{aligned} [E_{3-0-0}] &= \text{Rot}(Z, \alpha) \\ &= \begin{bmatrix} \cos \alpha & -\sin \alpha & 0 \\ \sin \alpha & \cos \alpha & 0 \\ 0 & 0 & 1 \end{bmatrix} \dots \dots \dots (3) \end{aligned}$$

The second angle, β, is a rotation about the new transformed X' axis.

$$\begin{aligned}
 [E_{3-1-0}] &= \text{Rot}(X', \beta) \cdot \text{Rot}(Z, \alpha) \\
 &= \text{Rot}([\cos \alpha \quad \sin \alpha \quad 0], \beta) \cdot \text{Rot}(Z, \alpha) \\
 &= \begin{bmatrix} \cos \beta + \sin^2 \alpha \cdot (1 - \cos \beta) & \sin \alpha \cdot \cos \alpha \cdot (1 - \cos \beta) & \sin \alpha \cdot \sin \beta \\ \sin \alpha \cdot \cos \alpha \cdot (1 - \cos \beta) & \cos \beta + \sin^2 \alpha \cdot (1 - \cos \beta) & -\cos \alpha \cdot \sin \beta \\ -\sin \alpha \cdot \sin \beta & \cos \alpha \cdot \sin \beta & \cos \beta \end{bmatrix} \cdot \begin{bmatrix} \cos \alpha & -\sin \alpha & 0 \\ \sin \alpha & \cos \alpha & 0 \\ 0 & 0 & 1 \end{bmatrix}
 \end{aligned}$$

$$[E_{3-1-0}] = \begin{bmatrix} \cos \alpha & -\sin \alpha \cdot \cos \beta & \sin \alpha \cdot \sin \beta \\ \sin \alpha & \cos \alpha \cdot \cos \beta & -\cos \alpha \cdot \sin \beta \\ 0 & \sin \beta & \cos \beta \end{bmatrix} \dots \dots \dots (4)$$

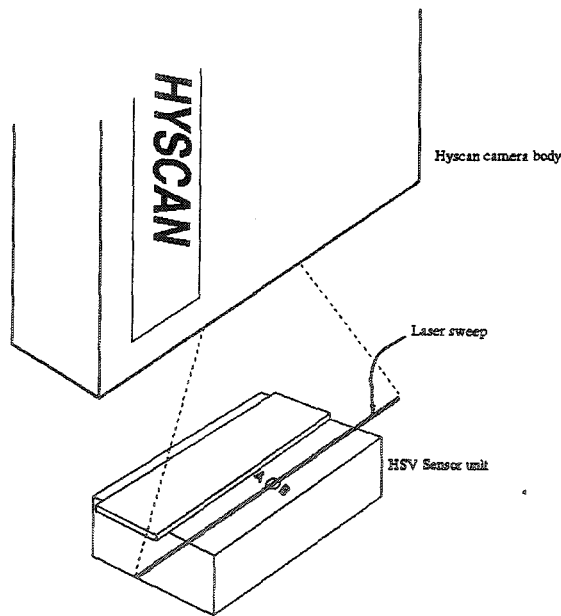


Figure 4-6 Optical Vernier [Hymarc]

At this point the Z'' axis is aligned with the W axis of the laser digitizer. The W axis extends positively outwards from the scanner back, perpendicular to the scan plane. The α and β angles can be determined, using an optical vernier such as the Hyscan optical vernier alignment device (HSV) (see Figure 4-6) to detect the location of the scan

plane. The HSV contains a dual photodiode detector and two LEDs to indicate on which side of the sensor the laser light is concentrated. Using the joystick, the CMM (and digitizer) is moved to three well-spaced points where the laser beam lands on the fixed HSV. The $[X \ Y \ Z]$ coordinates of the three discrete points in the scan plane are used to compute an equation of the scan plane in point vector format. Only the normal vector passing perpendicular through the plane $[x_p \ y_p \ z_p]$ is needed to compute the α and β angles.

$$\beta = \cos^{-1} z_p \dots\dots\dots(5)$$

$$\alpha = \sin^{-1} \left(\frac{x_p}{\sin \beta} \right) \dots\dots\dots(6)$$

The third Euler angle is rotated γ about the new Z" axis.

$$[E_{3-1-3}] = \begin{bmatrix} \cos \alpha \cdot \cos \gamma - \sin \alpha \cdot \cos \beta \cdot \sin \gamma & -\cos \alpha \cdot \sin \gamma - \sin \alpha \cdot \cos \beta \cdot \cos \gamma & \sin \alpha \cdot \sin \beta \\ \cos \alpha \cdot \cos \beta \cdot \sin \gamma + \sin \alpha \cdot \cos \gamma & \cos \alpha \cdot \cos \beta \cdot \cos \gamma - \sin \alpha \cdot \sin \gamma & -\cos \alpha \cdot \sin \beta \\ \sin \beta \cdot \sin \gamma & \sin \beta \cdot \cos \gamma & \cos \beta \end{bmatrix} \dots\dots\dots(7)$$

The γ angle can be determined by scanning a planar surface while moving the CMM, and fitting the data.

Alternatively, the $[E_{3-1-3}]$ rotation matrix for attitude can be expressed in terms of unit vectors in the laser digitizer coordinate reference frame (L). The unit vector in the

digitizer \bar{u} direction is $[\lambda_1 \ \mu_1 \ v_1]^T$. The unit vector in the digitizer \bar{v} direction is $[\lambda_2 \ \mu_2 \ v_2]^T$. The unit vector in the digitizer \bar{w} direction is $[\lambda_3 \ \mu_3 \ v_3]^T$.

$$[E_{3-1-3}] = \begin{bmatrix} \lambda_1 & \lambda_2 & \lambda_3 \\ \mu_1 & \mu_2 & \mu_3 \\ v_1 & v_2 & v_3 \end{bmatrix} \dots\dots\dots (8)$$

4.4. Laser Digitizer Alignment Calibration

The Euler Angle HTM accounts for the angular pose attitude of the digitizer. To complete the transformation of UV points into XYZ coordinate data a reference point is required. The calibration sphere on the ball tower is used for this. (See Figure 4-7.) The sphere is scanned and the scale readings $[D_0 \ E_0 \ F_0]$ are recorded when the CMM is located such that the origin of the laser digitizer coordinate system is aligned with the centre of the reference sphere. The scale readings are obtained from the opto-isolator in μm and the measurand is reported in mm. For any digitizer pose mount attitude, the alignment data is stored as six numbers $[\alpha \ \beta \ \gamma \ D_0 \ E_0 \ F_0]$. When measurements are taken, the $[U \ V]$ data are converted to three dimensional $[X \ Y \ Z]$ point coordinates with the following:

$$\begin{bmatrix} X \\ Y \\ Z \\ 1 \end{bmatrix} = \begin{bmatrix} \lambda_1 & \lambda_2 & \lambda_3 & -D_0 \\ \mu_1 & \mu_2 & \mu_3 & -E_0 \\ v_1 & v_2 & v_3 & -F_0 \\ 0 & 0 & 0 & 1 \end{bmatrix} \cdot \begin{bmatrix} u \\ v \\ 0 \\ 1 \end{bmatrix} + \begin{bmatrix} 1 & 0 & 0 & 0 \\ 0 & 1 & 0 & 0 \\ 0 & 0 & 1 & 0 \\ 0 & 0 & 0 & 1 \end{bmatrix} \cdot \begin{bmatrix} D \\ E \\ F \\ 1 \end{bmatrix} \dots\dots\dots (9)$$

where

$X Y Z$ = Position in global coordinates relative to the reference optical sphere used for alignment (R).

$u v$ = Position of measured point in the scan plane relative to the digitizer origin

D_0, E_0, F_0 = Offset of the laser digitizer mount position from model coordinates

$D E F$ = quadrature counts of scales on the CMM axes.

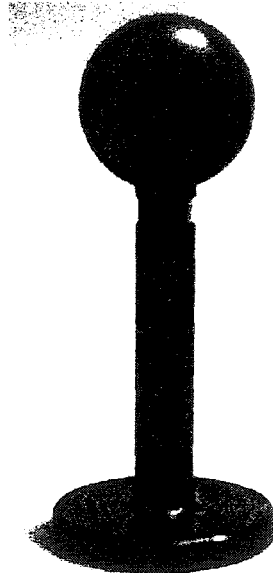


Figure 4-7 Ball Tower Calibration Sphere [Hymarc]

Since the trunnion accurately repositions the scanner at each incremental stop, any coordinate frame transformation that is computed can be stored in an alignment file to be recalled later.

Chapter 5

Error Compensation

For any structure of a CMM, such as moving bridge or horizontal arm, it is possible to create a geometric model of the CMM showing the relationship of each axis carriage to the end position of the measurement transducer [Bosch 1995]. A conventional coordinate measuring machine has three axis carriages mounted in orthogonal directions, providing a Cartesian coordinate system. Without loss of generality, the case presented here is a moving bridge XYZ kinematic CMM. (See Figure 1-1.) The X axis is mounted on the table; the Y axis is mounted on the bridge and the Z axis is mounted on the ram. Each axis or carriage has six inherent error sources: position in three dimensions and rotations about three axes. (See Figure 3-2.) There are three squareness errors identifying any deviation of the axes from being exactly 90° to each other.

5.1. Implementation Of Error Correction Scheme

Error compensation is applied to the pose of a laser digitizer, its position and attitude. The factors listed in Table 18 are used to generate error estimates. Position correction $[e_x \ e_y \ e_z]$ is calculated and applied as given in section 5.2. The use of homogeneous transformation matrices (HTM) is discussed in section 5.3. The attitude

correction for the scan plane of the laser digitizer is given in section 5.4. Measurements provided by the laser digitizer are adjusted and compensated as given in section 5.5.

Table 18 Pose Factors For Data Correction

Pose Factors Used to Correct Data; all are functions of (D, E, F)	
e_x	Total positional error in X direction $e_x = \delta_x(X) + \delta_x(Y) + \delta_x(Z)$
e_y	Total positional error in Y direction $e_y = \delta_y(X) + \delta_y(Y) + \delta_y(Z)$
e_z	Total positional error in Z direction $e_z = \delta_z(X) + \delta_z(Y) + \delta_z(Z)$
ϵ_x	Total angular error as a rotation about the X axis $\epsilon_x = \epsilon_x(x) + \epsilon_x(y) + \epsilon_x(z)$
ϵ_y	Total angular error as a rotation about the Y axis $\epsilon_y = \epsilon_y(x) + \epsilon_y(y) + \epsilon_y(z)$
ϵ_z	Total angular error as a rotation about the Z axis $\epsilon_z = \epsilon_z(x) + \epsilon_z(y) + \epsilon_z(z)$

To improve the overall accuracy, integration of the CMM error compensation with the laser digitizer scan plane coordinates was implemented accounting for quasi-static temperature variations.

5.2. CMM Position Error Compensation

With an X-Y-Z kinematic chain of the CMM, the angular errors of the X axis mounted on the table affect the true position of the bridge and the ram. The angular errors of the Y axis mounted on the bridge affect the true position of the ram. The angular errors of the Z axis mounted on the ram do not affect position, but will affect the transducer mounted on the ram. Kunzmann *et al.* [1995] listed the error factors for an Y-X-Z kinematic chain using VDI/VDE 2617 notation. Equation 10 provides the basic compensation, where the scale reading of the X axis is D, the scale reading of the Y axis is E, and the scale reading of the Z axis is F. The corrected position of the end of the ram of the CMM $[X \ Y \ Z]^T$ is given in equation 10 by a combination of the scale readings and the calculated errors. Equations 11 to 13 yield the measurement position errors in three directions at a given position $[D \ E \ F]^T$ indicated on the linear scales of the axes. The angular error terms use the measured angles in radians directly, using the small angle assumptions of $\cos \theta \approx 1$ and $\sin \theta \approx \theta$.

$$\begin{bmatrix} X \\ Y \\ Z \end{bmatrix} = \begin{bmatrix} D \\ E \\ F \end{bmatrix} + \begin{bmatrix} e_x \\ e_y \\ e_z \end{bmatrix} \dots\dots\dots (10)$$

$$e_x = \delta_x(x) + \delta_x(y) + \delta_x(z) - E \cdot \epsilon_z(x) + F \cdot \epsilon_y(x) + F \cdot \epsilon_y(y) - E \cdot S_{xy} - F \cdot S_{xz} \dots (11)$$

$$e_y = \delta_y(x) + \delta_y(y) + \delta_y(z) - F \cdot \epsilon_x(y) - F \cdot \epsilon_x(x) - F \cdot S_{yz} \dots\dots\dots (12)$$

$$e_z = \delta_z(x) + \delta_z(y) + \delta_z(z) + E \cdot \epsilon_x(x) \dots\dots\dots (13)$$

5.3. HTM For Laser Digitizer Alignment

The HTM for digitizer calibration alignment developed in chapter 4 uses the position of the optical calibration sphere as its reference point (R) for the values of [X Y Z] calculated from the digitizer [u v] coordinates measured from the laser origin (L).

$${}^R \begin{bmatrix} X \\ Y \\ Z \\ 1 \end{bmatrix} = \begin{bmatrix} & D - D_0 \\ [E_{3-1-3}] & E - E_0 \\ & F - F_0 \\ 0 & 0 & 0 & 1 \end{bmatrix} \cdot {}^L \begin{bmatrix} U \\ V \\ W \\ 1 \end{bmatrix} \dots\dots\dots (14)$$

To apply CMM error correction it is necessary to expand the information to include the CMM home point (H) from which geometric component errors are measured. The position of the CMM is located using an up/down quadrature counter that starts at zero when power is applied to the CMM controller. To enable software compensation, the CMM is manually moved to the extreme end of all axes where "end of travel" limit switches are detected and a home (H) position is defined for the global coordinate system.

$${}^H \begin{bmatrix} X \\ Y \\ Z \\ 1 \end{bmatrix} = \begin{bmatrix} & D \\ [E_{3-1-3}] & E \\ & F \\ 0 & 0 & 0 & 1 \end{bmatrix} {}^L \begin{bmatrix} U \\ V \\ W \\ 1 \end{bmatrix} \dots\dots\dots (15)$$

An intermediate step requires determining the location (P) at the end of the ram, which determines the pose of the digitizer. (See Figure 5-1.) The origin (L) of the laser digitizer [u v] scan plane is located outside the laser digitizer box and is shown located at the centre of the calibration sphere. The point in the trunnion that is the centre of rotation in two directions is defined as the mount point (P). The distance in the \bar{v} direction from the origin of the digitizer coordinates to the mount point is V1. The distance in the \bar{w} direction from the origin of the digitizer coordinates to the mount point is W1.

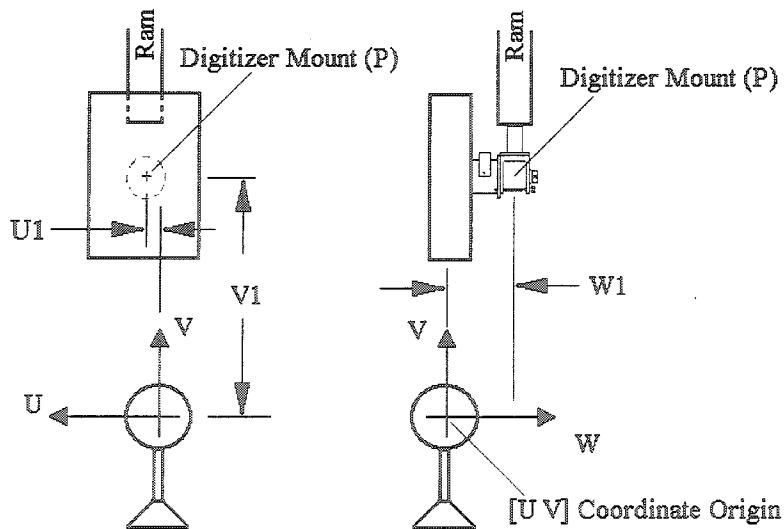


Figure 5-1 Laser Digitizer At $\gamma = 0^\circ$

The physical distance from the laser origin to the pose point is constant and given by $[U_1 \ V_1 \ W_1]$. These values can be obtained by evaluating the $[D_0 \ E_0 \ F_0]$ values obtained from three different laser digitizer alignments:

- 1) The W axis aligned with the X axis ($\alpha = 90^\circ, \beta = 90^\circ$) and a γ angle of 0° ,
- 2) The W axis aligned with the X axis and a γ angle of 90° , and
- 3) The W axis aligned with the Y axis ($\alpha = 180^\circ, \beta = 90^\circ$) and a γ angle of 0° .

The ball tower calibration sphere, Figure 4-7, is located on the CMM in a fixed position $[D_0 \ E_0 \ F_0]$ and the position of the end of the ram is determined when the origin of the digitizer coordinate system is aligned with the centre of the calibration sphere. The coordinates of the ram when the digitizer is in alignment 1 are designated $[D_1 \ E_1 \ F_1]$. Likewise the ram coordinates when the digitizer is in alignment 2 are designated $[D_2 \ E_2 \ F_2]$ and alignment 3 are designated $[D_3 \ E_3 \ F_3]$. This yields the following equations for the position of the reference sphere in terms of ram coordinates and digitizer dimensions:

$$[D_0 \ E_0 \ F_0] = [(D_1 - W_1) \ (E_1 - U_1) \ (F_1 - V_1)] \dots\dots\dots (16)$$

$$[D_0 \ E_0 \ F_0] = [(D_2 - W_1) \ (E_2 + V_1) \ (F_2 - U_1)] \dots\dots\dots (17)$$

$$[D_0 \ E_0 \ F_0] = [(D_3 + U_1) \ (E_3 - W_1) \ (F_3 - V_1)] \dots\dots\dots (18)$$

Of the nine axis dimensional component equations, only six are independent. For example, by inspection $D_1 = D_2$ and $F_1 = F_3$.

$$U_1 = \frac{1}{2}(E_1 - E_2 + F_2 - F_1) \dots\dots\dots(19)$$

$$V_1 = \frac{1}{2}(E_1 - E_2 + F_1 - F_2) \dots\dots\dots(20)$$

$$W_1 = \frac{1}{2}(D_1 + 2 \cdot D_3 - E_2 + F_2 - F_1) \dots\dots\dots(21)$$

For the Hyscan 45C used, these values were $U_1 = 1.001$ mm, $V_1 = 264.505$ mm, $W_1 = 129.575$ mm. The uncertainty associated with each of the dimensions of the digitizer was approximately 40 μ m caused by 1) the 9 μ m probing uncertainty of the digitizer measurement, 2) the 10 μ m uncertainty of the sphere fitting program that calculates the centre of the reference sphere, and 3) the uncertainty caused by scale error (2 μ m for X, 16.5 μ m for Y and 1 μ m for the Z scale). The scale uncertainty was determined using the range of values for measured positions. For example, the range of X scale values used was 276 mm to 405 mm and testing was done at ambient temperature, so the error map of appendix B is used. The X scale linear error at 275 mm is 4 μ m, and at 425 mm is 8 μ m, giving an average scale error of 6 ± 2 μ m, or an uncertainty of ± 2 μ m for the X scale value. The 10 μ m uncertainty of the sphere fitting program is related to a three dimensional position, so the contribution to an individual axis component reading, either D, E or F, is $\frac{10}{\sqrt{3}} = 5.8$ μ m. We are trying to measure the size of the digitizer as three dimensions in orthogonal coordinates. The final size is the distance from the end of the ram to the imaginary point in front of the digitizer in three dimensional coordinates [U V W]. The imaginary point is approximately positioned

60 mm in front of the digitizer. This distance is measured by using data from three different alignments of the digitizer measuring a sphere in space. Data from the CMM, the digitizer and the calculation of the centre of the sphere is used for this. The final three dimensional coordinates of this distance are reported as $[U \ V \ W]$ (perpendicular coordinate frame) as outlined in Figure 5-1. These values are calculated using equations 19, 20, 21 with scale readings $[D_1 \ E_1 \ F_1]$, $[D_2 \ E_2 \ F_2]$, $[D_3 \ E_3 \ F_3]$ from the CMM $[X \ Y \ Z]$, 20,000 data points from the digitizer measuring the surface of the sphere, and the calculated centre of the sphere from the surface points (using the NIST algorithm Ref. Rosenfeld NISTIR 5674), for the three different digitizer alignments. Each of the values for these three measurements has uncertainty. The underlying relationships of uncertainties for these equations are captured in equations 22, 23, 24 which are based on the directional components of the error map coming from the CMM, the error coming from the digitizer which is limited to the UV plane and in this case is aligned with the direction of interest in each of the three cases and the error from the calculation of the centre of the sphere.

The directional components of the error map were measured as $2\mu\text{m}$ for X, $16.5\mu\text{m}$ for Y, and $1\mu\text{m}$ for Z. The uncertainty of the error from the digitizer is based on the manufactures specification of $9\mu\text{m}$. This value is used as the uncertainty for each of the three components of distance reported by the digitizer. This conservative estimate is used because there is no data available to relate the UV coordinates with the XYZ reported point on the surface of the sphere. The $10\mu\text{m}$ value for the calculation of the centre of

the sphere is based on a NIST standard (Ref. Rosenfeld NISTIR 5674). The treatment of this centre uncertainty is that its value is the same in all three coordinate directions so a volumetric approach can be taken which evenly distributes this uncertainty over the three orthogonal coordinate directions. $10 = \sqrt{5.8^2 + 5.8^2 + 5.8^2}$ which is $\frac{10 \mu\text{m}}{\sqrt{3}}$. Once the uncertainties are all in a three coordinate direction form they can be consistently handled in equations 22, 23 and 24.

For the uncertainty of U_1 , $u(U_1)$, the uncertainties of E_1 and E_2 are equivalent and can be combined, and the uncertainties of F_1 and F_2 are equivalent and can be combined using: [ISO GUM 1995, equation 10].

$$\begin{aligned}
 u^2(U_1) &= \frac{1}{4}(u^2(E_1) + u^2(E_2) + u^2(F_2) + u^2(F_1)) \\
 &= \frac{1}{4}(2 \cdot u^2(E_1) + 2 \cdot u^2(F_1)) \\
 &= \frac{1}{2}(u^2(E_1) + u^2(F_1)) \dots\dots\dots(22) \\
 &= \frac{1}{2}((9^2 + 5.8^2 + 16.5^2) + (9^2 + 5.8^2 + 1^2)) \\
 u(U_1) &= 35.1 \mu\text{m}
 \end{aligned}$$

$$\begin{aligned}
 u^2(V_1) &= \frac{1}{4}(u^2(E_1) + u^2(E_2) + u^2(F_1) + u^2(F_2)) \\
 &= u^2(U_1) \dots\dots\dots(23) \\
 u(V_1) &= 35.1 \mu\text{m}
 \end{aligned}$$

$$\begin{aligned}
 u^2(W_1) &= \frac{1}{4} \left(u^2(D_1) + 4 \cdot u^2(D_3) + u^2(E_2) + u^2(F_2) + u^2(F_1) \right) \\
 &= \frac{1}{4} \left(5 \cdot u^2(D_1) + u^2(E_1) + 4 \cdot u^2(F_1) \right) \\
 &= \frac{5}{4} u^2(D_1) + \frac{1}{4} u^2(E_1) + u^2(F_1) \quad \dots\dots\dots(24) \\
 &= \frac{5}{4} (9^2 + 5.8^2 + 2^2) + \frac{1}{4} (9^2 + 5.8^2 + 16.5^2) + (9^2 + 5.8^2 + 1^2) \\
 u(W_1) &= 39.9 \mu\text{m}
 \end{aligned}$$

Including uncertainty, the dimensional values of the offset from the laser digitizer origin to the end of the ram are $U_1 = 1.00 \pm 0.04$ mm, $V_1 = 264.51 \pm 0.04$ mm, and $W_1 = 129.58 \pm 0.04$ mm. While being aware of the limitations of the determined uncertainties, compensation calculations were performed with numbers to the 1 μm level. Because we are dealing with accuracy obtained by a complex compensation algorithm, we carry as many digits of resolution as reasonable to reduce computer round-off error. At the end of all computations, the uncertainty of the result is considered.

The effect of the uncertainty of the U_1 , V_1 and W_1 values was evaluated to have minimal effect as follows. The position of the spot measured by the digitizer is to be compensated using the angular error from the error map and the digitizer dimensions. The maximum value of rotational error is 3.8 arc-seconds on the Z axis and the maximum squareness error is the XY error of 169.4 arc-seconds for a worst case angle of 173.2 arc-seconds. The correction factor is the tangent of the error angle times the dimension. The resulting uncertainty in the compensation of pose due to uncertainty in digitizer dimensions is $u = 40 \mu\text{m} \cdot \tan(173.2 \text{ a-s}) = 0.04 \mu\text{m}$. This uncertainty is two

orders of magnitude less than the 9 μm measurement variability that will be seen in chapter 6.

When converting to a coordinate reference frame aligned with the global CMM coordinate frame, the displacement offset from the laser origin (L) to the pose origin is affected by whatever angles have been selected for the digitizer pose. The measurement data, aligned with the world coordinate system and relative to the pose origin, is given by equation 25.

$${}^P \begin{bmatrix} X \\ Y \\ Z \\ 1 \end{bmatrix} = \begin{bmatrix} [E_{3-1-3}] & \begin{bmatrix} [E_{3-1-3}] \cdot \begin{bmatrix} -U_1 \\ -V_1 \\ -W_1 \end{bmatrix} \\ 1 \end{bmatrix} \end{bmatrix} \cdot {}^L \begin{bmatrix} U \\ V \\ W \\ 1 \end{bmatrix} \dots\dots\dots (25)$$

5.4. Error Correction For Attitude Of Laser Digitizer Mount

To develop a concise homogeneous transformation matrix, the rotation error measurements are combined. Nine terms describing the cosines of the solid angles of the new reference frame are required for the rotation part of the HTM.

$$\epsilon_X = \epsilon_X(X) + \epsilon_X(Y) + \epsilon_X(Z) \dots\dots\dots (26)$$

$$\epsilon_Y = \epsilon_Y(X) + \epsilon_Y(Y) + \epsilon_Y(Z) \dots\dots\dots (27)$$

$$\epsilon_Z = \epsilon_Z(X) + \epsilon_Z(Y) + \epsilon_Z(Z) \dots\dots\dots (28)$$

To maintain an orthogonal coordinates system, the measured plane angles are combined for each axis of rotation and then the axis directions are calculated.

The angular errors of the CMM accumulate to provide a pose attitude that is not aligned with the world coordinate system as indicated by the previous $[E_{3-1-3}]$ matrix.

A new HTM is developed to correct for the orientation error. Taking the Z-axis as the axis of primary concern, we combine two angular rotation errors, ϵ_X and ϵ_Y , to find the orientation of the \vec{Z}_p axis in terms of its direction cosines in the world coordinate system. $\vec{Z}_p = fn(\epsilon_X, \epsilon_Y)$

$$[\vec{Z}_p] = \begin{bmatrix} \frac{\tan \epsilon_Y}{\sqrt{1 + \tan^2 \epsilon_X + \tan^2 \epsilon_Y}} \\ \frac{-\tan \epsilon_X}{\sqrt{1 + \tan^2 \epsilon_X + \tan^2 \epsilon_Y}} \\ 1 \\ \sqrt{1 + \tan^2 \epsilon_X + \tan^2 \epsilon_Y} \end{bmatrix} \dots\dots\dots (29)$$

Taking the X axis next, we include the third angular error to find the \vec{X}_p axis as the intersection of two planes, one defined normal to \vec{Z}_p and one defined by ϵ_Z .

$$\vec{X}_p = fn(\epsilon_X, \vec{Z}_p)$$

$$\left[\bar{X}_P \right] = \begin{bmatrix} \frac{1}{\sqrt{1 + \tan^2 \epsilon_Z + (\tan \epsilon_X \cdot \tan \epsilon_Z + \tan \epsilon_Y)^2}} \\ \frac{-\tan \epsilon_Z}{\sqrt{1 + \tan^2 \epsilon_Z + (\tan \epsilon_X \cdot \tan \epsilon_Z + \tan \epsilon_Y)^2}} \\ \frac{-(\tan \epsilon_X \cdot \tan \epsilon_Z + \tan \epsilon_Y)}{\sqrt{1 + \tan^2 \epsilon_Z + (\tan \epsilon_X \cdot \tan \epsilon_Z + \tan \epsilon_Y)^2}} \end{bmatrix} \dots\dots\dots (30)$$

The Y-axis is calculated as a cross product of the other two axes to make an orthogonal

system. $\bar{Y}_P = fn(\bar{X}_P, \bar{Z}_P)$

$$\left[\bar{Y}_P \right] = \left[\bar{Z}_P \right] \times \left[\bar{X}_P \right] \dots\dots\dots (31)$$

The rotation correction matrix is

$$\left[\text{HTM} \right]_{\text{Rcorrection}} = \begin{bmatrix} \left[\bar{X}_P \right] & \left[\bar{Y}_P \right] & \left[\bar{Z}_P \right] & 0 \\ 0 & 0 & 0 & 1 \end{bmatrix} \dots\dots\dots (32)$$

5.5. Laser Digitizer Pose Attitude And Position Compensation

The measured data relative to the pose origin can be corrected with equation 33 for the orientation error based on the CMM position. The corrected position data, with respect to the home of the CMM is given by:

$${}^H \begin{bmatrix} X \\ Y \\ Z \\ 1 \end{bmatrix} = \begin{bmatrix} & & & D+e_x \\ [\bar{X}_p] & [\bar{Y}_p] & [\bar{Z}_p] & E+e_y \\ & & & F+e_z \\ 0 & 0 & 0 & 1 \end{bmatrix} {}^P \begin{bmatrix} X \\ Y \\ Z \\ 1 \end{bmatrix} \dots\dots\dots (33)$$

where $[D \ E \ F]^T$ represents the moving coordinate frame of the CMM, $[e_x \ e_y \ e_z]^T$ represents the positional errors, $[\bar{X}_p \ \bar{Y}_p \ \bar{Z}_p]$ represents the angular errors and all twelve of the error terms of the homogeneous transformation matrix are functions of (D, E, F).

5.6. Interpolation Between Map Points

The HTM that corrects for position and attitude can be applied, based on the measured values of position and angular error at the recorded $[D \ E \ F]^T$ coordinates. For each CMM coordinate, the error table is searched for the closest points on each axis, and the position and angle error values are linearly interpolated for the 18 position and angular errors. Linear interpolation was selected instead of a higher order approximation because the error map points are closely spaced compared to the length of the CMM axis and the range of error measurements at any point (i.e. see Figure 3-13) was comparable to the difference in error measurement between mapped points. The squareness error is considered constant to calculate the HTM.

The corrected position data, with respect to the home of the CMM is given by:

$${}^H \begin{bmatrix} X \\ Y \\ Z \\ 1 \end{bmatrix} = \begin{bmatrix} [\bar{X}_P] & [\bar{Y}_P] & [\bar{Z}_P] & D+e_x \\ 0 & 0 & 0 & E+e_y \\ & & & F+e_z \\ & & & 1 \end{bmatrix} \cdot {}^P \begin{bmatrix} X \\ Y \\ Z \\ 1 \end{bmatrix} \dots\dots\dots (34)$$

where $[D \ E \ F]^T$ represents the moving coordinate frame of the CMM and all the terms of the homogeneous transformation matrix are functions of (D, E, F).

The transformation given in equation 35 provides error compensation and converts from $[u \ v]$ scan plane coordinates to $[X \ Y \ Z]$ CMM global coordinates.

$${}^H \begin{bmatrix} X \\ Y \\ Z \\ 1 \end{bmatrix} = \begin{bmatrix} [\bar{X}_P] & [\bar{Y}_P] & [\bar{Z}_P] & D+e_x \\ 0 & 0 & 0 & E+e_y \\ & & & F+e_z \\ & & & 1 \end{bmatrix} \cdot \begin{bmatrix} [E_{3-1-3}] & \begin{bmatrix} -U_1 \\ -V_1 \\ -W_1 \end{bmatrix} \\ 0 \ 0 \ 0 & 1 \end{bmatrix} \cdot {}^L \begin{bmatrix} U \\ V \\ W \\ 1 \end{bmatrix} \dots\dots (35)$$

The values of $[U_1 \ V_1 \ W_1]^T$ only need to be measured once. The digitizer alignment values that provide the $[E_{3-1-3}]$ matrix need to be measured every time the laser digitizer is repositioned on the CMM ram. The error compensation values $[\bar{X}_P]$, $[\bar{Y}_P]$, $[\bar{Z}_P]$, and $[e_x \ e_y \ e_z]^T$ need to be calculated for each point.

5.7. Summary

The equations in this chapter provide a conversion from $[u \ v]$ laser digitizer scan plane coordinates and $[D \ E \ F]$ CMM scale coordinates to $[X \ Y \ Z]$ global CMM

coordinates, including compensation for both the geometric errors of the CMM at various temperatures and the angular errors affecting the pose of the laser digitizer mounted at the end of the CMM ram.

Chapter 6

Test Results And Analysis

6.1. Tests

To implement the error compensation, the scan plane coordinates, the CMM axis scale positions and temperature were recorded simultaneously in real time. The CMM error compensation data was then used to post process the scan plane coordinates to obtain improved global part coordinates. Three sets of tests were performed to validate the algorithm developed in the previous section.

The first set of tests was the evaluation of crossed ballbars using different camera alignments. These tests, called "Initial Squareness Tests", are given in section 6.2 and confirm that the algorithm is valid for various alignments of the camera.

The second set of tests was a volumetric evaluation of the CMM at ambient temperature, using the ballbar positions recommended in ASME standard B89 [1997]. These tests are given in section 6.3 and confirm that the compensation was valid over the volume of the coordinate measuring machine.

The third set of tests was a volumetric evaluation of the CMM at three different temperatures. These tests are given in section 6.4 and demonstrate the effectiveness of the compensation at different temperatures.

The evaluation of the results is done, based on the auto-calibration techniques of section 2.6, with an analysis of the dispersion of the measured ballbar length at various positions. To report accuracy, the ASME B89 CMM Calibration Standard (section 2.6.1) gives a single number representing the maximum error measured at any of the twenty positions. Here in this chapter on tests and analysis, the accuracy is reported by a single number representing the differences measured at all positions. The number is called the "rms accuracy error" and is calculated using the following formula:

$$\text{rms accuracy error} = \sqrt{\frac{1}{n-1} \sum_{i=1}^n (X_i - \bar{X})^2} \dots\dots\dots (36)$$

where $(X_i - \bar{X})$ is the error of an individual measurement of the ballbar length.

This ensures the improvement reported for the compensation represents the entire measuring volume rather than just the one worst case position. The ballbar is a constant length and the differences in measured length are primarily due to the geometric error of the coordinate measuring machine with a small residue due to measurement uncertainty. In the first set of tests, given in section 6.2, the accuracy of uncompensated data was of the order of 200 μm and the accuracy of compensated data was of the order of 10 μm . The accuracy of the uncompensated data may be considered to be composed of geometric error and measurement uncertainty. The accuracy of the compensated data may be considered to be composed of only the measurement uncertainty. The reported improvement in accuracy, the difference between uncompensated and compensated values, represents the average reduction of geometric error throughout the entire working volume of the CMM.

6.1.1. Equipment

Measurements were made on a ballbar artefact. To avoid problems with specular reflections, a special ballbar was made with optically coated spheres at each end. The spheres were obtained by removing them from calibration towers (see Figure 4-7) purchased from Hymarc. The grey painted spheres were made of grade 200 ball bearings, which were 76.25 mm in diameter. The bar was approximately 404 mm between the sphere centres.

The CMM was a DEA model Iota 1102 and it had 11 type-E thermocouples mounted on it interfaced to a temperature-recording computer. There were three thermocouples on each axis, one on the top of the granite table and one on the bottom of the granite table.

6.1.2. Measurements On Sphere

The digitizer was aligned at an angle suitable for scanning the spheres at the ends of the ballbar and its calibration was stored prior to measurements. For the initial tests with crossed ballbar positions, the W axis of the digitizer was aligned with both the X axis and with the Y axis. For the rest of the measurements, the W axis of the digitizer was always aligned with the X axis and the γ angle selected based on the position of the ballbar. Each time the γ angle was changed, the digitizer calibration was confirmed before taking measurements. The CMM was manually positioned near the sphere at the end of the ballbar and two of the CMM axes were locked. Scanning with the digitizer

was performed while moving one CMM axis, taking care to collect data from the sphere only and not the bar.

6.1.3. Calculation Of Sphere Centre

Measurements of the spheres at each end of the ballbar were taken, with the ballbar at various locations in the volume. The raw data was manually inspected to ensure that only points on the spheres were included. Points that were measured on the bar would cause errors in estimating the centre of the sphere, and were removed if they were included in the data set. The raw data was saved, and a MATLAB based computer program calculated the compensated values. For each of the data sets, uncompensated and compensated, a computer program was used to calculate the sphere centre using the NIST ATS program [Rosenfeld 1996]. The algorithm for sphere fitting calculates the centre point and radius using orthogonal least squares fitting.

6.1.4. Interpolation Between Error Map Points

For the testing at ambient temperature, the error map of Appendix B was used. For each CMM coordinate, the error table is searched for the closest points on each axis, and the position and angle error values are linearly interpolated for the 18 position and angular errors. The squareness error is considered constant.

For the testing at controlled temperatures, the three error maps were based on the data presented in the graphs in Chapter 3.

6.2. Initial Squareness Tests (22 °C)

6.2.1. Measurements Of XY Squareness Using Ballbar

To verify the developed algorithm, an initial set of tests was performed at an ambient temperature of 22 °C. The ballbar unit was placed at various positions on the table and the spheres were scanned with the laser digitizer. Position 1 was near the home position with the bar pointing at 45°. (See Figure 6-1.) The bar was then rotated 90 degrees and the spheres were measured in their new position. Position 2 of the ballbar is also shown in Figure 6-1. Likewise, each pair of test positions overlapped.

Four positions were measured with the laser digitizer aligned such that the W axis was collinear with the CMM X axis, as illustrated in Figure 4-2 and photographed in Figure 6-3. The same four positions were measured with a different orientation of the laser digitizer. The laser digitizer was re-oriented so that the W axis was collinear with the Y axis. To identify the difference in digitizer alignment, the test data was identified as positions 5 to 8.

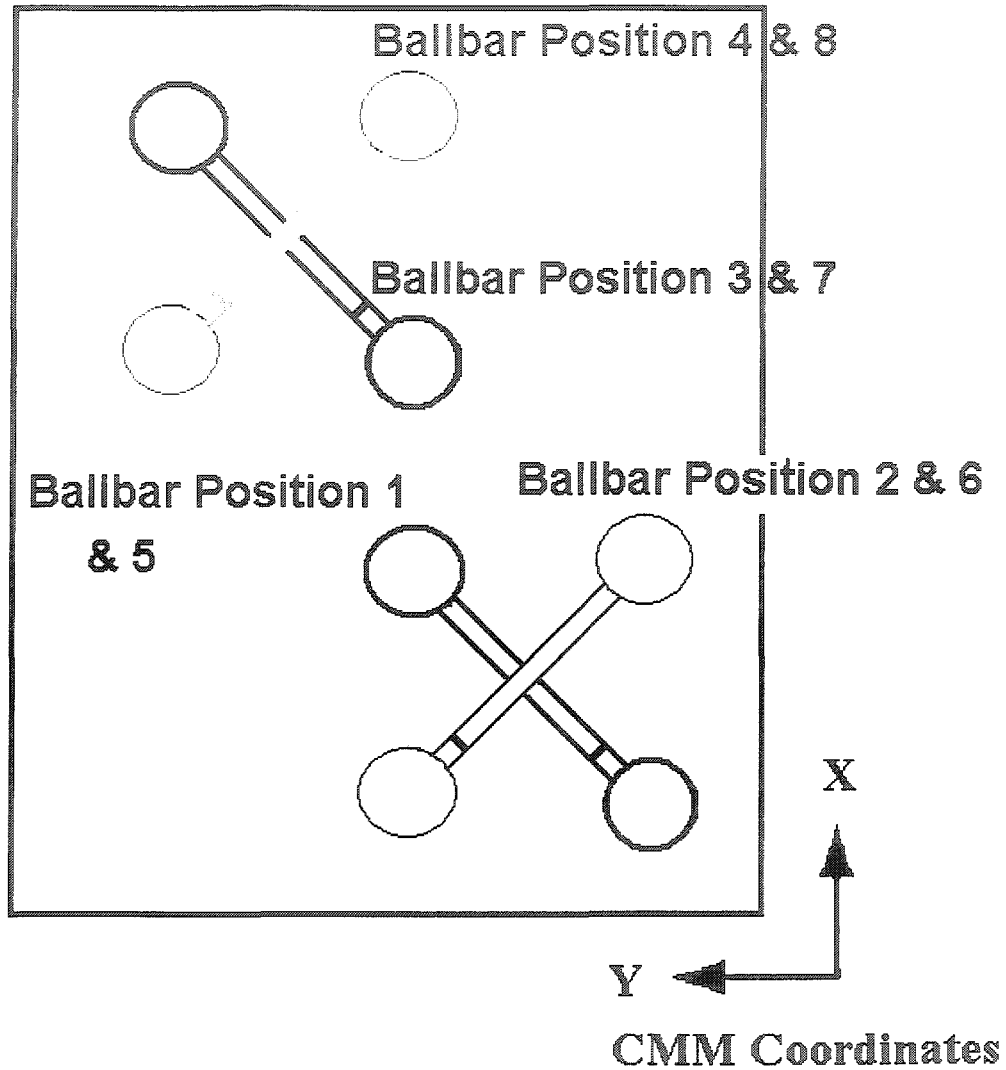


Figure 6-1 Ballbar Position For Squareness Tests

The first four positions were measured with the laser digitizer aligned ($\alpha = 90^\circ$, $\beta = 90^\circ$, $\gamma = 0^\circ$) such that the W axis was collinear with the CMM X axis, as shown in Figure 5-1 and Figure 4-2. The laser digitizer was re-oriented ($\alpha = 0^\circ$, $\beta = -90^\circ$, $\gamma = 0^\circ$) so that the W axis was collinear with the Y axis before repeating the measurements.

Position 1 was identified when the digitizer W axis was aligned with the CMM X axis and was identified as position 5 when the digitizer was aligned with the Y axis.

Approximately 12,000 points were collected for each sphere. Only the top portion of the sphere, visible to the laser digitizer above it, was recorded. Data collection included the uncompensated XYZ position reported by the laser digitizer, the U-V scan plane coordinates and the DEF axis scale readings. The CMM error map was known from laser interferometer measurements. The laser digitizer pose alignment was known from the camera calibration data.

6.2.2. Results Of Squareness Tests

Sphere centres were calculated using the NIST ATS least squares fit algorithm [Rosenfeld 1996], from the uncompensated XYZ measurements and the length of the ballbar was determined, and plotted on Figure 6-4. With a single measurement uncertainty of 26 μm , the length had an rms accuracy error of 171 μm for the eight positions measured. In the compensation of the measurements, we are correcting for the geometric error of the CMM at different locations in the working volume and the effect it has on the digitizer mount, so it is appropriate to compare accuracy using rms accuracy error, which contains the variability at all measured positions. New values of XYZ were calculated from the U-V scan plane coordinates and the DEF axis scale readings using the proposed error compensation algorithm. The sphere centres and ballbar length were calculated for the compensated values. These are also plotted in Figure 6-4. The

accuracy of the length of the ballbar, using compensated data, had an rms accuracy error of $6 \mu\text{m}$ with a single measurement uncertainty of $20 \mu\text{m}$.

6.2.3. Analysis Of Squareness Tests

A definite periodicity is seen in the results shown in Figure 6-4. Positions 1 and 5 are the same position on the CMM table; the difference is the orientation of the digitizer. The results are the same whether the digitizer is oriented in the direction of the X axis (positions 1 to 4) or in the direction of the Y axis (positions 5 to 8). The two orientations of the laser digitizer were used to confirm the correctness of angle directions and associated signs in the developed equations.

The calculated length of the ballbar using raw, or uncompensated, data shows a definite sensitivity to the bar orientation. Positions 1, 3, 5 and 7 show an elongation of the measured ballbar length. Positions 2, 4, 6 and 8 show a contraction of the measured ballbar length. This indicates a significant squareness error component in the error map of the machine. The XY squareness error of the IOTA 1102 was measured as 169 arc-seconds. Using the uncompensated sphere centres the XY squareness error is estimated at 152 arc-seconds.

The eight estimates of length, based on uncompensated data, had an rms accuracy error of $171 \mu\text{m}$. When the compensated data was used there was much less variation, the ballbar length measurements had an rms accuracy error of $6 \mu\text{m}$. The uncertainty in the rms accuracy error is the same as the uncertainty in ballbar length. For the uncompensated data, the uncertainty of a single measurement was $\pm 26 \mu\text{m}$ as given

in section 6.4.1 for 20 °C measurements. For the compensated data, the uncertainty of a single measurement was $\pm 20 \mu\text{m}$ as given below. The uncertainty of the rms accuracy error was the uncertainty of single measurement divided by the square root of 8 which was the number of positions. The pose error compensation scheme provided the digitizer data with an order of magnitude improvement in accuracy.

The effectiveness of the proposed compensation has been confirmed and the compensation algorithm correctly handled various digitizer pose attitudes. For the 400 mm length of the ballbar the geometric errors of the CMM are significant and are corrected for by the proposed algorithm. The uncertainty of the sphere centre using compensated measurement is composed of two elements, the $\pm 9 \mu\text{m}$ digitizer point accuracy [Hymarc] and the $10 \mu\text{m}$ uncertainty of sphere centre fitting algorithm (displayed in the column labelled “Fit” in Figure C-2) [Rosenfeld 1996]. Using: [ISO GUM 1995, equation 10], there is a variance of $u_p^2 = (9^2 + 10^2)$, or $\pm 14 \mu\text{m}$ uncertainty for the sphere centre at each end of the ballbar, so there is a variance of $u_L^2 = (14^2 + 14^2)$ or a $\pm 20 \mu\text{m}$ uncertainty in an individual calculation of the length of the ballbar. When many measurements are taken and the covariance of the measurements is zero, the uncertainty of the mean is divided by the square root of the number of measurements. This results in a length measurement uncertainty of $\frac{20}{\sqrt{8}} = 7 \mu\text{m}$ which is of the same order of magnitude as the rms accuracy error of $6 \mu\text{m}$ of the compensated measurements and much less than the $171 \mu\text{m}$ rms accuracy error of uncompensated measurements.

This shows that the variability in uncompensated measurements can be attributed to geometric error. The pose error compensation scheme provided the digitizer data with an order of magnitude improvement for the squareness error.

6.3. Volumetric Tests At Ambient Temperature (22 °C)

A second set of test measurements was taken at an ambient temperature of 22 °C. Measurements were made on the ballbar throughout the entire volume of the CMM, specifically at the 20 positions specified in B89.4 figure 26 [ASME 1997] reproduced as Figure 6-2. The spheres were 76.25 mm in diameter and the bar was approximately 404 mm between the sphere centres. The error table given in Appendix B was used.

For each intended pose orientation, the laser digitizer was calibrated to obtain the alignment parameters. The ballbar was then measured at the 20 specified positions. For each point, the $[U \ V \ W]^T$ and $[D \ E \ F]^T$ coordinates were collected. Approximately 17,000 points were measured on each sphere. The sphere centres and ballbar lengths were calculated as before using the matrix procedure described in Chapter 5 to compensate each point, and the sphere centres were located using orthogonal least squares.

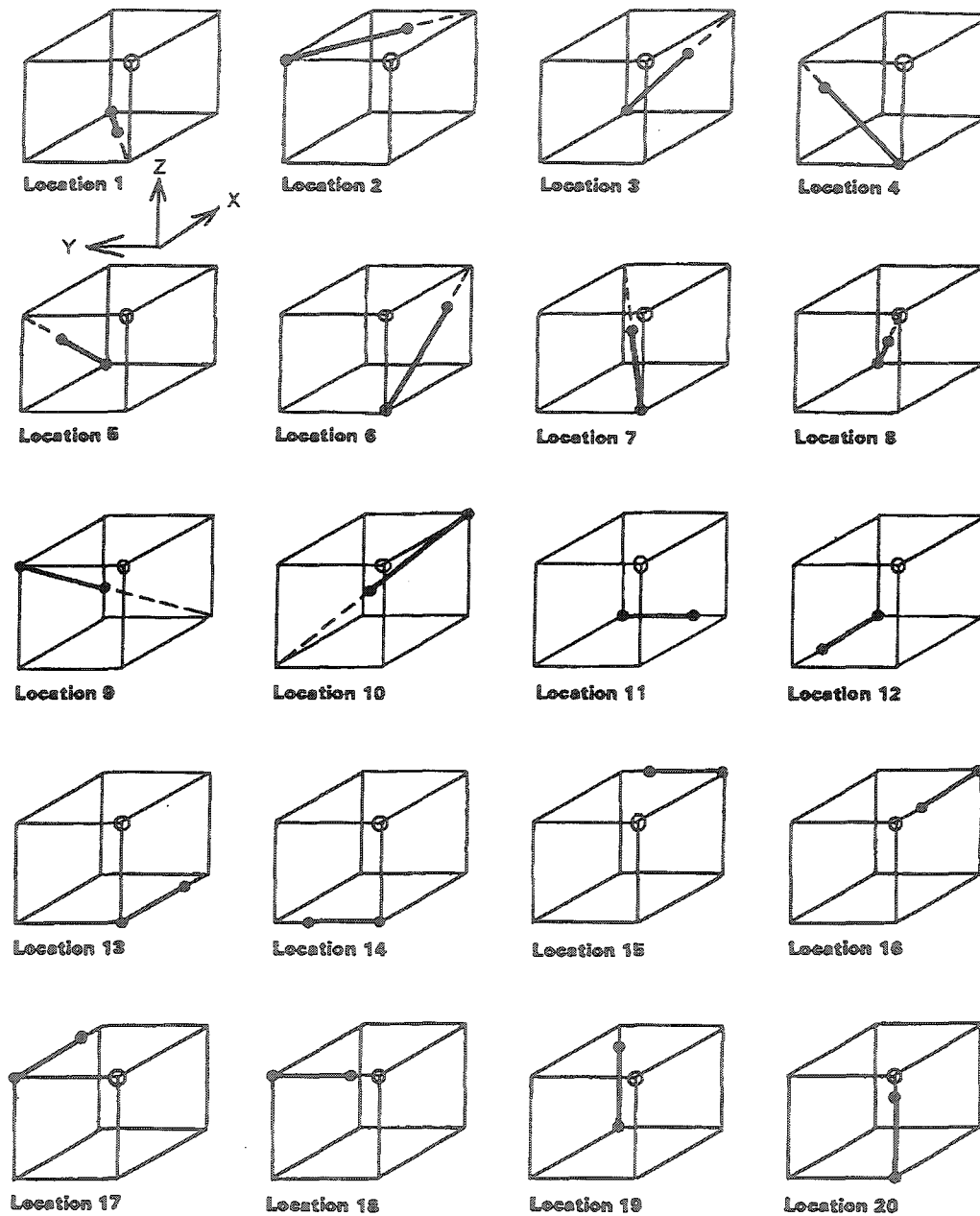


FIG. 26 RECOMMENDED BALL BAR POSITIONS FOR MACHINES WITH NEARLY CUBIC WORK ZONES

Figure 6-2 B89 Test Positions [ASME 1997]

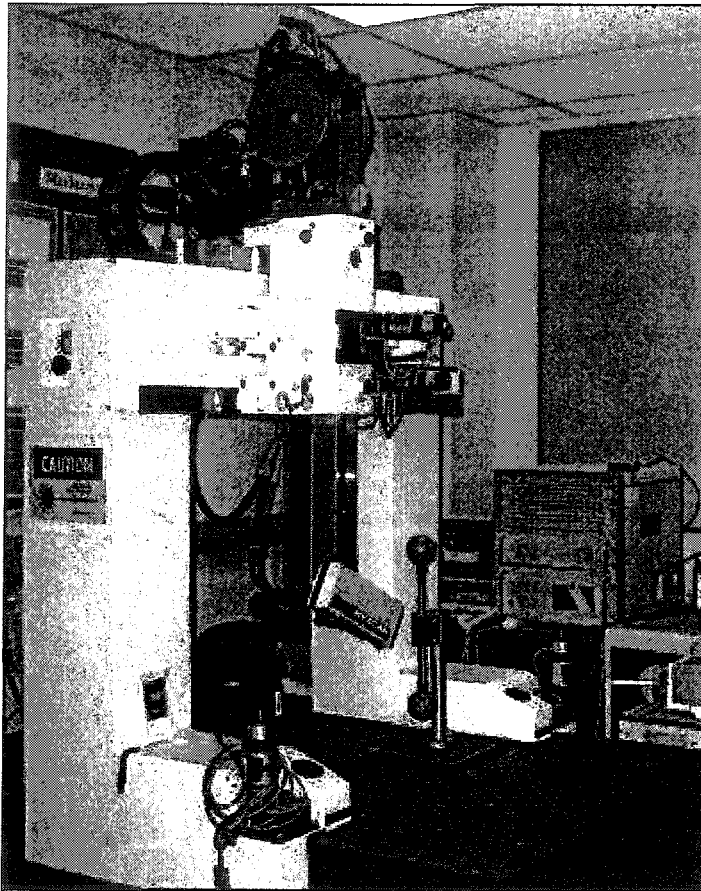


Figure 6-3 Digitizer W Aligned With X Axis, $\gamma = -60^\circ$

6.3.1. Results At Ambient Temperature

As was shown in section 6.2.3, the effect of geometric errors is represented by the accuracy of the population of measurements. The accuracy of measurement, using the twenty determinations calculated from the uncompensated measurements, had an rms accuracy error of $71 \pm 6 \mu\text{m}$. The accuracy of measurement, as calculated from the compensated measurements, had an rms accuracy error of $22 \pm 5 \mu\text{m}$. The results are

given graphically in Figure 6-5. Using compensated data, there is a 65% improvement in the accuracy of the calculated length of the ballbar, throughout the working volume of the CMM.

6.3.2. Analysis Of Results At Ambient Temperature

The most significant CMM flaw is the 160 arc-second squareness error. Test positions 1 and 2 are designed to test XY squareness of the CMM. The uncompensated values at positions 1 and 2 exhibit the largest variation from the mean value. In self-calibration the mean value of length is assumed to be the best estimate of the true value of length. The compensated values are much closer to the mean value and demonstrate the effectiveness of compensating the digitizer data.

The other test positions that exhibit a large deviation from the mean values are 7, 8, 9 and 10. These are the body diagonals of the CMM volume and are affected by the XY squareness error of the machine used for testing. The physical squareness error could have been reduced with maintenance, but was left in the machine to be compensated for by software (for thesis purposes).

Positions 4, 19 and 20 give the smallest apparent corrected length of the ballbar. Test positions 19 and 20 are the farthest away from the mean value, and very similar to the uncompensated values. Those two test positions are measuring the ballbar in an upright or vertical position, so they are designed to test the linearity of the Z axis. The error map used for this series of measurements shows there is very little error in the

linearity of the Z axis (less than 5 μm), so there is only the pose angle variation error to be compensated.

The ballbar length, using uncompensated measurements, had an rms accuracy error of $71 \pm 6 \mu\text{m}$. The ballbar length, using compensated measurements, was more accurate and had an rms accuracy error of $22 \pm 5 \mu\text{m}$. Based on the published laser digitizer point measurement accuracy ($\pm 9 \mu\text{m}$ at the 1σ level [Hymarc]), and the measured CMM error, this 65% improvement in the data accuracy, as measured by rms accuracy error, is consistent with expectations.

To determine if the view of the sphere at the end of the ballbar might have caused an abnormality due to a variation in roundness, the quality of the ball was examined. Computer simulations of looking at the sphere in its most out-of-round view showed that the error would likely be zero, and in all cases would be less than 3 μm . (See Appendix A.)

The copious cloud of data measured, up to 22,000 points on each sphere, did not appreciably improve the accuracy of the calculated sphere centre. A subset of data was evaluated for several sphere locations. The sphere fitting error, the RMS value of the error of all data points from an ideal sphere, was consistently 10 μm for the large data sets used. The sphere fitting error did not change from the 10 μm value for data sets as small as 300 points, and the centre point moved less than 0.3 μm . As long as the solid angle measured on the sphere was maintained, the number of data points had little influence on the calculation.

These measurements and those of section 6.2 were done with the same ballbar on different days. The mean compensated length of the ballbar during the initial squareness tests was 404.084 ± 0.007 mm, and for these volumetric tests was 404.073 ± 0.005 mm. The difference in apparent length between the two sets of measurements at ambient is less than 0.004%.

The results expressed as equivalent B89 accuracy measurements are 0.163 mm/404 mm for the uncompensated measurements and 0.054 mm/404 mm for the compensated measurements, an improvement of 67%.

6.4. Measurements Over Volume At Controlled Temperature

Sets of measurements were taken at each of three temperatures. By using the temperature at the time of measurement, it is possible to select the appropriate error map data using a linear interpolation of the two closest calibration temperatures.

The entire volume of the CMM was used and the ballbar was placed at the 20 positions recommended in B89.4 [ASME 1997]. The spheres at each end of the ballbar were measured with the laser digitizer and the data from the digitizer and CMM scales was recorded with a time stamp. Data collection included the uncompensated XYZ position reported by the laser digitizer, the U-V scan plane coordinates and the DEF axis scale readings. Approximately 17,000 points were measured on each sphere. Simultaneously, the temperature readings of the 11 thermocouples were recorded along with their time stamp in a separate data log.

When the compensation adjustments are made, the time stamp from the measurements is used to query the temperatures recorded on the CMM at the time of measurement. The temperature is then used to select the closest two temperature error maps and a linear interpolation is made of the 21 parametric errors to be used for the compensation. In this case, the temperature was controlled and the single matching error map was selected. The CMM error compensation data was then used to post process the scan plane coordinates using a new HTM to obtain improved global part coordinates. The sphere centres and ballbar lengths were calculated as before.

Length of Ball Bar

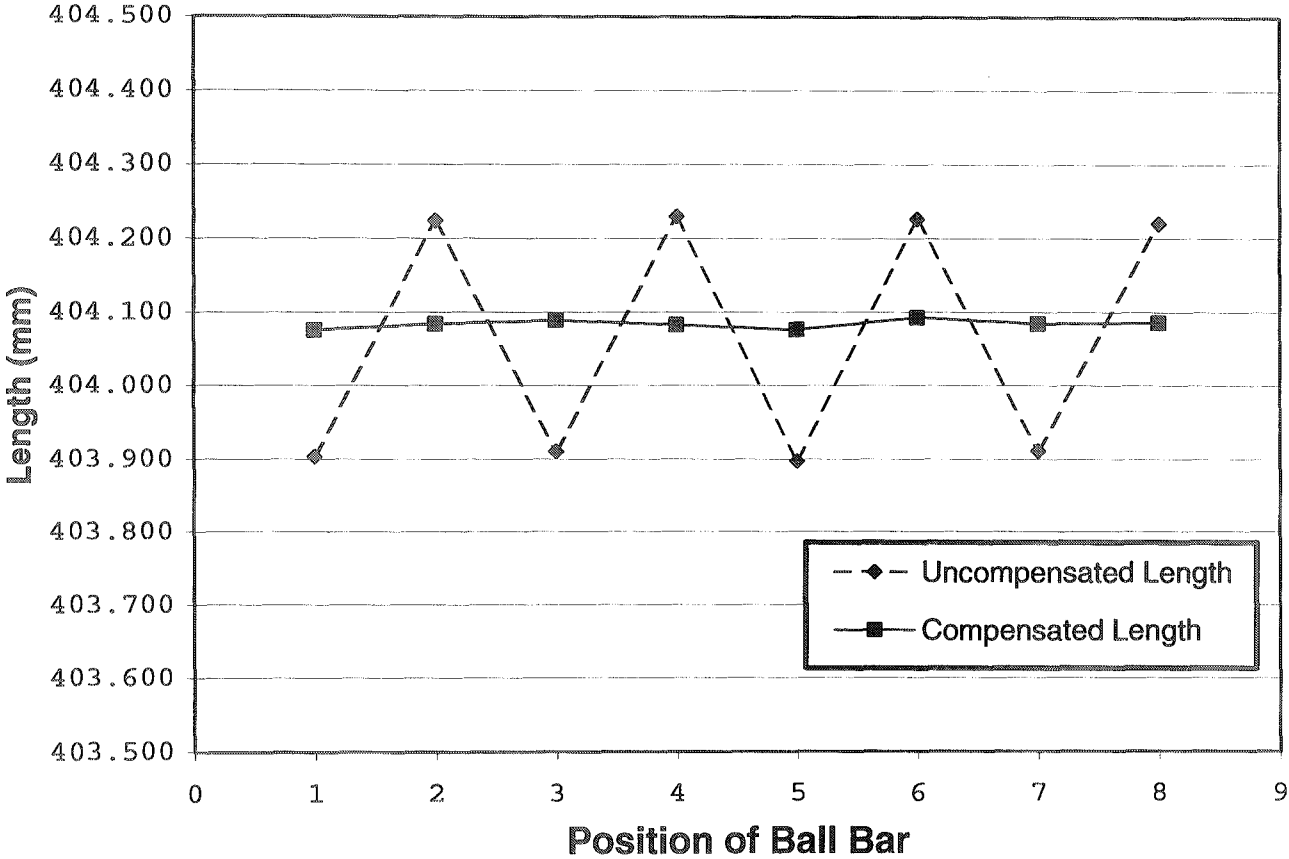


Figure 6-4 Results Of Initial Test

CMM Volumetric Measurements

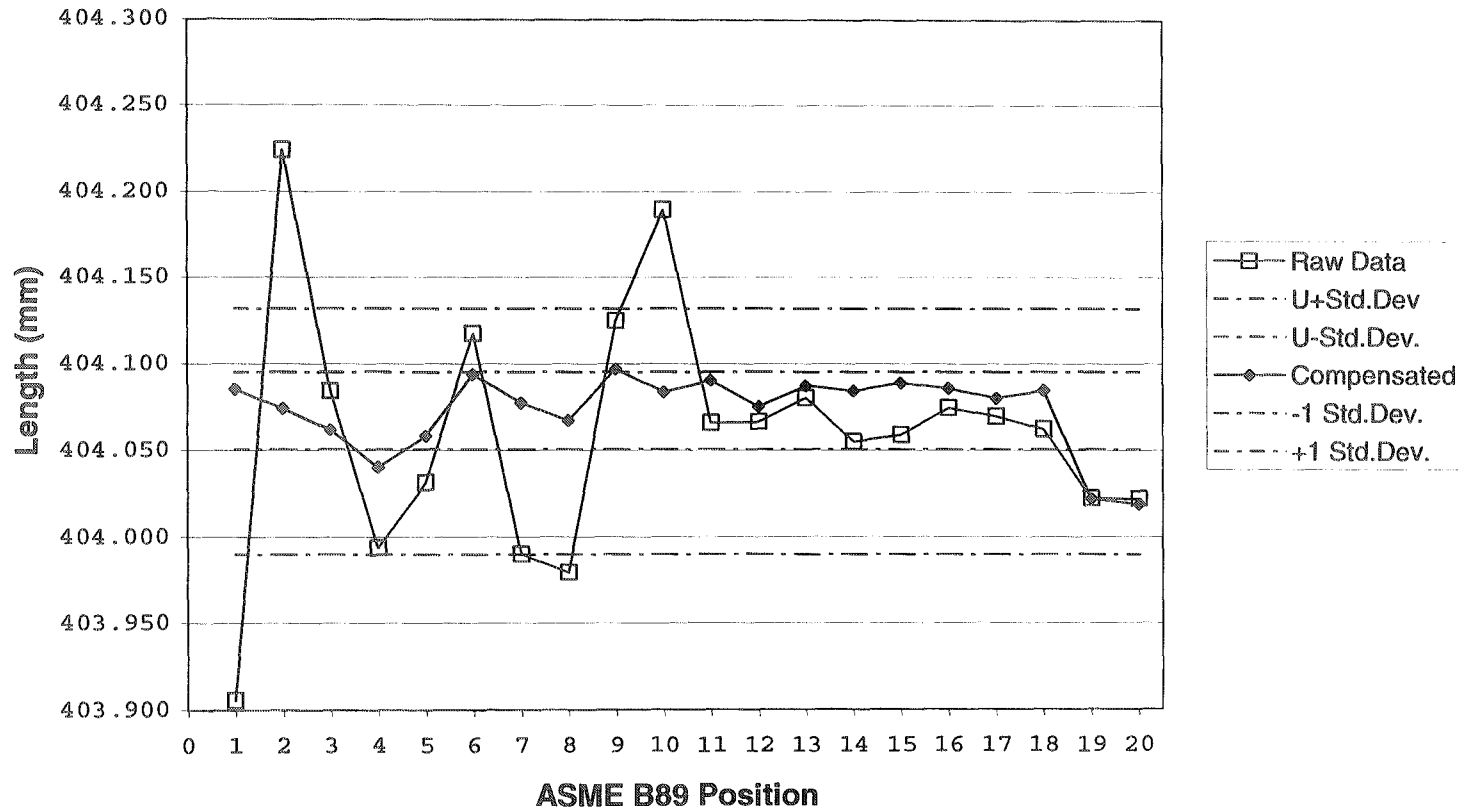


Figure 6-5 Volume Measurements At Ambient

Ballbar Length (20 °C)

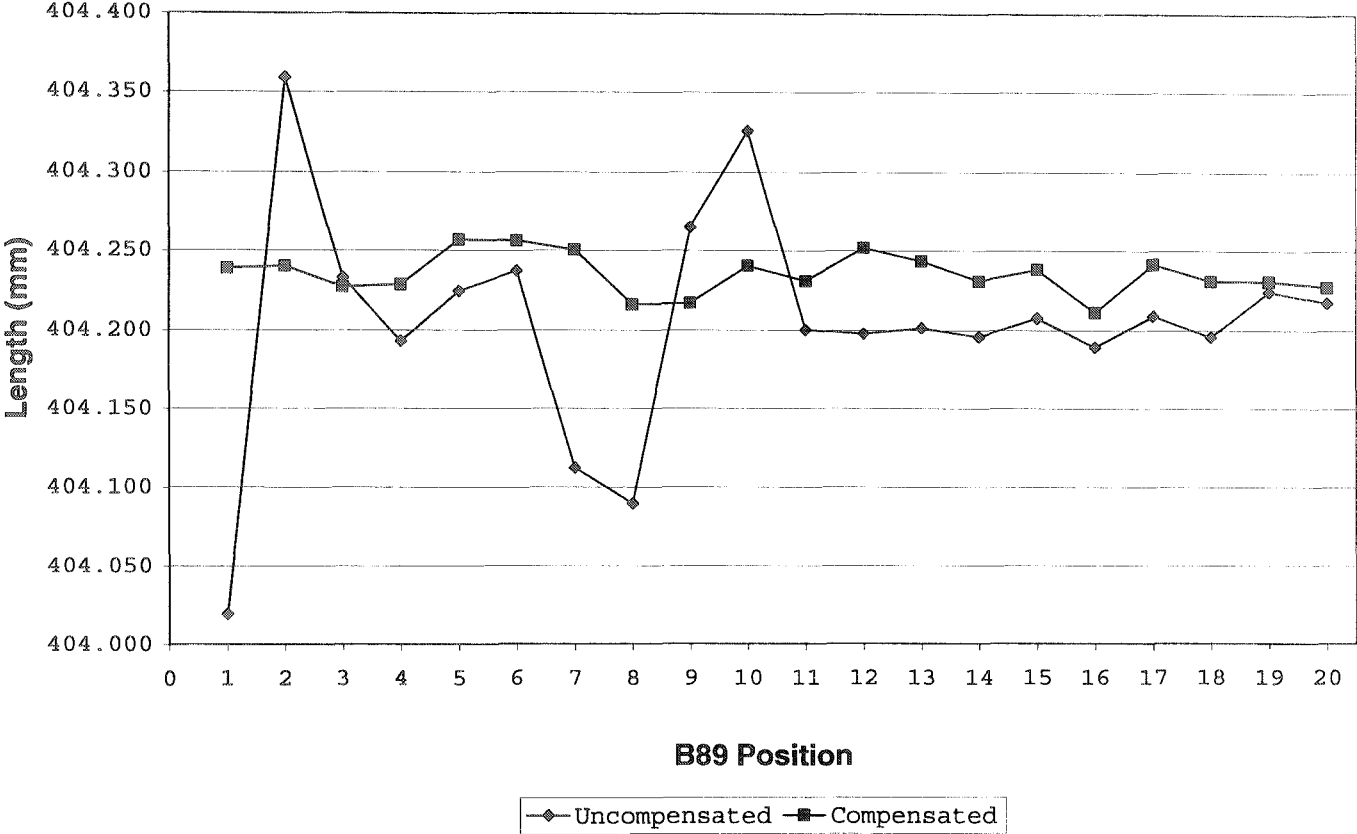


Figure 6-6 Results At 20 °C

Ballbar Length (25 °C)

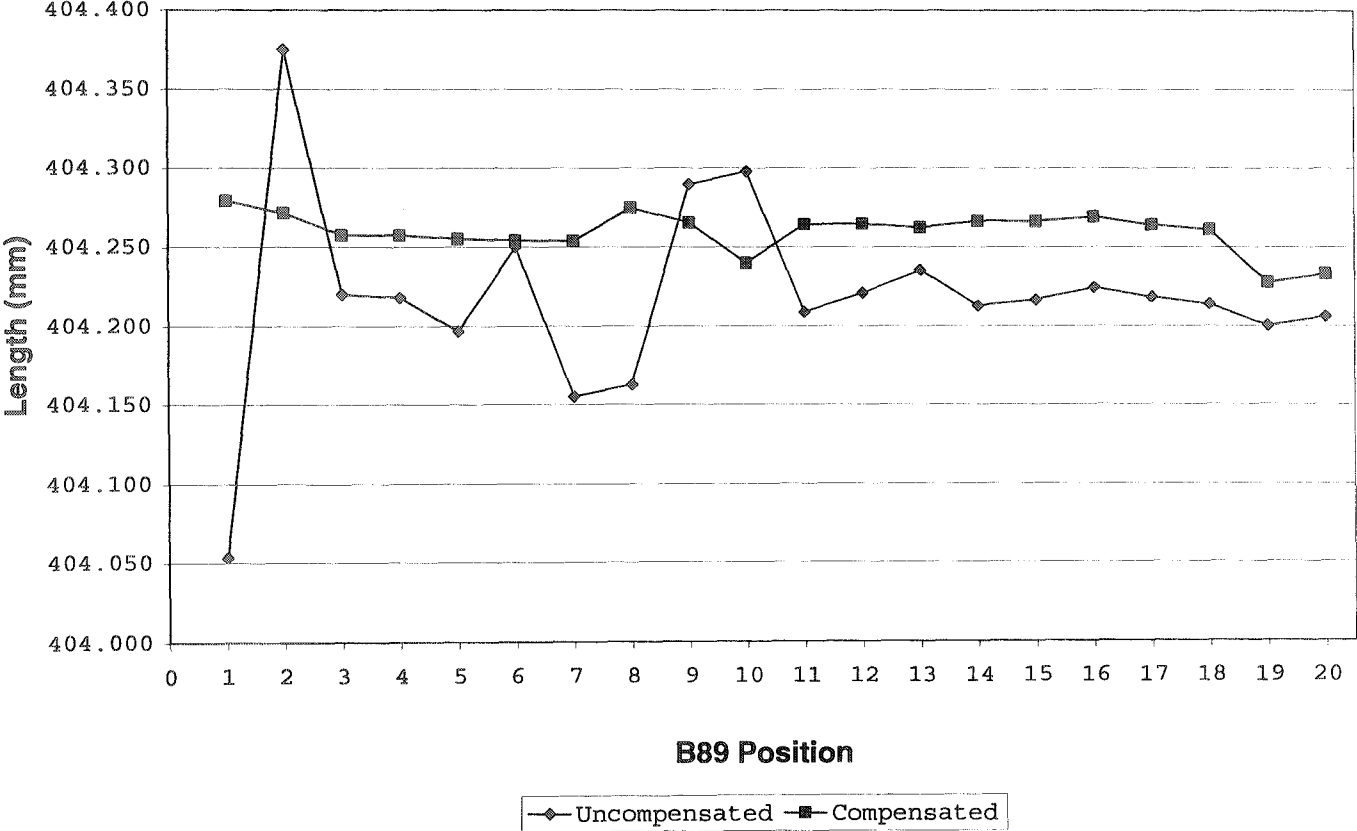


Figure 6-7 Results At 25 °C

Ballbar Length (30 °C)

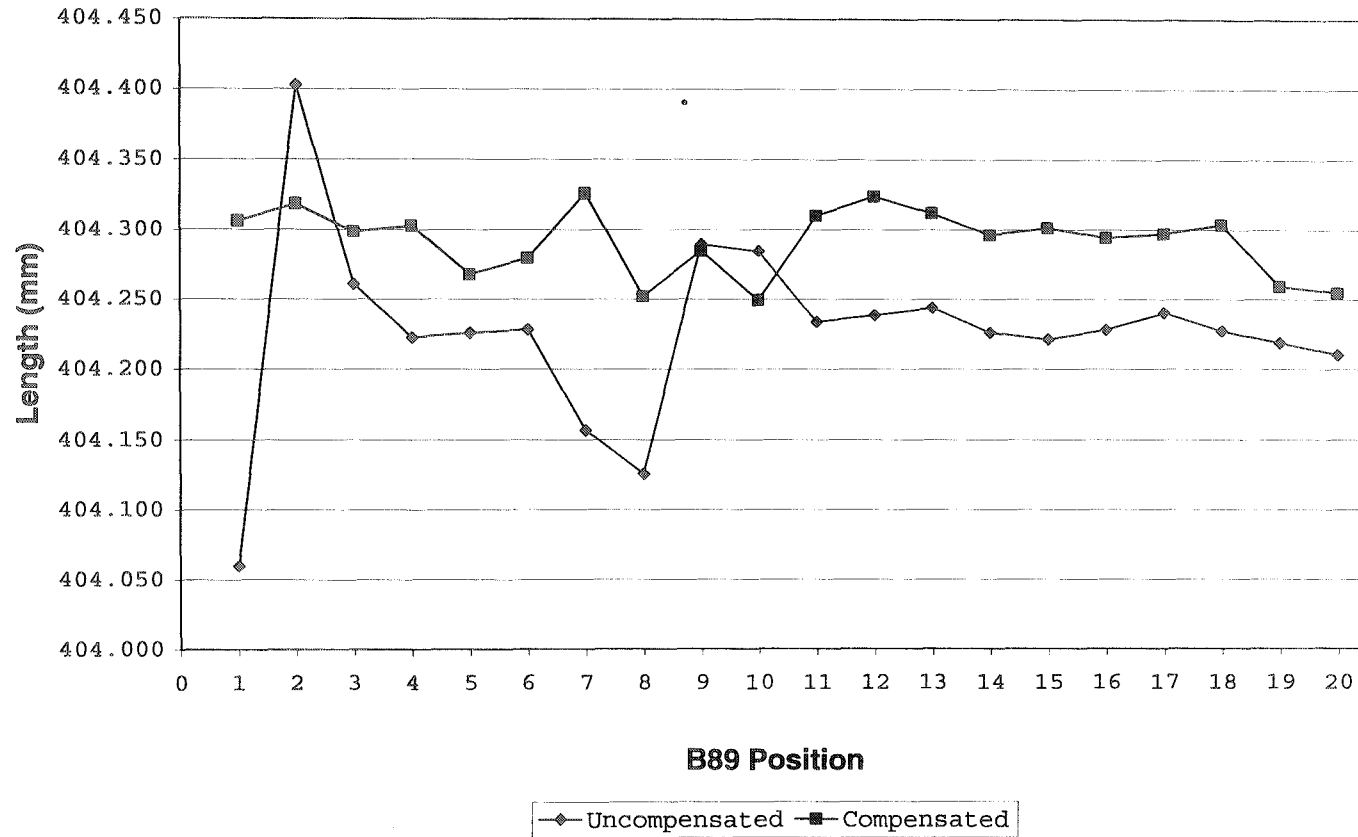


Figure 6-8 Results At 30 °C

6.4.1. Results At Controlled Temperature

At 20 °C, using the uncompensated data, the length of the ballbar measured at twenty different positions had an accuracy, as measured by rms accuracy error, of $73 \pm 6 \mu\text{m}$. At 25 °C, the length of the ballbar had an rms accuracy error of $62 \pm 10 \mu\text{m}$. At 30 °C, the length of the ballbar had an rms accuracy error of $66 \pm 12 \mu\text{m}$. As was shown in section 6.2.3, the effect of geometric errors is represented by the rms accuracy error of the measurements at all positions within the working volume. The results of ballbar length are given in Figure 6-6 to Figure 6-8. Table 19 gives the accuracy results expressed as rms accuracy error and the improvement with the geometric and quasi-static temperature error compensation. The improvement is 82% at 20 °C, 79% at 25 °C and 63% at 30 °C.

Table 19 Summary Of Controlled Temperature Results

Temperature	Uncompensated	Compensated	
	rms accuracy error	rms accuracy error	Improvement
20 °C (20 measurements)	0.0732 mm ± 0.006 mm	0.0128 mm ± 0.005 mm	82 %
25 °C (20 measurements)	0.0618 mm ± 0.010 mm	0.0130 mm ± 0.005 mm	79 %
30 °C (20 measurements)	0.0663 mm ± 0.012 mm	0.0240 mm ± 0.005 mm	63 %
All Temperatures (60 measurements)	0.0671 mm ± 0.009 mm	0.0166 mm ± 0.003 mm	75 %

For comparison, the results are expressed in terms of B89 accuracy in Table 20. The improvement is 87% at 20 °C, 81% at 25 °C and 76% at 30 °C. As expected, the improvement appears better when only the maximum error within the CMM working volume is considered.

Table 20 Summary Of Results Per ASME B89

Temperature	Uncompensated	Compensated	
	accuracy	accuracy	Improvement
20 °C	0.186 mm/404 mm	0.024 mm/404 mm	87 %
25 °C	0.165 mm/404 mm	0.032 mm/404 mm	81 %
30 °C	0.176 mm/404 mm	0.043 mm/404 mm	76 %

Because the scales on the CMM were mounted on steel and the test object (ballbar) was steel, they both should expand at the same rate. The uncompensated data provide a consistent length measurement independent of temperature. Using the uncompensated data from measurements at all three temperatures, the length had a mean of 404.217 ± 0.009 mm (see Table 21). The uncertainty of the uncompensated values consists of three components: 1) the $9 \mu\text{m}$ digitizer point accuracy, 2) the $10 \mu\text{m}$ uncertainty of sphere fitting algorithm for each end of the ballbar, and 3) the possible scale error over a length of 404 mm. From the plots of geometric error measured in chapter 3, the worst case scale error to be encountered at 20°C is ± 0.012 mm on the X scale, ± 0.018 mm on the Y scale, and ± 0.006 mm on the Z scale. Since a length measurement is being performed only the uncertainty in the direction of measurement from the digitizer is applied to the length in question. The uncertainty perpendicular to the length measurement does not have a significant affect on the uncertainty in length hence the value of $9 \mu\text{m}$ is used. The same applies to the uncertainty associated with the

sphere centre fitting algorithm. The value of $10\ \mu\text{m}$ from this algorithm does not need to be broken down into coordinate directions because it is being applied to the length of the ball bar that could be arbitrarily aligned in space. The uncertainty of a single position measurement is $u_{20} = \sqrt{9^2 + 10^2 + 12^2 + 18^2 + 6^2} = 26\ \mu\text{m}$. At 25°C the scale error is $\pm 0.021\ \text{mm}$ on the X scale, $\pm 0.030\ \text{mm}$ on the Y scale, and $\pm 0.012\ \text{mm}$ on the Z scale. The uncertainty of a single position measurement at 25°C is $u_{25} = \sqrt{9^2 + 10^2 + 21^2 + 30^2 + 12^2} = 41\ \mu\text{m}$. At 30°C the scale error is $\pm 0.026\ \text{mm}$ on the X scale, $\pm 0.038\ \text{mm}$ on the Y scale, and $\pm 0.020\ \text{mm}$ on the Z scale. The uncertainty of a single position measurement is $u_{30} = \sqrt{9^2 + 10^2 + 26^2 + 38^2 + 20^2} = 52\ \mu\text{m}$. The uncertainty in the coordinates of a sphere centre location measurement due to geometric error is affected differently in all three dimensions. The net uncertainty in the length of the ballbar due to geometric error is the square root of the sum of the square of the scale errors because the length is determined by the three dimensional coordinates. For multiple length measurements the uncertainty of the mean, assuming uncorrelated errors, is divided by the square root of the number of measurements.

The thermal expansion of the ballbar can be seen in the compensated measurements. The compensated length of the ballbar was calculated as $404.236 \pm 0.005\ \text{mm}$ at 20°C , $404.259 \pm 0.005\ \text{mm}$ at 25°C , and $404.292 \pm 0.005\ \text{mm}$ at 30°C , showing the expansion of the part. In metrology, measurements are reported at a standard temperature of 20°C . When corrected for the thermal expansion of steel ($12\ \mu\text{m}/\text{m}\ ^\circ\text{C}$), the length measurements from compensated values had means of

404.236 ± 0.005 mm at 20 °C, 404.235 ± 0.005 mm at 25 °C and 404.244 ± 0.005 mm at 30 °C. Using the compensated data from measurement at all three temperatures, and correcting for thermal expansion, the length had a mean of 404.238 ± 0.003 mm.

Table 21 Length At Standard Temperature

Temperature	Uncompensated	Compensated	
	Measured Length (mm at 20 °C)	Measured Length (mm)	Standardised Length (mm at 20 °C)
Ballbar at 20 °C	404.205 ± 0.006	404.236 ± 0.005	404.236 ± 0.005
Ballbar at 25 °C	404.219 ± 0.010	404.259 ± 0.005	404.235 ± 0.005
Ballbar at 30 °C	404.227 ± 0.012	404.292 ± 0.005	404.244 ± 0.005
All Temperatures (3 determinations)	404.217 ± 0.009		404.238 ± 0.003

6.4.2. Analysis Of Results At Controlled Temperature

The rms accuracy error of all length measurements at all three temperatures was 67 ± 9 µm for the uncompensated values and 17 ± 3 µm for the compensated values. The improvement, shown as a reduction in dispersion of the results, was 75%.

In estimating the true length of the ballbar, all 20 measurements at each temperature need to be averaged to account for the geometric and quasi-static thermal error. The uncertainty of the length is not related to the rms accuracy error of the 20 measurements, but rather to the uncertainty of the measurement as described in section 6.4.1. Referring to Table 21, the uncompensated length has uncertainty due to digitizer measurement uncertainty, sphere fitting algorithm uncertainty and scale uncertainty. The compensated length has uncertainty due only to digitizer measurement uncertainty and sphere fitting algorithm uncertainty. The scale uncertainty for the length determined with compensation has been removed by measuring an error map at different temperatures. The compensated length measurement at elevated temperature shows the thermal expansion of the ballbar because the thermal expansion of the scales have been incorporated into the error maps at different temperatures. The uncompensated length measurement shows minimal thermal expansion of the ballbar because the thermal expansion of the scales is not identified. For the three determinations of length at the three temperatures, the mean uncompensated length of 404.22 ± 0.01 mm and the mean compensated thermal adjusted length of 404.238 ± 0.003 mm (the 0.005 mm uncertainty of a single length determination using the average of the 20 positions measurement has been divided by $\sqrt{3}$ to account for the 3 temperature sample size) have overlapping uncertainties and are equivalent. In this case the length of the ballbar is different from that reported in section 6.3, 404.073 ± 0.005 mm, because the ballbar had been disassembled for storage and then reassembled for the controlled temperature tests.

It is often assumed that when the measuring device and the measurand are made of materials with similar thermal expansion coefficients that a valid measurement can be obtained at temperatures other than the standard 20 °C. To quote Bryan [1995], “If the work is made of steel and the scale is steel, the two expand together and the resultant errors tend to cancel. Two wrongs make a right.” One of the reasons for this research was to allow new non-ferrous materials to be measured, but it was observed that even when the scales and the work are steel, there is a difference in measured length due to the temperature effect. The uncompensated results have a $22 \pm 12 \mu\text{m}$ difference in length between 20 and 30 °C. When the compensated length of the ballbar was corrected for thermal expansion, the results improved to within $9 \pm 7 \mu\text{m}$ between 20 and 30 °C (equivalent to the 1σ limit for the laser digitizer).

At 20 °C, the variability of length due to geometric and quasi-static thermal errors, as represented by the rms accuracy error of the population, is reduced from $73 \pm 6 \mu\text{m}$ to $13 \pm 5 \mu\text{m}$, an improvement of 82%. At 25 °C the variability of length is reduced from $62 \pm 10 \mu\text{m}$ to $13 \pm 5 \mu\text{m}$, and at 30 °C from $66 \pm 12 \mu\text{m}$ to $24 \pm 5 \mu\text{m}$. This is an improvement in accuracy between 59 and 75% at these temperatures.

Measuring an artefact with the laser digitizer tested the performance of the system. Software compensation incorporating position and angular error terms is shown to significantly improve accuracy.

6.5. Summary

To implement the integrated error compensation, the scan plane coordinates and the CMM axis scale positions were recorded simultaneously in real time. The CMM error compensation data was then used to post process the scan plane coordinates using a new HTM to obtain improved global part coordinates. Inclusion of the angular error compensation terms is shown to significantly improve accuracy.

The results obtained with crossed ballbar positions were particularly good. The accuracy of the uncompensated data had an rms accuracy error of $171 \pm 9 \mu\text{m}$. With compensation applied, the rms accuracy error was only $6 \pm 7 \mu\text{m}$, an improvement of 95%.

The results obtained over the entire volume of the CMM were also significant. The uncorrected rms accuracy error of $71 \pm 6 \mu\text{m}$ was reduced to an rms accuracy error of $22 \pm 5 \mu\text{m}$, an improvement of 65%.

The difference in apparent lengths between the two sets of measurements at ambient, which were taken on different days, is less than 0.004%.

The most significant CMM flaw is the 160 arc-second XY squareness error. This showed up with the crossed ballbars of the squareness test and at positions 1 and 2 of the volumetric tests. The proposed compensation procedure with the pose attitude term handled this well.

Using controlled temperatures from 20°C to 30°C and measurements throughout the entire volume, the accuracy of a laser equipped CMM is improved by

75%, the rms accuracy error of the length of the test artefact being reduced from $67 \mu\text{m}$ to $17 \pm 5 \mu\text{m}$.

Chapter 7

Conclusion

7.1. Conclusions

The objective was to provide improved accuracy of the data points measured with a laser digitizer by using software error compensation. This has been accomplished by the development of a set of equations for compensating the pose position and attitude of a laser digitizer mounted on a CMM, and introduction of a standard ballbar test.

To implement the error compensation, the scan plane coordinates of the laser digitizer and the CMM axis scale positions were recorded simultaneously in real time along with temperature. The geometric component errors of the CMM were previously measured at three static temperatures and could be interpolated for the temperature of measurement. The data were compensated for errors in the digitizer, both pose position and attitude, to obtain improved global part coordinates. The correctness of the algorithm was verified by measurements on a ballbar under controlled temperature conditions. For the 400 mm length of the ballbar, the geometric errors of the CMM are significant and are compensated by the proposed algorithm. There is a 63 to 90% improvement in the accuracy of the data.

Thermal error has a great influence on measurement accuracy, especially when the CMM is put on the factory floor to perform inline inspection. Testing showed one of

the most significant effects is the expansion of the scales of the axes. By evaluating the error at several temperatures, it was possible to include thermal effects in the error compensation.

Measuring an optical ballbar artefact with the laser digitizer tested the performance of the system. The use of optically coated spheres on the ballbar avoids the specular reflections that come from the typical polished stainless steel spheres and is a significant improvement to the method.

7.2. Suggestions For Further Work

This thesis compensated for the effects of the CMM geometric component errors and the laser digitizer alignment. The accuracy of the laser digitizer was assumed constant. Other researchers [Feng 2001] have examined the effects of the scan depth and the projected angle on the accuracy of a laser digitizer. It would be interesting to investigate accuracy improvement, by incorporating the bilinear factors for the angle between the tangent of the workpiece surface and the incident laser beam.

For flexible measurement, a laser triangulation sensor can be mounted on the end of an industrial robot arm, which is then programmed to move the sensor into position to perform a number of different dimensional measurements. The equations developed for a Cartesian CMM could be modified to apply to a rotary joint device, such as a Faro Arm.

Because the touch probe is so well known, it is the basis for calibration procedures. To permit the permanent installation of a digitizer, one could develop the

calibration of a laser digitizer equipped CMM, based on measurements of a ballbar with optically coated spheres.

Appendix A Effect Of Sphericity

Since the laser scanner can only see the top half (2π steradians) of the spheres at the ends of the ballbars, the sphericity of the spheres was a potential source of error in evaluating the ballbar length.

Sphericity is a measure of the degree to which the axes of an object are the same lengths. In highly spherical objects (ball or cube) the axes are equal, in objects of low sphericity (disc or rod shaped) they are of different lengths. For ball bearings, the term sphericity is used as a synonym for roundness and measured as the difference between the largest diameter and the smallest diameter measurable on a single ball.

The optically coated spheres used for the test measurements were made from grade 200 ball bearings. They had a nominal diameter of 76.25 ± 0.025 mm. A grade 200 ball bearing has a sphericity rating of 200 microinch, which is shown in metric in Table 22. Surface roughness indicates the allowable finely spaced surface irregularities of the ball. To prevent specular reflections, the balls were painted with an optical coating.

Table 22 Grade 200 Ball Tolerance

Basic Diameter	76.25 mm
Diameter Tolerance	$\pm 25.4 \mu\text{m}$
Sphericity	$5.08 \mu\text{m}$
Surface Roughness	$0.20 \mu\text{m}$

A worst case analysis was performed by creating two data sets. The assumption was that the camera was looking at the worst possible variation in a ball diameter, one looking at an oblate spheroid where the width is greater than the height and one looking at a prolate spheroid. In both cases the centre of the sphere was $[0 \ 0 \ 0]$. Points were selected at 0.1 mm increments starting at the top, the polar axis, and extending for various solid angle coverage, as would be typical with a laser digitizer. A simplified side view for the oblate sphere is shown in Figure A 1. The azimuth or longitude angle is 360° to extend all around the sphere. The colatitude or polar angle is used to identify the data set. The NIST ATS algorithm was used to calculate sphere centre and radius for the data sets. As shown in Figure A 1, when only a portion of the oblate sphere is viewed, the centre appears to be further away from the digitizer and the radius appears to be larger. The results are given in Figure A 2 and Figure A 3.

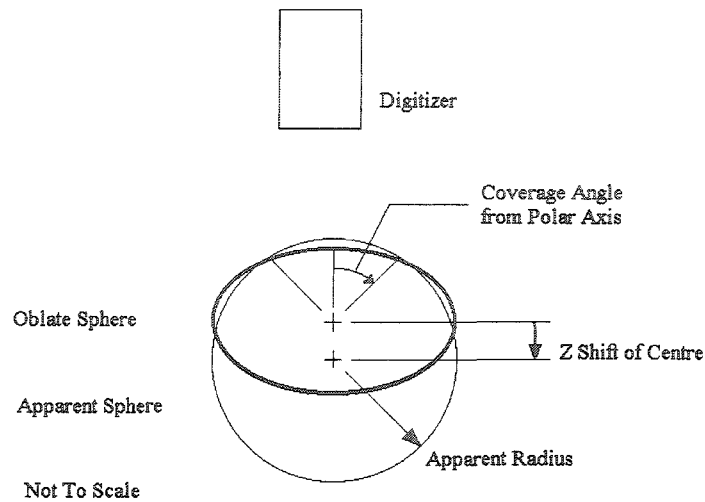


Figure A 1 Side View Of Oblate Sphere

For the oblate sphere, the equatorial radius was 38.125 mm and the polar axis was 38.1225 mm. The observed centre point was always located at $X=0$ and $Y=0$, but the apparent Z value changed. The less coverage of the sphere the larger the apparent errors. When data from only 0.4% of the surface area of the hemisphere (polar angle = 5°) the radius was calculated as 38.128 mm and the centre point was calculated as $[0 \ 0 \ -0.005]$. When data was selected from half of the hemisphere (π steradians, or polar angle = 60°) the radius was calculated as 38.126 mm and the centre point was calculated as $[0 \ 0 \ -0.004]$. When a typical measurement coverage was used (polar angle = 85°) the radius was calculated as 38.126 mm and the centre point was calculated as $[0 \ 0 \ -0.003]$.

For the prolate sphere, the equatorial radius was 38.125 mm and the polar axis was 38.1275 mm. When the data of the prolate sphere is examined, similar effects are

seen. At a polar angle 5° the apparent radius of the sphere is smaller by 0.003 mm, whereas for the oblate sphere it was larger 0.003 mm. The measured centre, $[0 \ 0 \ 0.005]$, is high in the Z axis direction by 0.005 mm, whereas for the oblate sphere it was low by 0.005 mm. When a typical measurement coverage was used (polar angle = 85°) the radius was calculated as 38.124 mm and the centre point was calculated as $[0 \ 0 \ 0.003]$.

It can be seen that the data fitting algorithm used is sensitive to the sphericity of the measured object. If there is 0.005 mm sphericity, it will be seen as a 0.003 mm shift in the calculated origin, either towards the laser digitizer or away from it. However, that is a worst case analysis. The ballbar was oriented in several directions during testing. Several pose attitudes of the laser digitizer were used during testing. The sphericity might not be aligned with the view seen by the laser digitizer. Thus, since there is equal probability of seeing a prolate or oblate distortion, the systematic component of error is likely 0, and definitely less than 0.003 mm.

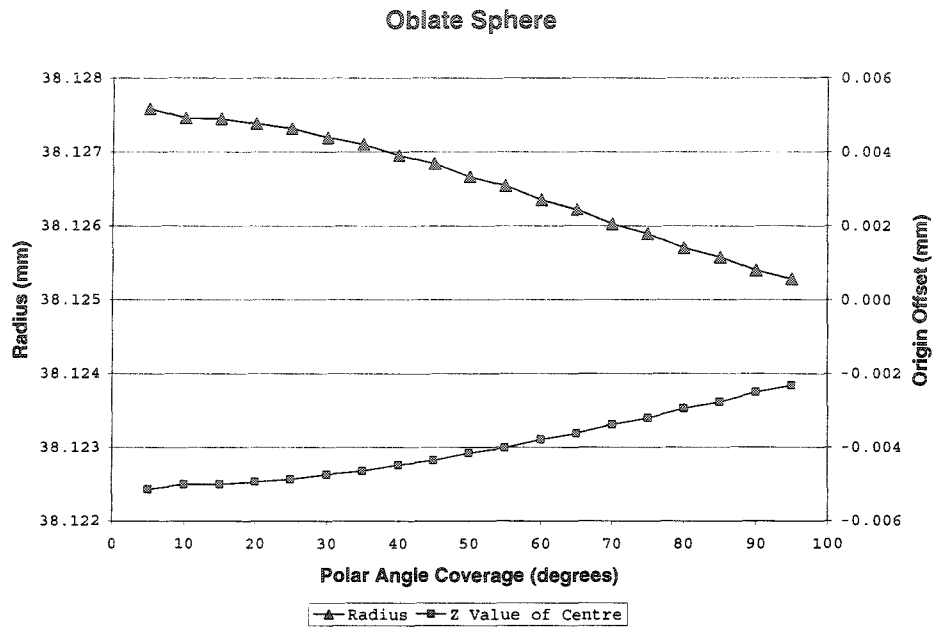


Figure A 2 Oblate Sphere

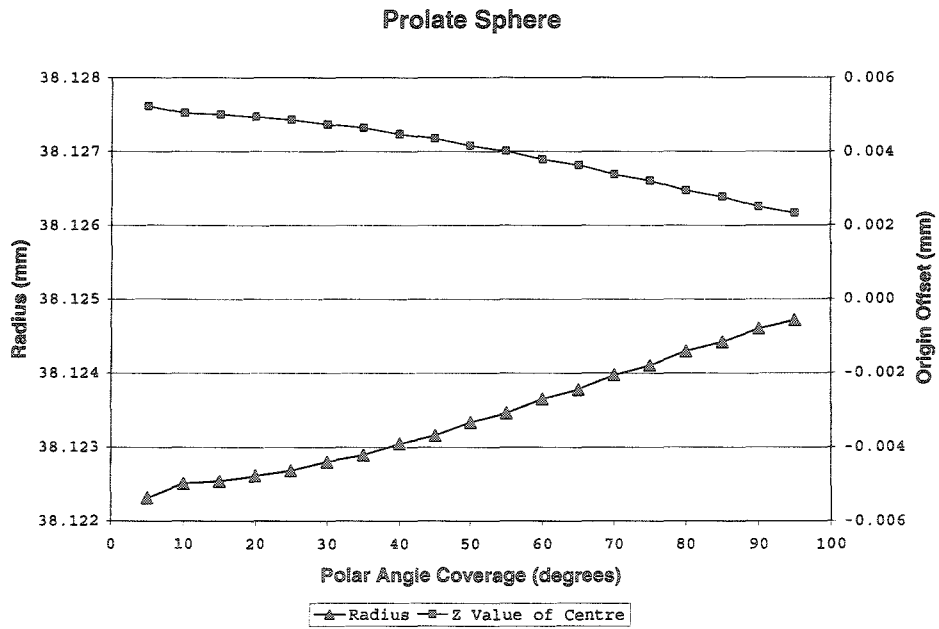


Figure A 3 Prolate Sphere

Appendix B CMM Error Map At Ambient

The following error map was generated at an ambient temperature of 22 °C

File Name: errors_1102.txt

CMM Style: Vertical Arm Main Carriage: X-Axis

Axis Parameters:

Axis Min Position Max Position Increment Probe Head

X 0 900 25 0

Y 0 550 25 0

Z -500 0 25 0

Squareness Parameters:

XY: 169.397

YZ: 33.979

ZX: -25.984

Engineer's ID: Neil- Canada

File ID: 4033289624401

Last Modified: Mon Jan 14 17:48:19 2002

Map Data: X Axis

X Position	X Linear	Y Straight	Z Straight	Y Rotation	Z Rotation	X Rotation
0	0.00	0.00	0.00	-0.60	-0.10	0.00
25	0.00	0.00	0.00	-0.80	0.30	0.00

X Position	X Linear	Y Straight	Z Straight	Y Rotation	Z Rotation	X Rotation
50	3.00	0.00	0.00	-0.90	0.15	0.00
75	2.00	0.00	0.00	-0.90	0.30	0.00
100	3.00	0.00	0.00	-0.80	0.50	0.00
125	2.00	0.00	0.00	-1.10	0.40	0.00
150	2.00	0.00	0.00	-0.80	0.55	0.00
175	1.00	0.00	0.00	-0.80	0.55	0.00
200	2.00	0.00	0.00	-0.95	0.25	0.00
225	2.00	0.00	0.00	-0.75	0.05	0.00
250	3.00	0.00	0.00	-0.65	0.20	0.00
275	4.00	0.00	0.00	-0.55	-0.10	0.00
300	5.00	0.00	0.00	-0.50	0.10	0.00
325	7.00	0.00	0.00	-0.20	0.10	0.00
350	6.00	0.00	0.00	-0.25	-0.10	0.00
375	8.00	0.00	0.00	0.05	-0.25	0.00
400	8.00	0.00	0.00	0.15	-0.10	0.00
425	8.00	0.00	0.00	0.30	-0.25	0.00
450	8.00	0.00	0.00	0.45	-0.15	0.00
475	9.00	0.00	0.00	0.55	0.25	0.00
500	11.00	2.00	0.00	0.65	0.55	0.00
525	11.00	2.00	1.00	0.65	0.80	0.00

X Position	X Linear	Y Straight	Z Straight	Y Rotation	Z Rotation	X Rotation
550	14.00	2.00	1.00	0.35	0.80	0.00
575	13.00	2.00	1.00	0.55	0.95	0.00
600	11.00	-1.00	0.00	0.60	0.95	0.00
625	13.00	-1.00	1.00	0.80	1.25	0.00
650	13.00	-1.00	0.00	0.85	1.20	0.00
675	11.00	-1.00	0.00	0.75	1.15	0.00
700	11.00	2.00	0.00	0.95	1.55	0.00
725	11.00	2.00	0.00	0.85	1.50	0.00
750	11.00	2.00	0.00	1.00	1.55	0.00
775	12.00	0.00	0.00	1.15	1.70	0.00
800	12.00	0.00	0.00	1.45	1.75	0.00
825	10.00	0.00	0.00	1.25	1.80	0.00
850	12.00	0.00	0.00	1.05	1.90	0.00
875	12.00	0.00	0.00	1.25	2.00	0.00
900	12.00	0.00	0.00	1.40	2.00	0.00

Map Data: Y Axis

Y Position	Y Linear	Z Straight	X Straight	X Rotation	Z Rotation	Y Rotation
---------------	-------------	---------------	---------------	---------------	---------------	---------------

Y Position	Y Linear	Z Straight	X Straight	X Rotation	Z Rotation	Y Rotation
0	0.00	0.00	0.00	-0.35	-0.20	0.00
25	2.00	0.00	0.00	-1.05	0.00	0.00
50	4.00	0.00	0.00	-1.10	0.15	0.00
75	8.00	0.00	0.00	-1.20	0.15	0.00
100	11.00	0.00	0.00	-1.15	0.10	0.00
125	11.00	0.00	0.00	-0.85	0.30	0.00
150	14.00	0.00	0.00	-0.95	0.15	0.00
175	15.00	0.00	-7.00	-0.85	-0.15	0.00
200	16.00	1.00	-7.00	-0.70	0.05	0.00
225	17.00	1.00	-10.00	-0.50	-0.10	0.00
250	20.00	1.00	-11.00	-0.75	-0.05	0.00
275	23.00	1.00	-10.00	-1.10	-0.20	0.00
300	25.00	1.00	-11.00	-1.05	0.10	0.00
325	27.00	1.00	-9.00	-1.60	0.30	0.00
350	31.00	-1.00	-10.00	-1.70	0.25	0.00
375	33.00	0.00	-5.00	-1.95	0.20	0.00
400	33.00	-1.00	-7.00	-1.45	0.40	0.00
425	34.00	-1.00	0.00	-1.40	0.35	0.00
450	35.00	-2.00	-1.00	-1.65	0.65	0.00
475	36.00	-2.00	-2.00	-1.85	0.70	0.00

Y Position	Y Linear	Z Straight	X Straight	X Rotation	Z Rotation	Y Rotation
500	38.00	-1.00	2.00	-1.60	0.95	0.00
525	39.00	0.00	6.00	-1.75	1.20	0.00
550	41.00	0.00	0.00	-2.20	1.00	0.00

Pagination by Microsoft's printer driver.

PhD Thesis - J. Harris McMaster - Mechanical Engineering

□Map Data: Z Axis

□Z Position□Z

Z Position	Z Linear	X Straight	Y Straight	X Rotation	Y Rotation	Z Rotation
-500	0.00	0.00	0.00	-1.50	-0.15	0.00
-475	0.00	0.00	0.00	-1.55	-0.05	0.00
-450	0.00	0.00	0.00	-1.85	-0.10	0.00
-425	0.00	0.00	0.00	-2.30	0.00	0.00
-400	0.00	0.00	0.00	-2.40	0.55	0.00
-375	0.00	0.00	0.00	-2.70	0.55	0.00
-350	0.00	0.00	0.00	-2.90	0.65	0.00
-325	0.00	0.00	0.00	-1.80	0.55	0.00
-300	-4.00	0.00	0.00	-1.05	0.40	0.00
-275	-4.00	0.00	0.00	-1.10	0.30	0.00
-250	-2.00	0.00	0.00	-0.75	0.25	0.00
-225	-2.00	0.00	0.00	-3.50	-0.15	0.00
-200	-2.00	0.00	0.00	-3.30	-0.45	0.00
-175	-2.00	0.00	-1.00	-3.55	-0.65	0.00
-150	-2.00	0.00	0.00	-3.55	-1.05	0.00
-125	-2.00	0.00	-1.00	-3.55	-1.20	0.00
-100	-2.00	0.00	-2.00	-3.70	-1.60	0.00
-75	-2.00	0.00	0.00	-3.60	-1.85	0.00

Z Position	Z Linear	X Straight	Y Straight	X Rotation	Y Rotation	Z Rotation
-50	-2.00	0.00	0.00	-3.75	-2.20	0.00
-25	-5.00	0.00	0.00	-3.65	-2.55	0.00
0	-5.00	0.00	0.00	-3.80	-3.20	0.00

Appendix C Ballbar Data

The data in this appendix was taken and measured at 20°C. It is representative of the sphere data measured at each end of the ballbar during testing.

PhD Thesis - J. Harris McMaster - Mechanical Engineering

Uncompensated

Position	Ball	Points	Fit	Radius	B1 X	B1 Y	B1 Z
1	1	13799	0.012	38.1732	-496.6823	-134.2409	27.7912
2	1	8569	0.011	38.1638	-463.6166	98.8370	26.1378
3	1	17087	0.010	38.1592	-480.4967	-161.3865	235.0341
4	1	10736	0.013	38.1505	-470.6128	-167.4699	-30.1317
5	1	12613	0.010	38.1427	-242.7957	30.3372	-30.1308
6	1	13543	0.012	38.1615	-237.0059	4.4126	235.0254
7	1	11283	0.011	38.1723	-291.1321	105.3707	177.2970
8	1	8767	0.011	38.1735	-469.3263	-127.4794	177.2997
9	1	9819	0.010	38.1358	-263.6298	-101.5836	-87.8336
10	1	15028	0.008	38.1363	-401.5235	70.7335	-87.8334
11	1	9244	0.011	38.1798	-258.2077	-223.0165	27.7911
12	1	10667	0.010	38.1625	-165.4314	174.7068	26.1328
13	1	7274	0.010	38.1588	-567.5347	-168.4128	26.1354
14	1	11722	0.012	38.1552	-556.0627	230.0767	26.1412
15	1	8673	0.011	38.1564	-171.9902	-166.6456	26.1360
16	1	10509	0.012	38.1767	-73.7629	-233.1986	27.8981
17	1	8708	0.012	38.1696	-520.5358	-11.8186	26.1700
18	1	11722	0.012	38.1552	-556.0627	230.0767	26.1412
19	1	11228	0.009	38.1794	-208.4810	8.3186	-110.5010
20	1	8983	0.010	38.1669	-402.4176	-150.0854	293.7143
Mean		10999	0.011	38.1615			
Std.Dev.			0.001	0.0131			
Max		17087	0.013	38.1798			
Min		7274	0.008	38.1358			
Range			0.004	0.0440			

Figure C 1 Ballbar Sphere Data (1)

PhD Thesis - J. Harris McMaster - Mechanical Engineering

Uncompensated

Position	Ball	Points	Fit	Radius	B2 X	B2 Y	B2 Z	Length
1	1	14334	0.010	38.1618	-211.1357	151.5774	26.1370	404.0194
2	1	10168	0.010	38.1737	-166.5034	-175.4392	27.8002	404.3593
3	1	9988	0.011	38.1412	-485.3435	143.6879	-30.1272	404.2331
4	1	15739	0.012	38.1660	-473.9616	137.5785	235.0217	404.1931
5	1	14627	0.008	38.1444	-547.8584	26.8435	235.0520	404.2244
6	1	13522	0.012	38.1635	-542.1203	6.9595	-30.1283	404.2373
7	1	8891	0.013	38.1396	-473.5901	-139.0006	-87.8420	404.1125
8	1	10634	0.008	38.1322	-268.8783	102.3327	-87.8338	404.0901
9	1	13692	0.009	38.1608	-470.2660	122.9880	177.3067	404.2651
10	1	9655	0.012	38.1691	-211.0731	-167.8381	177.2926	404.3261
11	1	12772	0.011	38.1607	-270.1514	181.0040	26.1405	404.2004
12	1	10327	0.011	38.1810	-569.5281	165.8097	27.7952	404.1981
13	1	10414	0.012	38.1840	-163.3789	-162.5568	27.7914	404.2016
14	1	13845	0.011	38.1796	-551.8353	-174.0938	27.7972	404.1960
15	1	7614	0.008	38.1594	-180.9785	237.4588	27.8255	404.2079
16	1	10561	0.012	38.1738	-477.9066	-239.0214	26.1655	404.1894
17	1	18314	0.012	38.1918	-116.3365	-14.0799	27.8826	404.2093
18	1	13845	0.011	38.1796	-551.8353	-174.0938	27.7972	404.1960
19	1	13465	0.011	38.1676	-207.6944	9.4429	293.7212	404.2245
20	1	10236	0.009	38.1606	-403.1642	-151.2474	-110.5010	404.2177
Mean		12132	0.011	38.1645				404.2051
Std.Dev.			0.002	0.0158				0.0732
Max		18314	0.013	38.1918				404.3593
Min		7614	0.008	38.1322				404.0194
Range			0.005	0.0596				0.3399

Figure C 2 Ballbar Sphere Data (2)

PhD Thesis - J. Harris McMaster - Mechanical Engineering

Pose Compensated

Position	Ball	Points	Fit	B1 Radius	B1 X	B1 Y	B1 Z
1	1	13799	0.012	38.1767	-496.5355	-134.2546	27.7874
2	1	8569	0.011	38.1671	-463.2719	98.8514	26.1335
3	1	17087	0.010	38.1633	-480.3646	-161.3817	235.0321
4	1	10736	0.012	38.1530	-470.4919	-167.4905	-30.1247
5	1	12613	0.010	38.1453	-242.4613	30.3356	-30.1433
6	1	13543	0.012	38.1669	-236.7088	4.4374	235.0143
7	1	11283	0.012	38.1693	-290.7511	105.4031	177.2942
8	1	8767	0.011	38.1677	-469.1558	-127.4744	177.3003
9	1	9819	0.010	38.1382	-263.4019	-101.6033	-87.8489
10	1	15028	0.008	38.1412	-401.1623	70.7295	-87.8517
11	1	9244	0.011	38.1821	-258.1060	-223.0345	27.7877
12	1	10667	0.010	38.1650	-164.9831	174.7268	26.1252
13	1	7274	0.010	38.1643	-567.4163	-168.4264	26.1310
14	1	11722	0.012	38.1607	-555.6103	230.1010	26.1352
15	1	8673	0.011	38.1592	-171.8304	-166.6591	26.1306
16	1	10509	0.012	38.1794	-73.5018	-233.2154	27.8900
17	1	8708	0.012	38.1727	-520.1003	-11.8167	26.1599
18	1	11722	0.012	38.1607	-555.6103	230.1010	26.1352
19	1	11228	0.008	38.1817	-207.9407	8.3089	-110.5254
20	1	8983	0.009	38.1711	-402.0784	-150.0661	293.7022
Mean		10999	0.011	38.1643			
Std.Dev.			0.001	0.0124			
Max		17087	0.012	38.1821			
Min		7274	0.008	38.1382			
Range			0.004	0.0439			

Figure C 3 Ballbar Sphere Data (3)

PhD Thesis - J. Harris McMaster - Mechanical Engineering

Pose Compensated

Position	Ball	Points	Fit	B2 Radius	B2 X	B2 Y	B2 Z	Length
1	1	14334	0.010	38.1646	-210.7104	151.5954	26.1314	404.2388
2	1	10168	0.010	38.1764	-166.3468	-175.4532	27.7948	404.2404
3	1	9988	0.011	38.1429	-484.9647	143.6969	-30.1200	404.2273
4	1	15739	0.012	38.1700	-473.5961	137.6167	235.0182	404.2286
5	1	14627	0.008	38.1518	-547.5657	26.8691	235.0417	404.2571
6	1	13522	0.012	38.1668	-541.8501	6.9567	-30.1379	404.2565
7	1	8891	0.012	38.1432	-473.4183	-139.0268	-87.8576	404.2508
8	1	10634	0.008	38.1351	-268.4713	102.3341	-87.8498	404.2162
9	1	13692	0.009	38.1650	-469.8823	123.0196	177.2963	404.2173
10	1	9655	0.012	38.1672	-210.9083	-167.8393	177.2877	404.2407
11	1	12772	0.011	38.1628	-269.7074	181.0267	26.1353	404.2312
12	1	10327	0.011	38.1861	-569.1338	165.8291	27.7894	404.2521
13	1	10414	0.012	38.1861	-163.2184	-162.5697	27.7865	404.2437
14	1	13845	0.011	38.1844	-551.7242	-174.1080	27.7932	404.2311
15	1	7614	0.008	38.1644	-180.4597	237.4836	27.8180	404.2384
16	1	10561	0.012	38.1765	-477.6676	-239.0381	26.1601	404.2115
17	1	18314	0.012	38.1933	-115.8685	-14.0739	27.8704	404.2418
18	1	13845	0.011	38.1844	-551.7242	-174.1080	27.7932	404.2311
19	1	13465	0.011	38.1718	-207.2149	9.4732	293.7033	404.2310
20	1	10236	0.009	38.1641	-402.7947	-151.2700	-110.5234	404.2280
Mean		12132	0.011	38.1678				404.2357
Std.Dev.			0.001	0.0157				0.0128
Max		18314	0.012	38.1933				404.2571
Min		7614	0.008	38.1351				404.2115
Range			0.005	0.0582				0.0456

Figure C 4 Ballbar Sphere Data (4)

Ballbar Length (20 °C)

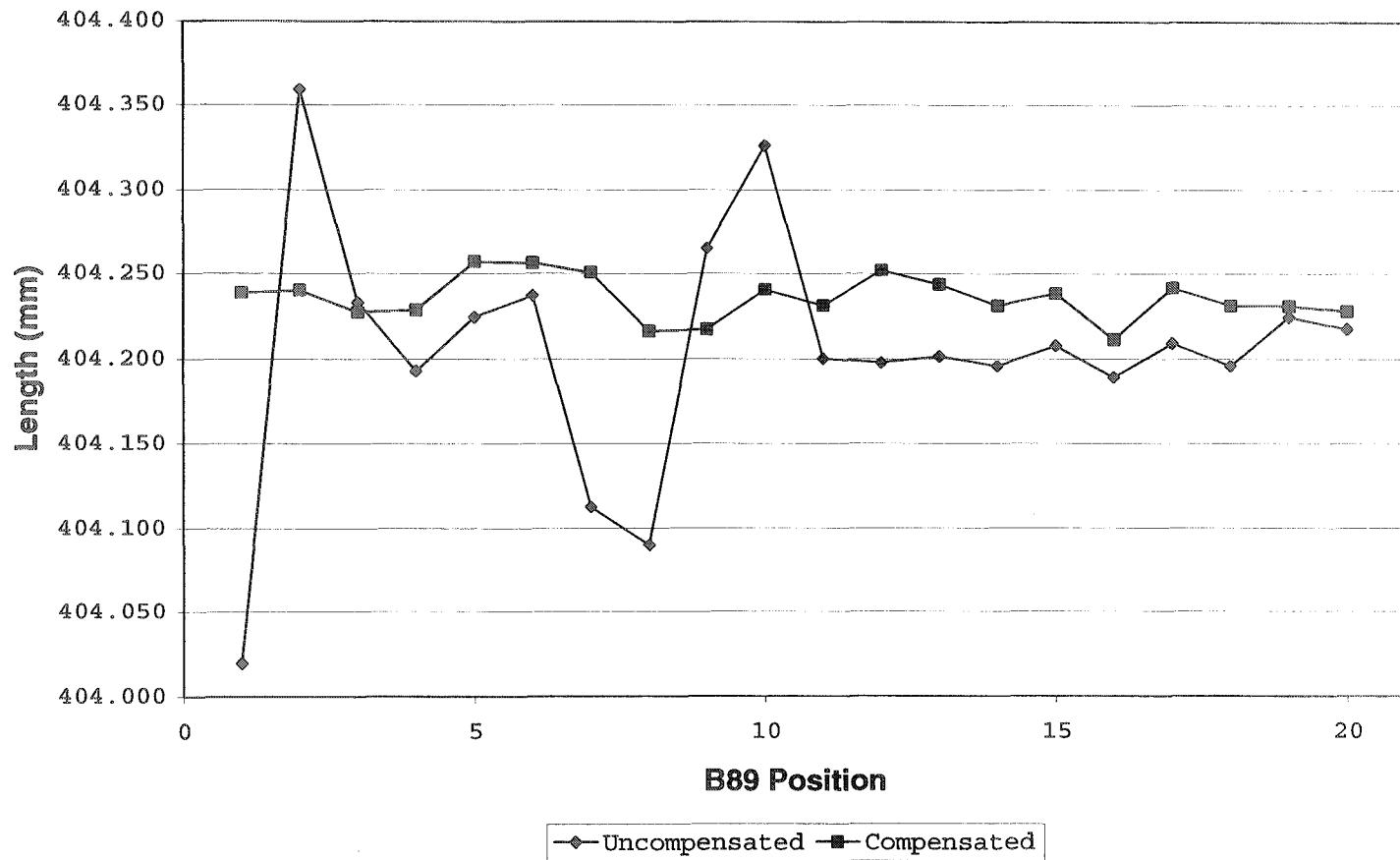


Figure C 5 Ballbar Lengths At 20 °C

Uncompensated Ball Data (20 °C)

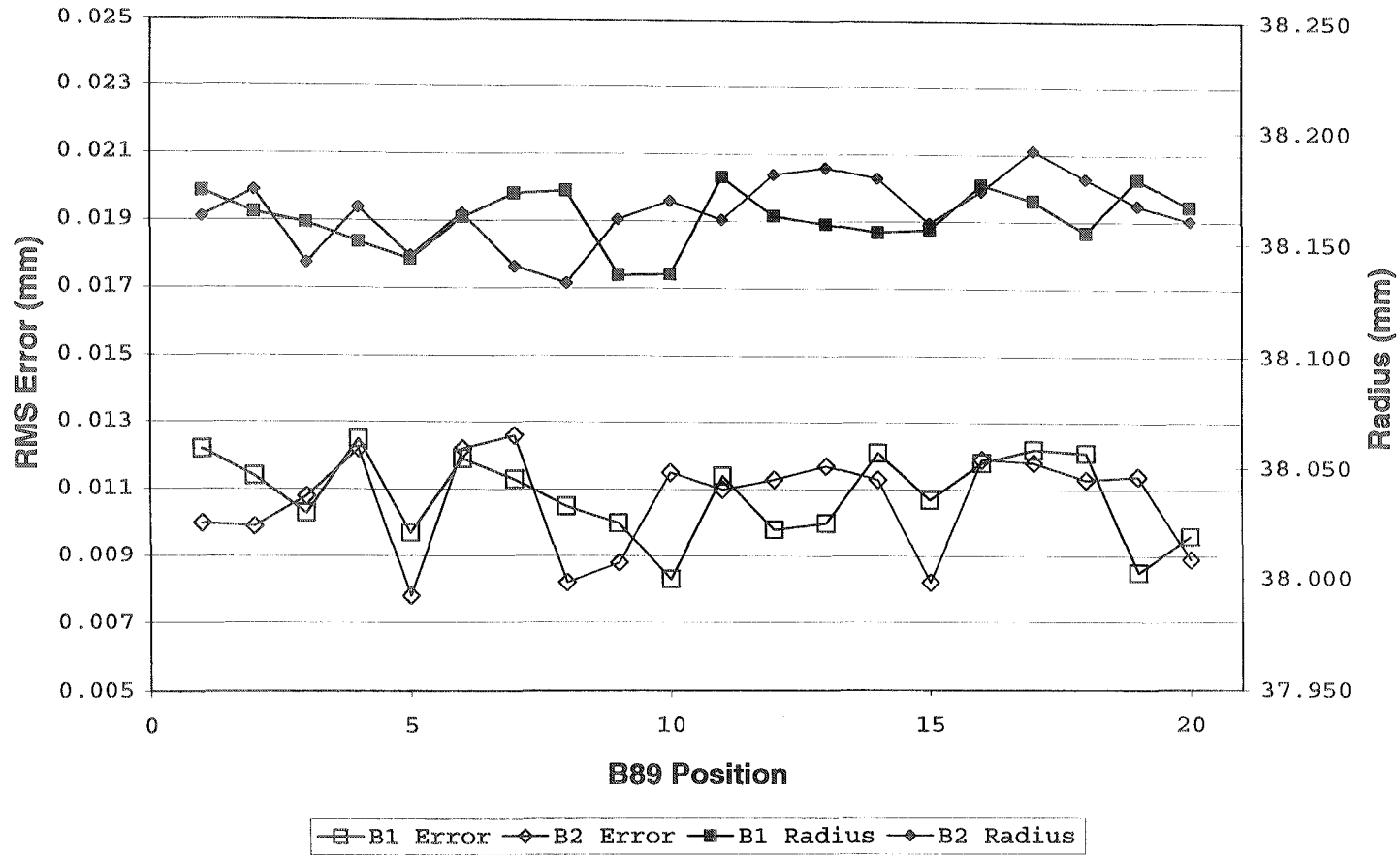


Figure C 6 Detailed Sphere Data, Uncompensated

Compensated Ball Data (20 °C)

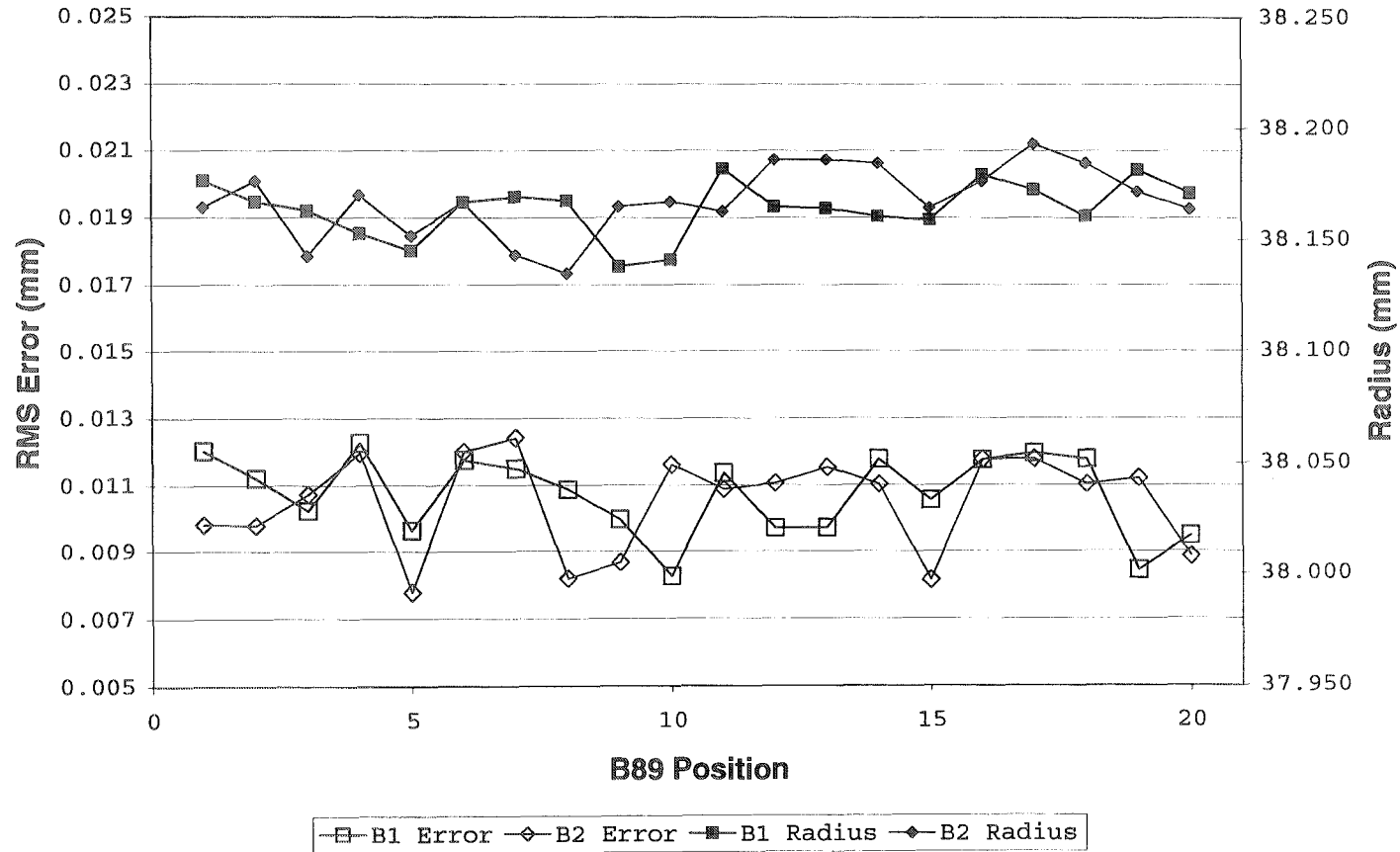


Figure C 7 Detailed Sphere Data, Compensated

References

- Ainsworth, I., M. Ristic, D. Brujic, "CAD-Based Measurement Path Planning for Free-Form Shapes Using Contact Probes", *International Journal of Advanced Manufacturing Technology*, V16/1, pp. 23-31, 2000.
- ASME B5.54, "Methods For Performance Evaluation Of Computer Numerically Controlled Machining Centers", An American National Standard, 1992.
- ASME B89.4.1, "Methods for Performance Evaluation of Co-ordinate Measuring Machines", An American National Standard, 1997.
- ASME B89.4.1b, "Methods for Performance Evaluation of Co-ordinate Measuring Machines, addenda", An American National Standard, 2001.
- Attia, M.H. and L. Kops, "Thermometric Design Considerations for Temperature Monitoring in Machine Tools and CMM Structures", *International Journal of Advanced Manufacturing Technology*, Vol. 8, pp. 311-319, 1993.
- Balsamo, A., "Effects of Arbitrary Coefficients of CMM Error Maps on Probe Qualification", *Annals of CIRP*, Vol. 44/1, pp. 475-478, 1995.
- Balsamo, A., D. Marques, S. Sartori, "A Method for Thermal - Deformation Corrections of CMMs", *Annals of CIRP*, Vol. 39/1, pp. 557-560, 1990.
- Belforte, G., *et al.*, "Coordinate Measuring Machines and Machine Tools Selfcalibration and Error Correction", *Annals of CIRP*, Vol. 36/1, pp. 359-364, 1987.

- Besl, P.J. and M. Ristic, "A Method for the Registration of 3D Shapes", IEEE Transactions on Pattern Analysis and Machine Intelligence, Vol. 14, No. 2, pp. 239-256, 1992.
- Birch, K.P. and M.J. Downs, "An Updated Edlén Equation for the Refractive Index of Air", Metrologia, Vol. 30, pp. 155-162, 1993.
- Bosch, J.A., ed., "Co-ordinate Measuring Machines and Systems", Marcel Dekker, Inc., New York, 1995.
- Bryan, J., "International Status of Thermal Error Research (keynote)", Annals of CIRP, Vol. 39/2, pp. 645-656, 1990.
- Bryan, J.B., "International status of thermal error research (keynote)", Annals of CIRP, Vol. 36 No. 2, pp. 203-215, 1968.
- Bryan, J.B., "Temperature Fundamentals", Chapter 8 in Co-ordinate Measuring Machines and Systems, J.A. Bosch, ed., Marcel Dekker, Inc., New York, pp. 227-264, 1995.
- Caskey, G.W., S.D. Phillips, B.R. Borchardt, "Results of NIST National Ball Plate Round Robin", Journal of Research of the NIST, V. 102, No. 1, 1997.
- Chan, H.L., A.D. Spence, M. Sklad, "Laser Digitizer Based Strain Measurement", in: Proceedings of the 16th Annual ASPE Meeting, Nov. 10-15, 2001, Crystal City, VA, pp. 369-372, 2001.
- Chang, D.W., P. Wu, J.O. Harris, J.E. Peterson, J. Heslip, A.D. Spence, "A Modular Multiple Sensor Embedded System CMM Motion Controller", ASPE 2003 Summer Topical Meeting, Charlotte, NC, 2003.

- Chen, G., J. Yuan, J. Ni, "A Displacement Measurement Approach for Machine Geometric Error Assessment", *International Journal of Machine Tools and Manufacture*, Vol. 41, No. 1, pp. 149-161, 2001.
- Craig, J., "Introduction to Robotics and Mechanics Control", Addison Wesley Publishing Company, 1989.
- Danzer, H. and H. Kunzmann, "Application of 3-Dimensional Co-ordinate Measuring Machines for Problem Investigation and Upstream Quality Assurance", *Annals of CIRP*, Vol. 36/1, pp. 369-372, 1987.
- Duffie, N.A. and S.M. Yang, "Generation Of Parametric Kinematic Error-Correction Functions From Volumetric Error Measurements", *Annals of CIRP*, Vol. 34/1, pp. 435-438, 1985.
- Edlén, B., "The Refractive Index of Air", *Metroligia*, Vol.2, No.2, pp. 71-80, 1966.
- EDS Corp., Imageware, Plano, TX, www.eds.com , 2000.
- Eggert, D.W., A.W. Fitzgibbon, R.B. Fisher, "Simultaneous Registration of Multiple Range Views for Use in Reverse Engineering of CAD Models", *Computer Vision and Image Understanding*, Vol. 69, No. 3, 1998.
- Eman, K., B. Wu, M. DeVries, "A Generalized Geometric Error Model for Multi-axis Machines", *Annals of CIRP*, Vol. 36/1, pp. 253-256, 1987.
- Feng, H-Y., Y. Liu, F. Xi, "Analysis of Digitizing Errors of a Laser Scanning System", *Precision Engineering*, Vol.25 No.3, pp. 185-191, 2001.
- Ferreira, P. and C. Liu, "A Contribution to the Analysis and Compensation of The Geometric Error of a Machining Centre", *Annals of CIRP*, Vol. 35/1, 1986.

Harris, J.O. and A.D. Spence, "Geometrically Compensated Measurement with a Laser Digitizer Equipped CMM", in: 17th Annual ASPE Meeting, St. Louis, MO, Oct. 20-25, 2002, 2002.

Harris, J.O. and A.D. Spence, "Integrated Geometric Error Compensation for a Laser Digitizer Equipped CMM", in: CSME Forum 2002, Queen's University, Kingston, ON, May 21-24, 2002, 2002.

Harris, J.O. and A.D. Spence, "Geometric and Quasi-static Thermal Error Compensation for a Laser Digitizer Equipped Co-ordinate Measuring Machine", International Journal of Machine Tools and Manufacture, Vol. 44, No.1, pp. 65-77, 2004.

Hocken, R.J., J.A. Simpson, B. Borchardt, J. Lazar, C. Reeve, P. Stein, "Three Dimensional Metrology", Annals of CIRP, Vol. 26/2, pp. 403-408, 1977.

Hymarc 3D Vision Systems, "Hyscan 45C 3-D Laser Digitizer", Hymarc 3D Vision Systems, Nepean, ON.

IACMM OSIS/WG2 Workgroup, "Optical Sensor Interface Standard Release RC1", International Association of Co-ordinate Measuring Machine Manufacturers http://www.iacmm.org/wgroups/osis/OSIS_WG2_DOCUMENTATION_VRC1.pdf accessed 2003-07-10, 2003.

ISO, "Guide to the Expression of Uncertainty in Measurement", International Organization for Standardization, Geneva, Switzerland, 1995.

ISO 10360, "Geometrical Product Specifications (GPS) Acceptance and reverification tests for co-ordinate measuring machines (CMM)", International Organization for Standardization, 2000.

- ISO 14253, "Geometrical Product Specifications (GPS) Inspection by measurement of workpieces and measuring equipment", International Organization for Standardization, 1998.
- Iwata, K., T. Moriwaki, S. Ueno, "Development of a Modular-Type Measuring System for Evaluation of Machining Accuracy", Annals of CIRP, Vol. 31/1, 1982.
- Jalkio, J.A., "The Use of Optical Probes for Co-ordinate Measuring Machines - Strengths and Weaknesses", in: SME Conference on Precision Metrology with CMMs, Minneapolis, IQ99-206, 1999.
- Jie-Chi, L., N. Duffie, J. Bollinger, "Two Dimensional Tracing and Measurement Using Touch Trigger Probes", Annals of CIRP, Vol. 31/1, 1982.
- Knapp, W., "Test of The Three-Dimensional Uncertainty of Machine Tools and Measuring Machines and its Relation to the Machine Errors", Annals of CIRP, Vol. 32/1, 1983.
- Knapp, W., "Accuracy of Length Measurement and Positioning: Statical Measurement and Contouring Mode", Annals of CIRP, Vol. 37/1, 1988.
- Kneppers, R., "HP Laser Interferometers", Vaisala News, Vol. 151, pp. 34-37, Helsinki, Finland, 1999. Available online at http://www.vaisala.com/DynaGen_Attachments/Att3429/3429.pdf.
- Kunzmann, H., J. Ni, F. Waldele, "Accuracy Enhancement", Chapter 10 in Co-ordinate Measuring Machines and Systems, J.A. Bosch, ed., Marcel Dekker, Inc., New York, 1995.

Kunzmann, H., E. Trapet, F. Waldele, "A Uniform Concept for Calibration, Acceptance Test, and Periodic Inspection of Co-ordinate Measuring Machines Using Reference Objects", Annals of CIRP, Vol. 39/1, pp. 561-564, 1990.

Kunzmann, H., E. Trapet, F. Waldele, "Results of The International Comparison of Ball Plate Measurements in CIRP and WECC", Annals of CIRP, Vol. 44/1, pp. 479 - 482, 1995.

Kunzmann, H. and F. Waldele, "On Testing Co-ordinate Measuring Machines (CMM) with Kinematic Reference Standards (KRS)", Annals of CIRP, Vol. 32/1, 1983.

Kunzmann, H. and F. Waldele, "Performance of CMMs", Annals of CIRP, Vol. 37/2, 1988.

Lau, K. and R. Hocken, "A Survey of Current Robot Metrology Methods", Annals of CIRP, Vol. 33/2, 1984.

Lingard, P., M. Purss, C. Sona, E. Thwaite, "Length-Bar and Step-Gauge Calibration Using a Laser Measurement System with a Co-ordinate Measuring Machine", Annals of CIRP, Vol. 40/1, 1991.

Liu, D., R. Che, Q. Huang, D. Ye, "An Error-model Study of a New Type of Co-ordinate-measuring Machine Based on the Parallel-link Mechanism", Measuring Science Technology, II, 2000, pp. 1721-1725, 2000.

McKeown, P.A., "The Role of Precision Engineering in Manufacturing of the future", Annals of CIRP, Vol. 36/2, 1987.

- Metrology Automation Association, "First ever CMM Industry Statistics",
http://www.metrologyautomation.org/firstcmmstats_release.htm accessed 2002-
Oct-03, 2000.
- Metrology Automation Association, "North American CMM Sales Fell 20% in 2002",
http://www.metrologyautomation.org/CMM_Sales_Fall_Release.html accessed
2003-Jun-27, 2002.
- Millett, J., "CMM Software Requirements for Profile Technology", SME Conference on
Precision Metrology with CMMs, Minneapolis, IQ99-208, 1999.
- Nakamura, O., M. Goto, K. Toyoda, Y. Tanimura, "Development of a Co-ordinate
Measuring System with Tracking Laser Interferometers", Annals of CIRP, Vol.
40/1, 1991.
- Nawara, L. and M. Kowalski, "Investigations on The Variability of Measurements
Realized by Multicoordinate Measuring Machines on Circular Sections with
Determined Types of Roundness Errors", Annals of CIRP, Vol. 30/1, 1981.
- Nawara, L. and M. Kowalski, "The Investigations on Selected Dynamical Phenomena in
The Heads of Multi-Co-ordinate Measuring Devices", Annals of CIRP, Vol. 33/1,
1984.
- Nawara, L., M. Kowalski, J. Sladik, "The Influence of Kinematic Errors on The Profile
Shapes by Means of CMM", Annals of CIRP, Vol. 38/1, 1989.
- Nijs, J., M. Lammers, P. Shellekens, A. Van der Wolf, "Modelling of a Co-ordinate
Measuring Machine for Analysis of its Dynamic Behaviour", Annals of CIRP,
Vol. 37/1, 1988.

- Ogura, K. and S. Kikuchi, "Development and Design Procedure of High-Accuracy Co-ordinate Measuring Machine", *Design Engineering*, Vol. 30, No. 11, 407, 1995.
- Okafor, A.C. and Y.M. Ertekin, "Vertical Machining Center Accuracy Characterization Using Laser Interferometer Part 2. Angular Errors", *Journal of Materials Processing Technology*, Vol. 105, pp. 407-420, 2000.
- Okafor, A.C. and Y.M. Ertekin, "Vertical Machining Center Accuracy Characterization Using Laser Interferometer Part 1. Linear Positional Errors", *Journal of Materials Processing Technology*, Vol. 105, pp. 394-406, 2000.
- Omni-Tech Corporation, "OTC5000 CMM Controller", Omni-Tech Corporation, Fenton, MI, 2001.
- Paul, R., "Robot Manipulators - Mathematics, Programming and Control", MIT Press, Cambridge, Mass. 1982, 1982.
- Peggs, G. and P. McKeown, "Creating a Standard Infrastructure for Co-ordinate Measurement Technology in the U.K.", *Annals of CIRP*, Vol. 38/1, 1989.
- Rosenfeld, D.A., "User's Guide for the Algorithm Testing System Version 2.0", NISTIR 5674, National Institute of Standards and Technology, Gaithersburg, MD, 1996.
- Sartori, S. and G. Zhang, "Geometric Error Measurement and Compensation of Machines (keynote)", *Annals of CIRP*, Vol. 44/2, pp. 599-609, 1995.
- Scarr, A.J.T., "Metrology and Precision Engineering", McGraw-Hill, New York, 1967.
- Schafrik, R.E., "Unit Manufacturing and Assembly Processes", Chapter 13.2 in *Mechanical Engineering Handbook*, Kreith, F. (ed), CRC Press, Boca Raton, 1999.

- Schultschick, R., "The Components of Volumetric Accuracy", *Annals of CIRP*, Vol. 25/1, pp. 233-227, 1977.
- Shen, Y-L. and N.A. Duffie, "Uncertainties in the Acquisition and Utilization of Co-ordinate Frames in Manufacturing Systems", *Annals of CIRP*, Vol. 40/1, pp. 527-530, 1991.
- Slocum, A., "Precision Machine Design", Chapter 11.8 in *Mechanical Engineering Handbook*, Kreith, F. (ed), CRC Press, Boca Raton, 1999.
- Spence, A.D., R.V. Fleisig, N.A. Barakat, "A Multiple Sensor, Geometrically Corrected Co-ordinate Measuring Machine System", in: *Proceedings of 33rd International MATADOR Conference*, pp. 217-222, 2000.
- Srivastava, A.K., S.C. Veldhuis, M.A. Elbesawi, "Modelling Geometric And Thermal Errors In A Five-Axis CNC Machine Tool", *International Journal of Machine Tools and Manufacture*, Vol. 35, No. 9, pp. 1321-1337, 1995.
- Tani, Y., K. Katsuki, H. Sato, Y. Kamimura, "Development of High-Speed and High-Accuracy Straightness Measurement of a Granite Base of a CMM", *Annals of CIRP*, Vol. 44/1, 1995.
- Teeuwesen, J., J. Soons, P. Schellekens, "A General Method for Error Description of CMMs Using Polynomial Fitting Procedures", *Annals of CIRP*, Vol. 38/1, 1989.
- Tong, Y.L., "Mathematics: Engineering Statistics", in: *Mechanical Engineering Handbook*, F. Kreith (Ed.), CRC Press, Boca Raton, 1999.

- Treib, T., "Error Budgeting - Applied to The Calculation and Optimization of The Volumetric Error Field of Multiaxis Systems", *Annals of CIRP*, Vol. 36/1, pp. 365-368, 1987.
- Turk, G. and M. Levoy, "Zippered Polygon Meshes from Range Images", *Proceedings of SIGGRAPH*, Orlando, FL, 1994.
- VDI/VDE 2617, "Accuracy of Co-ordinate Measuring Machines", Dusseldorf, 1989.
- Veldhuis, S.C. and M.A. Elbestawi, "A Strategy for the Compensation of Errors in Five-axis Machining", *Annals of CIRP*, Vol. 44/1, pp. 373-377, 1995.
- Weck, M., P. McKeown, R. Bonse, U. Herbst, "Reduction and Compensation of Thermal Errors in Machine Tools (keynote)", *Annals of CIRP*, Vol. 44/2, pp. 589-598, 1995.
- Weekers, W. and P. Schellekens, "Assessment of Dynamic Errors of CMMs for Fast Probing", *Annals of CIRP*, Vol. 44/1, 1995.
- Xi, F., Y. Liu, H-Y. Feng, "Error Compensation for Three-Dimensional Line Laser Scanning Data", *International Journal of Advanced Manufacturing Technology*, Vol. 18, pp. 211-216, 2001.
- Yonezawa, H., Y. Hirata, H. Sasai, "Positioning Table with High Accuracy and High Speed", *Annals of CIRP*, Vol. 39/1, 1990.
- Zeid, A.A. and R.R. Beck, "Dynamics of Rigid Bodies: Kinematics and Kinetics", *The Engineering Handbook*, R.C. Dorf, ed., CRC Press, Boca Raton, 2000.
- Zhang, G., "A Study on The Abbe Principle and Abbe Error", *Annals of CIRP*, Vol. 38/1, 1989.

Zhang, G. and Y. Fang, "A Method for Machine Geometry Calibration Using 1-D Ball Array", Annals of CIRP, Vol. 40/1, 1991.

Zhang, G., R. Veale, T. Charlton, B. Borchardt, R. Hocken, "Error Compensation of Coordinate Measuring Machines", Annals of CIRP, Vol. 34/1, 1985.